TÉCNICO LISBOA

Experimental demonstration of 10 Gbit/s fibre-to-the-home network downstream transmission employing an electro-absorption modulator

Jorge Eduardo Ribeiro da Costa Lima

Thesis to obtain the Master of Science Degree in

Electrical and Computer Engineering

Supervisors: Prof. Dr. Adolfo da Visitação Tregeira Cartaxo
Dr. Tiago Manuel Ferreira Alves

Examination Committee

Chairperson: Prof. José Eduardo Charters Ribeiro da Cunha Sanguino
Supervisor: Prof. Adolfo da Visitação Tregeira Cartaxo
Members of the Committee: Drª. Sílvia Medeiros Vaz Pato

May 2015

This dissertation was performed under the project “Metro networks based on multi-band orthogonal frequency-division multiplexing signals” (MORFEUS-PTDC/EEI-TEL/2573/2012) funded by Fundacão para a Ciência e Tecnologia from Portugal.

Acknowledgments

This dissertation would not have been possible without the support and encouragement of many people throughout my education, whether explicitly mentioned here or not, and to these people I express my deep gratefulness.

In this respect, I am grateful to Adolfo Cartaxo, and co-supervisor Dr. Tiago Alves for originally motivating this project, and supporting my work in this direction. They provided many valuable insights and have been always willing to take the time to explain things to me. Since the inception of this project, they have been a source of encouragement and enlightenment. I must also thank them for their time in helping me out of the practical difficulties while building my measurements setups.

Thanks are due to my parents and my family for their constant support over the years. The encouragement and love that they have selflessly and tirelessly invested in me is undoubtedly the greatest source of my ambition, inspiration, dedication and motivation. This work is dedicated to you: parents, Maria Costa and Júlio Lima, and grandmother. I also dedicate this work to my brother, Rui Lima.

I would also like to express my gratitude to Instituto de Telecomunicações (IT) for providing me access to their facilities and laboratory equipment.

I would like to thank also Ph.D. students Eng. Pedro Cruz, MSc. student João Rosário and MSc. Luís Mendes at the Group on Optical Fiber Telecommunications Systems of IT-Lisboa, for their availability to answer my questions, as well as in providing a friendly and entertaining working environment.

I feel it necessary to mention also the friends who have been with me in the past few years. Although they have perhaps not contributed directly to this work, their support and encouragement outside of my research is part of what kept me going those times when research wasn't going as well as I. Catarina Morgado, for all your support throughout this demanding and challenging journey. Filipe Rodrigues, André Mendes and Diogo Machado, for all the good moments and support you have provided to me along my graduation and master courses. Thank you all.

Abstract

Following the increasing demand in bit rate by end-users, an evolutionary step in fibre-to-the-home (FTTH) networks was made. Starting from the already deployed passive optical network (PON), this dissertation studies the possibilities of characterization of future PON trends. The evolution towards the future architecture of next generation passive optical networks (NG-PON) is described. Possible future solutions, like the NG-PON1 and NG-PON2, will also be presented and considered alongside their corresponding specification. To accomplish the bit rates intended for NG-PON1, external modulation is considered.

The characterization of an Electro-absorption modulator (EAM) is performed to measure the static and dynamic characteristic of the EAM. From the static characteristic it was possible to measure the optical power at the EAM output and from the dynamic characteristic it was possible to study the amplitude response of the modulator. Through the study of the amplitude response of experimental setup employing 100 km of fibre, the chirp and dispersion parameter were measured. The chirp parameter of the EAM at a wavelength of 1575 nm is between 3 and -2, approximately. The dispersion parameter has been measured and presented a value around 18 ps/(nm.km).

This dissertation focuses on experimental demonstration to evaluate the performance of a 10 Gbit/s signal transmitted in an optic link, which emulates the downstream direction of a Ten-Gigabit-Capable Passive Optical Network (XG-PON) architecture. From this experimental demonstration it has been concluded that the minimum extinction ratio scenario operating with a wavelength of 1575 nm presented the best performance.

Keywords: Fiber to the home, passive optical network, next generation passive optical network, electro-absorption modulator.

Resumo

Acompanhando o aumento da exigência no debito pelos end-users, um passo em direção à evolução nas redes de fibre-to-the-home (FTTH) foi dado. A partir da rede óptica passiva (PON) já instalada, esta dissertação estuda as possibilidade de caracterização de tendências futuras para as PON. A evolução para a futura arquitetura das redes ópticas passivas de nova geração (NG-PON) é descrita. Possíveis soluções futuras, assim com NG-PON1 e NG-PON2 serão também apresentadas e consideradas durante a sua correspondente especificação. A fim de conseguir os débitos destinados para a NG-PON1, a modulação externa foi considerada.

É realizada uma caracterização do modulador de electro-absorção (EAM), para medir a característica estática e dinâmica do EAM. Através desta característica estática, foi possível medir a potencia óptica à saída do EAM e através da característica dinâmica, foi possível estudar a resposta em frequência do modulador. Através do estudo da resposta em frequência do setup experimental com 100 km de fibra, o parâmetro de chirp e dispersão foram medidos. Foi concluído que o parâmetro de chirp do EAM está entre 3 e -2 aproximadamente. O parâmetro de dispersão foi medido e apresenta o valor de 18 ps/(nm.km).

Uma demonstração experimental é apresentada de forma a avaliar o desempenho de um sinal a 10 Gbit/s transmitido na ligação óptica que emula o sentido descendente de uma arquitetura XG-PON1. Desta demonstração experimental foi concluído que o cenário de menor razão de extinção com um comprimento de onda de 1575 nm apresenta melhor desempenho.

Table of Contents

List of Figures

List of Tables

List of Acronyms

AC	Alternate Current
ADSL	Asymmetric Digital Subscriber Line
AGC	Automatic Gain Control
APD	Avalanche Photo-Diode
APON	ATM Passive Optical Network
ATM	Asynchronous Transfer Mode
BER	Bit Error Ratio
BERT	Bit Error Ratio Tester
BPON	Broadband Passive Optical Network
CATV	Cable Television Services
CAS	Client Adaptation Layer
CDMA	Code Division Multiple Access
CWDM	Coarse Wavelength Division Multiplexing
DC	Direct Current
DBA	Dynamic Bandwidth Allocation
DSA	Digital Serial Analyzer
DSL	Digital Subscriber Line
DWDM	Dense Wavelength Division Multiplexing
EAM	Electro-Absorption Modulator
EDFA	Erbium Doped Fiber Amplifier
EPON	Ethernet Passive Optical Network
ESA	Electric Spectrum Analyzer
FEC	Forward Error Correction
FS	Framing Sublayer
FSAN	Full Service Access Networks
FTTX	Fiber To The X
FTTB	Fiber To The Building
FTTC	Fiber To The Curb
FTTCab	Fiber To The Cabinet
FTTH	Fiber To The Home
FTTN	Fiber To The Node

GEM	General Encapsulation Method
GEPON	Gigabit Ethernet Passive Optical Network
GPON	Gigabit Passive Optical Network
IEEE	Institute of Electrical and Electronics Engineers
ITU-T	Telecommunication Standardization Sector of the International Telecommunication Union
LTE	Long Term Evolution
MQW	Multiple Quantum Well
MZM	Mach-Zehnder Modulator
NGA	Next Generation Access
NT	Network Termination
NRZ	Non Return to Zero
NG-PON	Next Generation PON
ODN	Optical Distribution Network
OLT	Optical Line Terminal/Termination
ONT	Optical Network Terminal/Termination
ONU	Optical Network Unit
P2MP	Point-To-Multipoint
P2P	Point-to-Point
PAS	Physical Adaptation Sublayer
PIN	Positive-Intrinsic-Negative
PMD	Physical Media Dependent
PON	Passive Optical Network
POTS	Plain Old Telephone Service
QCSE	Quantum-Confined Stark Effect
RE	Reach Extender
RF	Radio Frequency
RS	Reed Solomon
SDH	Synchronous Digital Hierarchy
SDO	Standards Development Organization

TC	Transmission Convergence
TDM	Time Division Multiplexing
TDMA	Time Division Multiple Access
TIA	Transimpedance Amplifier
VEA	Variable Electric Attenuator
VOA	Variable Optical Attenuator
VDSL	Very-High-Bit-Rate Digital Subscriber Line
XG-PON	Ten-Gigabit-Capable Passive Optical Network
WBF	Wavelength Blocking Filter
WDM	Wavelength Division Multiplexing
WiFi	Wireless Fidelity
WiMAX	Worldwide Interoperability for Microwave Access

Chapter 1

Introduction

In this chapter, an assessment is performed on the legacy and evolution of passive optical networks (PONs). In section 1.1, entitled scope of the work, a description of these networks is presented. In subsections of section 1.1, a description of PONs and their history is made. In section 1.2, the Gigabit Passive Optical Network (GPON) system is introduced and its specifications are described in subsections of sections 1.2. Section 1.3 presents the motivation for this dissertation. Finally, in section 1.4, a description of the report structure is made and in section 1.5, the main original contribution of this work is presented.

1.1 Scope of the work

With the increasing demand in bandwidth by end-users, it is necessary to evolve the already deployed PON to answer this request in bandwidth. This dissertation focuses on experimental demonstration in order to evaluate the performance of a 10 Gbit/s signal transmitted in an optic link, which emulates the downstream direction of PON architecture. Considering the theme of this thesis, the electro-absorption modulator (EAM) is used. For transmitting signals several solutions for modulator are available and some are discussed in this dissertation.

This section of the report describes the history of PONs and its main components, devices and technology used.

1.1.1 Passive optical networks

Since the third quarter of the 20th century, fibre optics technology began to be deployed on metro/access networks [1]. Copper twisted pair and coaxial cable were the first stone of communication networks.

Since the creation of the World-Wide-Web in 1990, there has been a challenging demand in increasing the bandwidth for deploying online services and emerging multimedia content, such as cloud computing, video streaming, e-commerce, e-learning and other Internet based applications. This recent and enlarged interest in more bandwidth can be explained by the Nielsen's law of Internet bandwidth. This law states that each year, Internet connection bandwidth must increase by 50% on average, to accordingly respond to a high-end user needs [2]. This fact can be easily explained by the network evolution and new multimedia services and the other mentioned services. This increase of bandwidth is a natural response to the upsurge in data traffic, which doubles every 1 to 2 years with new applications and services.

In the past, homes were supplied with two kind of services delivered by access networks, the plain old telephone network (POTS), on a twisted pair network, and cable television services (CATV), on a coaxial cable network. Afterwards, the data services for Internet using a digital subscriber line (DSL) were added. These services functioned through the telephone network or through a cable modem service over the cable network [3]. Due to the increase of multimedia content, DSL technologies evolved to asymmetric digital subscriber line (ADSL) and very-high-bit-rate digital subscriber line (VDSL). ADSL was developed using 8 Mbit/s in the downstream and up to 800 kbps in the upstream over a distance of 5.5 km and the VDSL has 52 Mbit/s in the downstream and up to 16 Mbit/s in the upstream over a distance of 1.2 km [4].

Studies now show that optical networks have innumerous advantages, such as, smaller equipment size and weight, higher bandwidth, lower insertion loss, higher flexibility, scalability, durability and immunity to the environmental conditions [5]. The implementation of optical fibre in the metro/access networks, facilitates the upgrade of the already existing technology. With this upgrade it is possible to provide more forms of multimedia, like video on demand and high-definition television.

Optical fibre was viewed as the next step in communication evolution and so copper twisted pairs were replaced for the new fibre optics. Ultimately, copper twisted pairs are expected to be entirely replaced for an optical fibre connection.

The implementation of fibre optics in metropolitan networks was beneficial for consumers. This implementation led to immunity to electromagnetic interference and lower values of attenuation. Thanks to this fact, it was possible to extend the range of the access network as well as the data rates achieved.

The main optical fibre architecture subsystems are optical line terminal/termination (OLT) located at the service provider central office (CO) and the optical network unit (ONU) or the optical network terminal/termination (ONT) near end users.

The optical access architecture for fiber networks is show in figure 1.1.

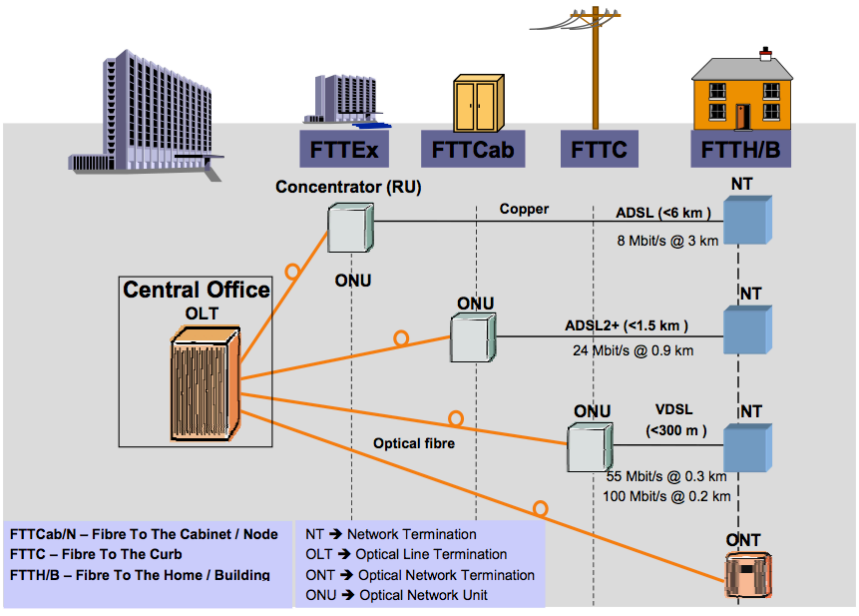

Figure 1.1 – Optical access architecture, adapted from [6]

It is possible to perceive from the figure, that the optical fibre is being deployed closer to the subscriber.

Optical fiber can be deployed in metro/access networks in different scenarios, depending on the extent of deployed fibre and on the fibre connection end-points. There are referred to as fibre-to-the-x (FTTX), where the x can stand for building (FTTB), curb (FTTC), cabinet (FTTCab), home (FTTH), exchange (FTTEx) and node (FTTN). In FTTH the optical fibre goes to the subscriber residence. The FTTC or FTTB topology is able to serve between 10 to 100 houses or buildings (located within less than 300 m of the subscriber). In this case, there is an additional distribution network between the ONU and the ONT that can be in copper wires (twisted pair or coaxial cable) or via radio. In the FTTCab solution, the ONU is distanced at a maximum distance of 1.5 km from the subscriber, with implies also an additional distribution network effort [6].

The FTTX system is deployed on business and residential networks and has a standard distance range between 10 and 20 km (it can be higher with some extensions), approximately, which can deliver services to several users [7].

The use of PONs represents the most suitable and efficient way to provide communications at significant lengths (around 20 km) with low transmission losses and reducing the total cost of the network. Sharing the opto-electronics in the CO and sharing part of the fiber infrastructure through passive splitters are some aspects that support the use of PONs [7].

While developing the optical access etwork, two architectures were created. One is the point-to-point (P2P) and the other is the point-to-multipoint (P2MP). The P2P topology consists in one dedicated fibre that is used to link each ONT/ONU to the OLT. This connection corresponds to a star physical topology and it can be viewed in figure 1.2. The P2MP connection is accomplished through a type of one-to-many connection. This solution means that it can provide several paths from a single location to multiple ONT/ONU with the aid of a passive optical splitter. The P2MP connectivity between OLT and various number of ONTs/ONUs is achieved using one or more passive branching devices in the fibre path. In this case, the feeder fibre, meaning the path between the splitting point and the OLT, is shared. This topology is described as a tree physical topology as shown in figure 1.3.

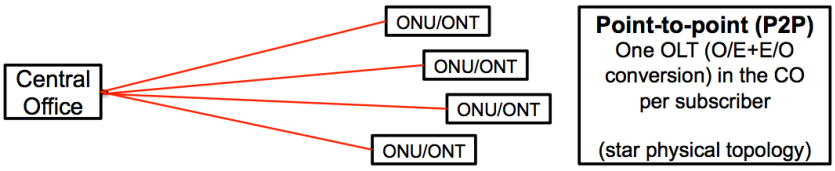

Figure 1.2 – Point-to-point

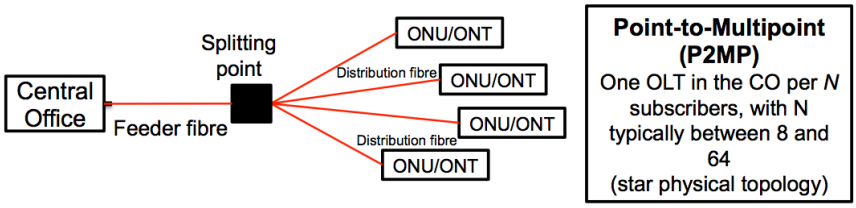

Figure 1.3 – Point-to-multipoint

The P2P topology can be configured to use two fibres, one for the upstream direction, between the OLT and each ONU, and another for the downstream direction, between each ONT/ONU and the

OLT. It can also operate in one single fibre at 1500 nm in downstream and 1300 nm in upstream, transmitting in the same distance range and data rate.

One other significant distinction between these two networks designs is the number of customers covered by each architecture. In P2P, each client gets a dedicated optical port located at the CO, while the P2MP can cover several clients, from typically 8 up to 64, sharing the same optical port from the same device [5].

PONs are mostly implemented in a P2MP passive architecture and usually work with two or three wavelengths. Its operating system can be described as a signal leaving the OLT port and transported through the optical fibre until it reaches the power splitter. This network element splits the optical fibre in to several links. From the power splitter, several output replicas of the signal are transmitted, with a lower level of power. This splitter device has a splitting factor of 1 to N (typically a power of two), which depends on the number of ONT or ONU that the network is able to provide. It is noticeable that each output port transmits a power level lower than 1 over N, of the original transmitted power by the OLT when approaching the remote node, meaning, the location of the power splitter [5].

The communication in PONs is be made in two different directions: upstream, defined by the communication between each ONU and the OLT and downstream, defined by the communication between the OLT and each ONU. The main difficulty of deploying PONs is the design of the networks operating system for the upstream direction. Although all ONUs share the same feeder fibre, it requires multiple access techniques to avoid collisions in the upstream direction [5].

To avoid the collisions, two types of PONs were created, the Time Division Multiplexing (TDM) PON and the Wavelength Division Multiplexing (WDM) PONs. TDM type can be explained by the multiple accesses in the time domain using the Time Division Multiple Access (TDMA) protocol [6]. Using this protocol, each ONU is given several timeslots, where it can transmit data in the upstream channel, meaning that different ONUs cannot transmit simultaneously, thus avoiding collisions. This transmission can be with a fixed or dynamic allocation, depending on the use of dynamic bandwidth allocation (DBA) algorithm. The DBA algorithm attributes time-slots to each ONU paying attention to the size of the data packets being transmitted and so, an ONU with bigger in formation receives a bigger time slot and vice-versa. The implementation of this algorithm guarantees an increase of efficiency and gives a fair allocation of the time slots and so, allowing a better way to explore the capacity of the available channels [8].

As it was stated, another type of PON created was the WDM PON that allows multiple accesses in the wavelength domain by exploring the Wavelength Division Multiple Access (WDMA). The creation of this protocol serves the same purpose of the TDMA, but now, improving the efficiency and fairness of the wavelengths allocation. Typically it uses WDM filters in the splitting locations. In other words, it is not possible for two ONUs to transmit in the same wavelength [6].

Figure 1.4 presents a road map for the future of the FTTH networks. From figure 1.4 it is possible to see that the network evolution will require coexistence. This is very important concept that will be introduced in this dissertation. The next sections of this chapter will present a historical perspective of PONs and specifications of PONs that are in used nowadays.

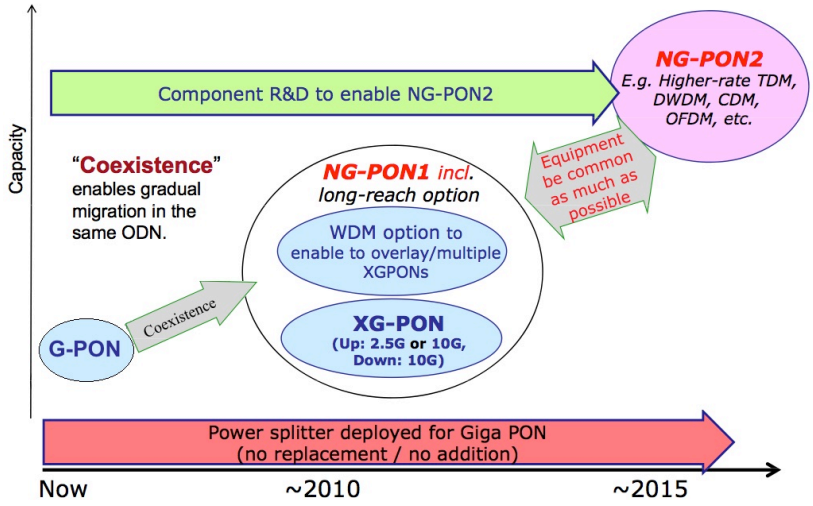

Figure 1.4 – NG-PON roadmap, adapted from [9]

1.1.2 Historical perspective of PONs

PONs technologies are available since the mid 90s, but in the last few year standards and know-hows have matured and commercial standards are being implemented [10].

The first PON developed was Asynchronous Transfer Mode Passive Optical Network (APON). The Full Service Access Network (FSAN) Group, which is associated with the Telecommunication Standardization Sector of the International Telecommunication Union (ITU-T), developed the standardization of this network in the year of 1995 and it took two years to be finished. This group has specialized in fibre access technology for many years. The APON uses an asynchronous transfer mode (ATM) cell at the core of its communication and depending on its covered distance could comprise up to 32 ONTs/ONUs. The APON had a downlink of up to 1.24 Gbit/s and up to 622 Mbit/s in the uplink stream [11].

The APON evolved to Broadband Passive Optical Network (BPON), which was backward compatible with APON as BPON it also operated using ATM cells [10]. The ITU-T issued several recommendations for this network, such as G983.3, G983.4 and G983.5. The main goal of these recommendations was to present major features that were not available in the APON. BPON introduced the video broadcast system at the 1550 nm wavelength and used wavelength division multiplexing method in the downstream direction [12]. Thanks to this advanced network, it was possible to have a date rate in the downlink up to 1.24 Gbit/s (about 20 Mbits/s per ONT/ONU, using a splitter of 1 to 32 [6]) and up to 622 Mbit/s in the uplink stream. DBA algorithms were also introduced to increase the performance of the upstream channels [13].

The description of the PONs developed is presented in figure 1.5. As shown in figure 1.5, following BPON, FSAN group defined the recommendation series G.984.1 through G984.4 and called Gigabit Passive Optical Network (GPON) to the next PON evolution. This network will be analyzed in the following section of this report.

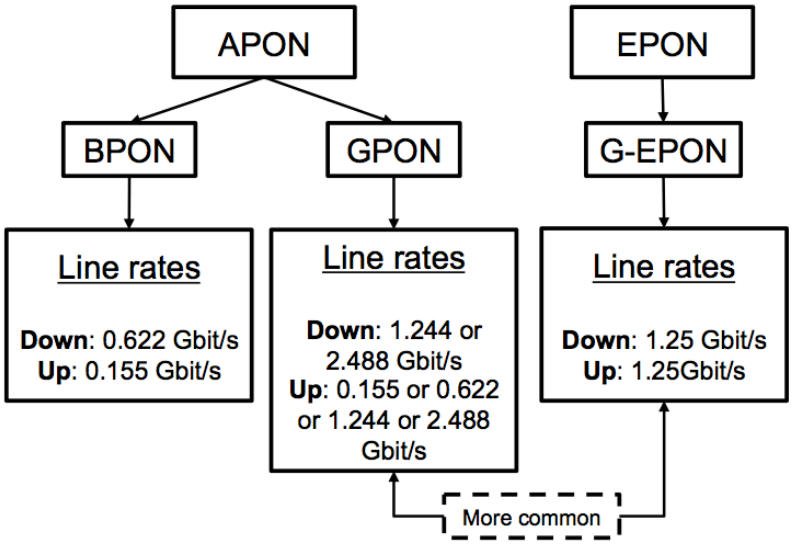

Figure 1.5 – PONs created

The Institute of Electrical and Electronics Engineers (IEEE) developed a network based on Ethernet packets called Ethernet Passive Optical Network (EPON), and created the P802.3ah standard. This network had no compatibility with APON and BPON [10]. This decision was taken due to the many disadvantages detected of Ethernet traffic over ATM networks. ATM cells were just not enough for the Ethernet frame and the cells needed to transmit 13% more bits than an Ethernet network [14].

1.2 Gigabit Passive Optical Network

Efforts to standardize PONs operating at above 1 Gbit/s were initiated in 2001 [15]. After the BPON, the next evolutionary step of the ITU-T FSAN group was the creation of the Gigabit Passive Optical Network (GPON) and the G.984 recommendation series. GPON has enhanced capability comparing with APON and BPON and is backward compatible. The G.984 standard defines the general characteristics of GPON, physical layer specification, transmission layer specification and ONU management and control specification, respectively [10]. The GPON standard was finished in early 2008 and published in early 2009.

By the time the GPON was developed, the ATM technology was starting to fade, mainly due to its lack of efficiency when transporting non-ATM traffic. Searching for a way to answer to this situation, ITU-T decided to introduce the General Encapsulation Method (GEM) as a method which encapsulates data over GPON. Although any type of data can be encapsulated, actual types depend on service situation. With this method, a broader range of traffic types, namely the TDM and Ethernet traffic, could be transmitted with higher efficiencies and more features [10].

Some specifications of GPON system will now be presented.

1.2.1 Wavelength plan

As far as this subject is concerned, ITU-T had defined telecommunication wavelength bands, as shown in figure 1.6. Figure 1.6 shows the wavelength bands for upstream, downstream and radio frequency (RF) services [16]. Figure 1.6 is used just to identify the wavelength bands. The ITU-T defined three operating windows. The first window is between 800 and 900 nm, the second window is around 1310 nm and the third around 1550 nm.

GPON followed the ITU-T definition related to wavelength allocation and its spectrum plan is presented in figure 1.7.

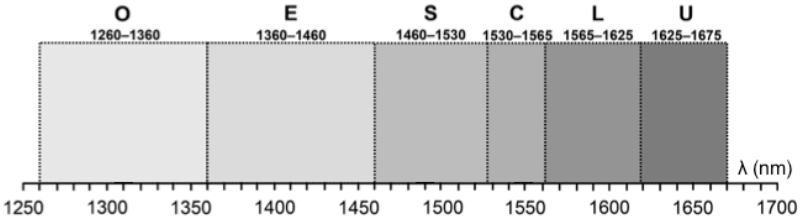

Figure 1.6 – ITU-T telecommunication wavelength bands, adapted from [16]

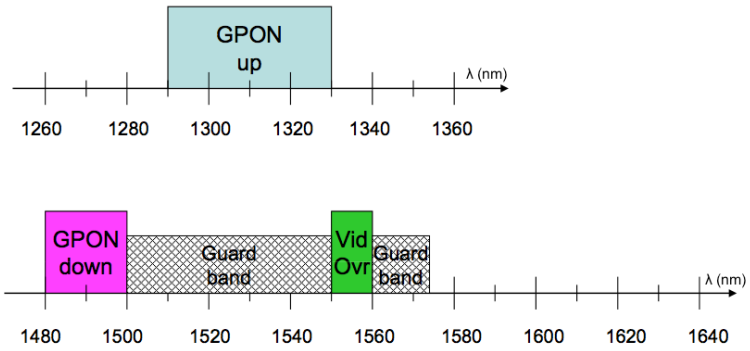

Figure 1.7 – GPON spectrum plan, adapted from [9]

As the figure 1.7 shows, the operating wavelength range established for GPON, was between the 1480 and 1500 nm, around the third window wavelength band, for the downstream direction and among 1290 and 1330 nm, throughout the second window wavelength band, for upstream direction. In addition, the wavelength range between 1550 and 1560 nm, also in the third window wavelength band, can be used for downstream RF video distribution.

1.2.2 Split ratio, reach and line rates

The active transmission equipment in GPON consists of OLT and ONU working over logical network architecture with different FFTX solutions shown in figure 1.1. Starting at the central office, only one single-mode optical fibre strand runs to a passive optical power splitter near users locations [10]. As shown in figure 1.3, the splitting device simply divides the optical power into a number (N) of separate paths to subscribers' home or businesses. The maximum split factor was increased to 128 but the 64 split factor is more likely to be used, due to power budget. The range covered by this PON is 20 km [10].

After different considerations for the line transmission rates for downstream and upstream direction, GPON was stated to work with data rates up to 2.488Gbit/s, in an asymmetrical manner, 2.488Gbit/s in the downstream and 1.244Gbit/s in the upstream, or in a symmetrical manner, in which both directions work at 2.488Gbit/s [16]. However, the major PONs deployment in the field uses only the asymmetric implementation due to costs reduction at ONU/ONT side. The 10 Gbit/s upstream system was still considered as a high cost system with limited application scenarios in the near future [16].

1.3 Motivation

Many studies have shown that there is an ever growing demand for higher bandwidth which historically has increased 6 to 10 times every 6 years [17], and that this trend will continue. After the standardization and approval of the GPON, It is clear from looking at open literature [17] and vendor forecasts that there are many speed drivers and new services being developed that will require a continuous growth in the bandwidth available to deliver content to the end user. The NG-PON, as an evolution of the GPON, tries to respond to this increasing requirement of the bandwidth. This dissertation focus on a 10 Gbit/s downstream signal and so the NG-PON was considered because it specifies the downstream direction bit rate as 10 Gbit/s.

The standard of the Ten-Gigabit-Capable Passive Optical Network (XG-PON), which is a solution of the NG-PON, was approved in 2012. This standard served as a motivation factor for this work because it provided vital information for the work to be developed in this dissertation. Addressing these network specifications was very interesting because it is a current question in the scientific community.

Considering the transmitters to be used in the XG-PON, EAMs are one type of optical modulators that can be used at the optical transmitter. Another type of external modulators are the Mach-Zehnder modulators (MZMs). However, MZMs present significant issues when employed in FTTH networks, namely, the big size and the difficulty of integration with the laser source. Contrarily, the EAMs can be developed quite small and they are easily integrated with the laser source, being a cost-effective solution to be employed in optical access networks. One critical challenge of using EAMs as optical transmitter in FTTH networks is the mitigation of the degradation induced by the fibre dispersion and EAM chirp on the double sideband optical signals [5]. This dissertation focuses on the experimental characterization of an EAM and on its application to enable the provisioning of 10 Gbit/s peak data-rate in the downstream of a FTTH network prototype developed in the laboratory. The experimental demonstration of this new XG-PON approved standard was a huge motivation of this dissertation.

1.4 Structure of the dissertation

The purpose of this work is to study and describe the sub-systems of the XG-PON network. It is also the purpose of this work to study and present a theoretical and experimental characterization of an electro-absorption modulator. Five chapters compose this report.

In Chapter 2, the next generation PON fundamentals and features are presented. In addition, the basic architecture of a PON evolution, known as NG-PON1 system is described, as well as, the techniques and devices used. The notion of XG-PON1 and XG-PON2 is introduced and a description centered in the physical layer of this next evolutionary step is made. The NG-PON2 system is also presented, as well as a brief migration scenario description and a protocol layer conception. The main components, such as the optical transmitter and receiver of the XG-PON1 are also presented.

In Chapter 3, the EAM characterization is performed. The static and dynamic characterization of the EAM is experimentally measured and presented. In this chapter, a measurement of the chirp and dispersion parameter for the experimental XG-PON1 system is presented.

In Chapter 4, an experimental demonstration is performed in order to measure the performance of a 10 Gbit/s signal in an optic link, which emulates the downstream direction of a XG-PON1 architecture. This performance measurement is realized by an experimental demonstration using different specifications.

In Chapter 5, the final conclusions of this dissertation are presented and proposals for future work on this subject are made.

In Appendix A, additional information and validation of EAM is presented. Additional information on the static and dynamic characteristic of the EAM and the chirp and dispersion parameter is presented. In this appendix, a comparison between experimental results and theoretical model approach to the amplitude response is presented.

In Appendix B, additional information for the experimental demonstration of a 10 Gbit/s signal in downstream transmission employing an EAM is presented. A calculation of the extinction ratio is also performed. Photos of the devices, equipment and experimental setup are presented.

1.5 Main original contributions

In the analysis performed in this work, several original contributions were introduced relative to other studies in the field. In the following, the list of the most important contributions of this work are presented:

- Implementation of a 10 Gbit/s laboratory system employing an EAM
- Performance measurement of the 10 Gbit/s laboratory system employing an EAM,

Chapter 2

PON Evolution

In this chapter, the next generation PON (NG-PON) is described. The two main evolutionary steps of NG-PON are introduced in section 2.1. In subsections of section 2.1, an approach of NG-PON1, NG-PON2 systems and NG-PON2 migration scenarios are presented.

In section 2.2,the specifications of the XG-PON1 physical layer are presented. In subsections of section 2.2 a more detailed analysis on the XG-PON1 physical layer is performed. The wavelength plan, line rates, code, split ratio, reach, loss and power budgets are presented

In section 2.3, the subsystems of NG-PON1 are presented and in its subsections the types NG-PON1 transmitters and receivers are analyzed.

In section 2.4, a brief notion of NG-PON1 protocol layer is made.

2.1 Next Generation PON

Beginning in late 2006, the FSAN group began to consider the system that would follow after GPON [18]. The network's incapacity to respond to future needs of the telecommunications world lead to the idea of an evolution network. This incapacity is explained by the network inability to satisfy major subscriber needs. Over the last few years, it has been a well-known fact that there is a rapidly increasing demand of higher bandwidth that needs to be answered. The appearance of new online services, now taking a more important role in people's lives, can explain the rising bandwidth demand, mainly in the downstream direction.

Initially, the motivation of this work towards GPON evolution was to develop additional specifications and features. This course of action had, as its goal, to improve the applicability of the already deployed network system that would enable a smoother migration to whatever system came afterwards. At the time, this work resulted in the creation of the G.984.5 recommendation that refined the spectrum plan used for GPON and defined a wavelength blocking filter in the network's ONU. The wavelength blocking filters are used when GPON, video and next generation access (NGA) share the same optical distribution network (ODN). This optical filter to prevent an optical receiver from receiving unwanted optical signals with different wavelengths. Hereafter, the way was then clear to more consideration towards the next generation PON (NG-PON) [19].

The ITU-T started to standardize their PON for this next evolutionary step, entitled as 10-GPON, also called Ten-Gigabit-Capable Passive Optical Network XG-PON in late 2009. The XG-PON G.987 recommendation series was published by ITU-T in March of 2010 [20]. The XG-PON G.987 standard series is described by the G.987.1 to G.987.3 recommendations, which define general requirements of XG-PON, physical media dependent (PMD) layer specification and transmission convergence (TC) specification, respectively.

The NG-PON had to fulfill some requirements needed for an efficient and successful migration to this new and evolved network. Among the previously mentioned higher bandwidth demand, NG-PON had to reduce the cost of existing services, serve as backhaul of mobile networks, provide affordable migration conditions, maximum utilization of the already installed fibre plans, flexible upgradeability and use of optimized technology in term of cost, performance and energy savings [6].

In late 2007, with the attention drawn towards defining the new system, a very wide range of architectures were raised as possible candidates, including TDM-PONs, WDM-PON, Code Division Multiple Access (CDMA) PONs. With so many types of systems and different architectures, it was very difficult to compare them in order to reach a fair conclusion [18]. As such, a division was made so as to present the solution in two groups. One group is called NG-PON1 and the other one is nominated as NG-PON2. Both of these groups are explained in the following subsections.

2.1.1 Next Generation PON 1

The evolution of the GPON to the NG-PON was contemplated in two major phases, next generation PON 1 (NG-PON1) and next generation PON 2 (NG-PON2). The most important feature regarding NG-PON1 is the ability to include systems that were able to coexist with the already deployed network used for the GPON. As a consequence, they used the same optical distribution network (ODN). In general, NG-PON1 inherits the multiplexing method, framing and management from the previous GPON and also provides full-service operations via four times higher rate and two times larger split than GPON [16].

There were many goals set out for this evolutionary step, goals to be achieved through this migration. These goals can be described as providing higher bandwidth (bit rates) per ONU, support more end-clients, better performance, reducing the cost of existing services, serving as backhaul of mobile networks (wireless fidelity (WiFi), worldwide interoperability for microwave access (WiMAX) and long term evolution (LTE)), providing the maximum utilization of the already installed fibre plants, [6]. From the previous list of objectives, it can be considered that the two general requirements of NG-PON1 were to provide higher transmission rates than its predecessor (GPON) and the reuse of outside plant. In addition to this fact, it is also expected that this evolutionary phase is able to bring leverage to existing optical deployments. Hence, FSAN and ITU-T specified the NG-PON1 backward compatibility with the legacy GPON deployments to protect the initial GPON investments of operators. Due to this backward compatibility feature, NG-PON1 is considered as a mid-term migration upgrade scenario [21]. With NG-PON1, it is conceivable to upgrade the network while, at same time, the investment made with GPON was protected, and so, it was possible to offer low costs, large capacity, wide coverage and other services [21].

NG-PON1 would be able to support equipment power saving. The reduction of the load during power failures will directly influence the level of durability in a given size battery. To achieve this goal, it is required to lower the use of power at all times, so that consumption of electricity can be reduced to the greatest extent possible.

Another new feature of this next evolution PON are the improvements made to security. The old legacy GPON just assumed that the upstream channel was physically secure, and so, the security covering connection was relatively weak. The NG-PON1 system was required to support the option of strong mutual authentication and use it to protect the integrity of the PON management messages and encryption keys [18].

NG-PON1 was created with two configurations, XG-PON1 and XG-PON2. In XG-PON1, an asymmetric bandwidth approach was considered with 10 Gbit/s in the downstream direction and 2.5 Gbit/s in the upstream link, using a different wavelength in each direction. The XG-PON2 is defined by a symmetric approach of 10 Gbit/s in both downstream and upstream directions [18]. In this dissertation the XG-PON2 option will not be considered because, according to the standard, this option will only be addressed in a later phase, when the technology becomes more mature [20]. Therefore this work will attend to the XG-PON1 option.

2.1.2 Next Generation PON 2

As far as NG-PON2 is concerned, the FSAN/ITU-T community has still not achieved a definite solution for the direction of this network deployment. In the case of XG-PON1, it was clear that it needed to coexist with GPON infrastructure to leverage the existing optical deployments, and therefore, protect the initial investments of operator made for the legacy PON ODN. In this regard, the NG-PON2 was considered as a long-term solution of PON that could be deployed over new ODNs not paying much attention to GPON standards [21]. This meant that NG-PON2 was not constrained by co-existence requirements, although co-existence was not precluded. Various technical solutions were pondered such as higher data rate TDM, DWDM CDM and OFDM. [22]. The NG-PON2 system is still under ongoing study but the topics needing some attention are activation, security, protection switching, dynamic bandwidth allocation and management [16].

In March of 2013 the ITU-T approved the standard recommendation for NG-PON2. The NG-PON2 presented some line rates for the downstream and upstream directions. The downstream and upstream nominal line rates can be defined with at least 40 Gbit/s downstream and at least 10 Gbit/s upstream. The downstream target ceiling capacity is 160 Gbit/s and in upstream is 80 Gbit/s [23]. NG-PON2 must support a fiber reach of at least 40 km [23]. NG-PON2 OLTs must support a split ratio of at least 1:256 [23].

Considering the migration scenarios, there are two major solutions. One is considered as the PON brown field migration scenario. In this case the standard refers to the deployment scenario where a PON system has already been deployed and network operators decide to leverage this existing fibre infrastructure to offer higher bandwidth carrier services, using the NG-PON2 options. Concerning this case, some subscribers on an existing PON system, might require an upgrade to such higher speed tier service. The network operator may therefore choose to move over these subscribers to the NG-PON2 system, while other subscribers remain on the legacy PON. In a slightly different migration scenario, it may be desirable to replace an existing PON with NG-PON2 completely. In this case, it would still be useful to operate both legacy PON and NG-PON2 systems at the same time on the ODN

and update customers one at a time. The timeframe for this type of upgrade is generally much shorter. Considering this scenario, there are some general requirements to be held in mind. One of these requirements is the coexistence between legacy PON and NG-PON2 systems on the same fibre must be supported for the situation where the fibre resource is not necessarily abundant. Another requirement assured the minimal service interruption for the non-upgrade subscribers [23].

The other migration scenario considered to NG-PON2 is the PON green field migration scenario. This scenario predicts the renovation of the access network infrastructure. The renovation is the biggest investment of service providers and may take a long time. When NG-PON2 technology becomes mature, service providers might be interested in using NG-PON2 to replace copper-based infrastructure or to deploy in a brand new development area for the benefit or higher bandwidth and/or higher splitting ratios. PON green filed is related to an area where PON had not ben deployed before. This scenario may help service providers achieve better economics while supporting the same or better bandwidth offer per user as PON. In this scenario, the requirement of coexistence with PON is not necessary. [23]

2.2 Specifications of XG-PON1 Physical Layer

XG-PON1 was considered the next step towards PON evolution. As mentioned earlier, the XG-PON1 has backward compatibility to protect the already deployed GPON. Issues as wavelength plan, split ratio and power budget needed some careful rethought in order to assure a feasible update to the GPON system. The GPON configuration, already presented, was the breaking ground in order to give some consideration to the XG-PON1 physical layer, also commonly referred to PMD. The development of the XG-PON1 PMD was a subject of considerable debate. This development was complex matter. The design of this XG-PON1 PMD would surely have huge impacts on operator-visible features, such as the compatibility with fibre plants or other systems already deployed or exploited [18].

2.2.1 Wavelength plan

The first hot topic was precisely the wavelength plan that was discussed in FSAN by telecommunication and operators venders. Due to the market evolution in optical transceivers, the FSAN chose the 1575 to 1580 nm wavelength band to the downstream direction to, therefore, promote the technology maturity [21]. As presented, the idea of coexistence between XG-PON1 and GPON was a must have feature. This means that both GPON and XG-PON1 must work at the same time. Therefore, the coexistence method had to be chosen. After much consideration the WDM coexistence method would be the one used for both downstream and upstream directions of the system. Therefore, the XG-PON1 would require two wavelengths that needed to be sufficiently separated from other wavelengths to ensure proper functioning.

Considering the downstream direction for the XG-PON1, the G.987.1 recommendation stated that the downstream wavelength is the 6 nm band around 1577 nm. The downstream window has a 6 nm band wide, but it will require cooled laser sources.

With respect to the upstream direction, the wavelength specified by the G987.1 recommendation was between 1260 and 1280 nm [24]. The wavelength used for downstream and upstream directions are presented in figure 2.1.

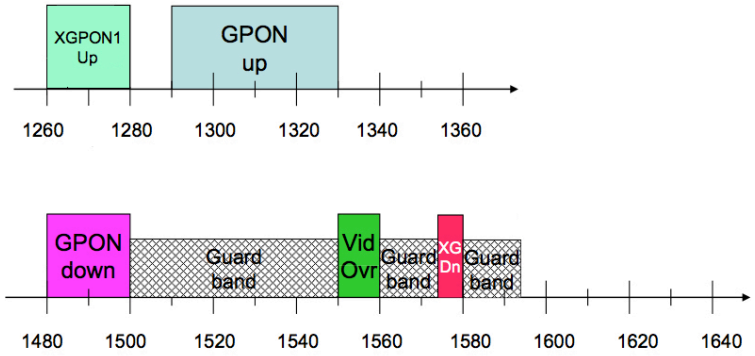

Figure 2.1– XG-PON1 spectrum plan, adapted from [9]

2.2.2 Line rates and code

The next issue in mind in the NG-PON1 is the line rate and code. To meet the ever-increasing demand and support continuous service enhancements, the next logical step of NG-PON1 was to be able to allow individual customers to have shared access to a maximum aggregate line rate of about 10 Gbit/s in the downstream link and 2.5 Gbit/s in the upstream direction, on XG-PON1 system [22].

For the downstream link, two solutions were considered, because they were already standardized for other applications and were commercialized already. The first solution was the 9.95328 Gbit/s synchronous digital hierarchy (SDH) rate, assumed to employ a non-return to zero (NRZ) coding. The second resolution was the 10.3125 Gbit/s Ethernet rate, assumed to use a 64b66b block coding. Given the two solutions, one had to be chosen. Bear in mind that the chosen solution had to be compatible with GPON and video overlay systems. It happens to also coexist with most EPON systems (due to the use of WDM). If the complete coexistence situation was desired, then the choice of line code was directed quite simply to use the Ethernet line rate and code. However, operators made a fateful decision that this kind of intra-generational coexistence would not be needed. It was considered unlikely that an operator would deploy both 10 Gbit/s EPON and XG-PON in the same network. Therefore the downstream link line rate selected was 9.985328 Gbit/s [18].

As for upstream link line rate, three solutions were well thought out. The first one had a line rate of 3.125 Gbit/s, which was about 25% higher than the desired 2.5 Gbit/s. The difference between these two values would be used for line conditioning coding (9b10b) and for forward error correction (FEC). The second solution ran a line rate coding of 2.577 Gbit/s (around one quarter of 10.3123 Gbit/s used for downstream). The third one was a bit rate of 2.488 Gbit/s (approximately one quarter of 9.985328 Gbit/s). Among these three choices, the first one was rejected because vendors believed it was hard to acquire optical equipment to work at that line rate. As conclusion, the selected upstream

link line rate was 2.488 Gbit/s because, after the selection of the downstream link rate as 9.985328 Gbit/s, it was the most logical choice [18]. Also this was the bit rate used in GPON upstream direction.

2.2.3 Filters

In order to assure coexistence between the legacy GPON and the XG-PON1 it was necessary to implement WDM filter, called WDM1r, deployed near the CO. This filter has the function of properly differentiating OLTs and ONUs according to its nature. With this element, the correct communication between OLTs and ONUs of each network system is respectively assured. Hence, the coexistence of the GPON system is assured, as shown in figure 2.2 [21].

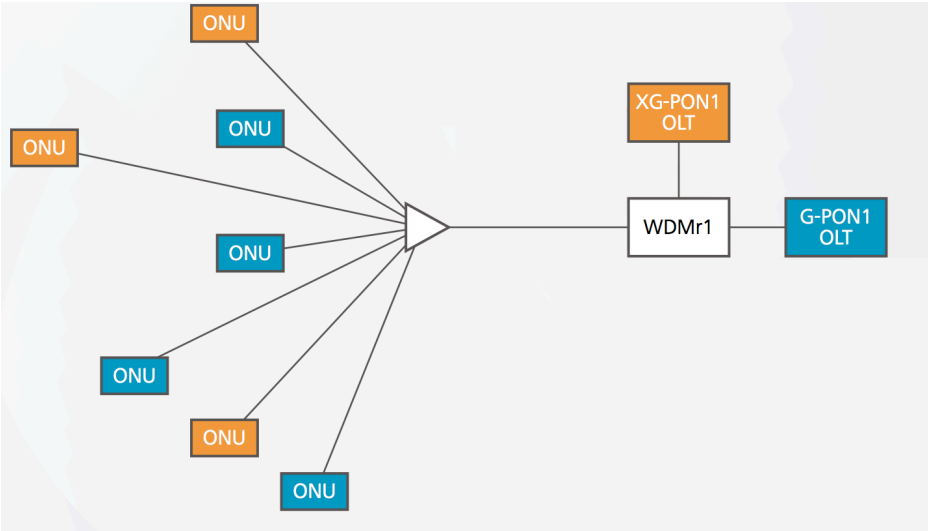

Figure 2.2– GPON and XG-PON1 coexistence, adapted from [21]

As mentioned earlier the downstream and upstream directions for XG-PON1 have different wavelengths and so, a new filter was needed inside the OLT and ONU system in order to assure the correct communication between these two network points. Thus, a WDM filter was deployed at the ONU and at the OLT, to properly distinguish the directions of the communications. This filter assures the correct selection of the direction considered and so, guarantees that the signal reaches its proper destination. This also happen in the GPON.

2.2.4 Split ratio and reach

The GPON ODN architecture was assembled to work with a 1 to 32 or a 1 to 64 split ratio. Therefore, it was reasonable that a 1 to 64 split ratio was the minimum requirement for XG-PON1 to allow coexistence with GPON. Figure 2.3 shows a possible configuration of the splitter deployment for XG-PON1.

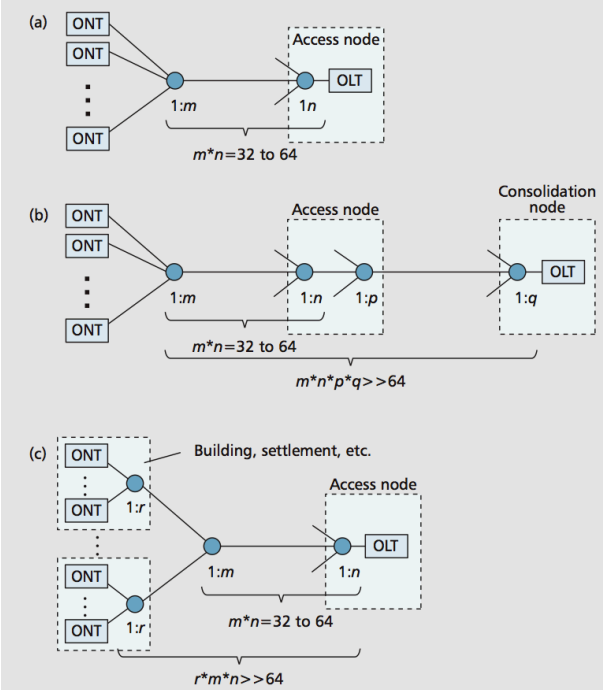

Figure 2.3 – XG-PON1 splitter configuration, extracted from [22]

In figure 2.3 a), a generic GPON splitter deployment is represented. It is easy to understand that a single split configuration with m equal to 64 and n equal 1 there is no need for a splitter at the access node. The ability of extending the split ratio from 64 to 128 or even 256 is a very appealing idea for the migration scenario to XG-PON1. As shown in figure 2.3 b), a higher split ratio is possible to achieve in the backhaul section, in other words, between the end of the core network and the last mile, or towards the end users as illustrated in figure 2.3 c) [22].

With respect to reach, GPON ODN infrastructure was conceived to have a 20 km maximum reach. Bearing in mind the evolutionary step to the XG-PON1, it was reasonable to assume that the minimum requirement reach for this new network would be 20 km. Reminding the idea of figure 2.3 b), extending the PON split on the backhaul side, according to the standard the XG-PON1 should support a maximum fibre distance of 40 km [20].

2.2.5 Loss and power budget

Respectably to the loss budget, the fundamental objective of XG-PON1 was to realize a nominal loss budget, without optical post or pre-amplifiers (i.e., external optical amplification in front of OLT transmitter/receiver), and also an extended loss budget with optical post or pre-amplifiers. With these goals the maximum value for the insertion loss, between the OLT and ONU, for the nominal budget, was specified between 28.5 and 31 dB with a bit error ratio (BER) of 10-12. The maximum insertion loss for extended loss budget was established as 4 dB higher than nominal loss budget. This allowed for an additional split in the ODN with suitable limits or an extent in the supported system reach [22].

Lastly, the loss budget regulates the maximum reach concerning the physical layer and if the reach exceeds the optical loss budget, it is necessary to add a mid-span reach extender (RE) [20].

The goal of using a mid-span RE is to provide additional optical budget with normal OLT and ONU performances, in order to enable, without it being at its maximum, the use of simultaneous full capability of the technology for both distance and split. The use of such REs must not require any change in the OLT and ONU requirements in order to avoid any interoperability issue [20].

The subject of power budget was considered to have a quite direct solution, because it was assumed that the XG-PON1 system shared the same ODN as GPON. Being so, NG-PON already had the specification of 28 dB of loss in between the 1260 to 1360 nm wavelength window and among the 1480 to 1580 wavelength window. Despite this motive, there were still two effects that made the uninterrupted reutilization of the same specifications not possible [18].

The first one was the introduction of a WDM1r filter, as stated in the section 2.2.2. This WDM1r filter was an important addition which makes the interconnection point between the GPON OLT and NG-PON1 OLT to the ODN. Unfortunately, the component had always some loss and was needed to be accounted for. Because GPON system was already deployed, and so, every effort had to be made to build the WDM1r filter, in order to minimize the loss in the GPON path.

The second effect considered was the knowledge of some deviation from the standards by real implementation of PON systems. This took place for commercial reasons because optics were developed having a higher value of loss margin in comparison to the standard requirement. The other reason was the fact that operators designed their ODNs using the 1310 nm value of fibre loss instead of 1260 nm value of fibre loss, as the standard indicated. Therefore this fact created an approximately 0.05 dB/km of differential loss between these two wavelengths. In fact, a PON with 20 km has a 1 dB higher loss at 1260 nm wavelength than at 1310 nm. Operators were keen to avoid the re-engineering of their ODNs for economic reasons [18].

In conclusion to this power budget feature, there was one more topic related to the detector type located in the ONU device. The ONU is considered a very cost sensitive system and like so, it is important to reduce its cost. Generically positive-intrinsic-negative (PIN) photodetectors have a more reduced cost in comparison to the avalanche photo-diode (APD) types. In addition, APD photodetectors are more sensitive than PINs, therefore a less powerful OLT transmitter is required. The standard recommend either type because as the network was being developed it was noted that both photodetectors had their advantages [18]. These photodetector devices are discussed and compared in detail in section 2.3.1 of this dissertation.

2.3 XG-PON1 subsystems

In order to better understand the XG-PON1 system it is important to provide a clarification regarding its subsystems, these subsystems being the optical transmitter and the optical receiver. Figure 2.4 shows the coexistence between the legacy GPON and the XG-PON1. In the same figure it is also possible to see the main elements inside both OLT and ONU systems. Some of these components were already addressed in this dissertation.

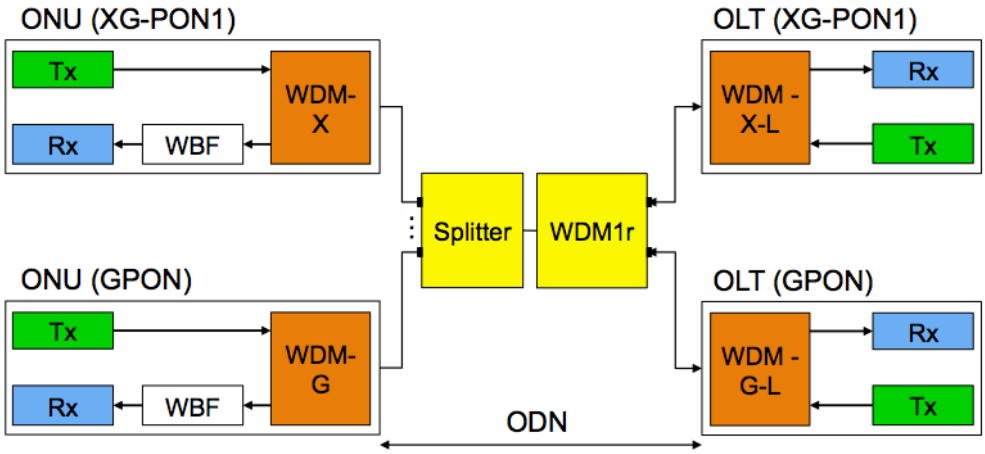

Figure 2.4 – XG-PON1 and GPON coexistence

2.3.1 XG-PON1 optical transmitter

The function of the transmitter element is to convert an electrical data signal into optical form and couple this optical signal into the communication channel. The transmitter typically consists of an optical source and some means of modulating that source either directly or externally, to encode the data onto the transmitted lightwave [25].

The optical source considered for the XG-PON1 was the laser diode (LD). The LD emits light through a stimulated emission process, with an average optical power coupled to the fibre going from 1 to 5 mW [5].

Considering optical modulators, they can either use direct modulation, which uses the optical source component to directly modulate the light, or external modulation, where the modulated data is imposed after the light is out of the LD.

Direct modulation for fibre optic transmitters presented some limitations, such as a high level of penalty due to chromatic dispersion associated with the modulated signal bandwidth and low extinction ratio [5]. This modulation type also presented some limitations to the bit rates greater than 1 Gbit/s and to the bandwidth. Although there has been laser with 20 GHz of bandwidth, but they are extremely expensive [5]. Direct modulation also presented a limitation in an effect designed as chirp. This effect, in telecommunication language, can be seen as a frequency modulation of the electrical field, which follows, in a way, the amplitude modulation of the electrical field [5]. The combination of chirp of dispersion in the optical fibre is a restrictive factor, which is relevant when the data transmission exceeds several Gbit/s in bit rate. The existence of frequency modulation leads to a wider spectrum, meaning, spectral components more apart, which represents propagation delays in the fibre [5].

In order to avoid these transmission limitations imposed by the high chirp values in higher bit rates (above several Gbit/s), external modulation of the optical source is used. Considering external modulation, the optical signal coming from the optical source is applied to the external modulator. This external modulator is affected by the electrical signal coming from the electrical signal generator which cuts-off or lets pass the optical signal. The laser source transmits a constant optical power, meaning

that there is not a variation in the optical frequency, which implicates that the signal generated by the optical source has no chirp. In practice, there has been measured some very small chirp values considering the implementation of external modulation [5]. The block diagram of an optical source with external modulation is presented in figure 2.5

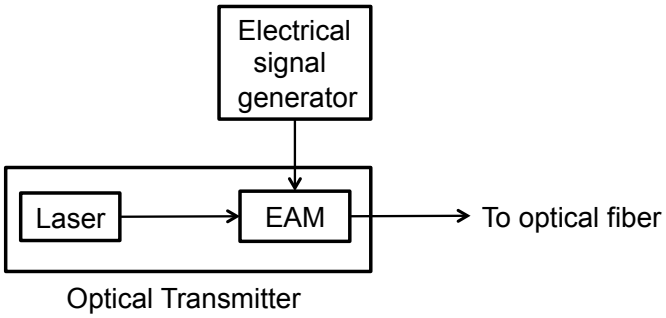

Figure 2.5 – Block diagram of an optical source with external modulation

In essence, modulators can be divided in two categories. The first one is the electro-optic modulator, which relies on the electro-optic effect to modify the actual index of a waveguide and modulates the phase of an optical signal. In other words, it changes the refractive index of a material with a voltage applied across the electrodes. The electro-optic modulator uses the geometry of the Mach-Zehnder interferometer, which currently dominates the market. The Mach-Zehnder modulator (MZM) is able to convert the phase change of the signal into an intensity modulation. Despite the fact that this type of modulator is considered to be satisfactory, there are significant issues considering its deployment in FTTX networks, because of their big size, high cost and the difficulty of integration with the laser source [25].

The other category of modulators is the EAM, which is an external modulator device and it is able to modify the absorption of an optical waveguide to control the intensity of a lightwave passing through it. The EAM is composed of multiple semi-conductor positive-negative layers with multiple quantum wells (MQW). EAM works with the quantum-confined Stark effect (QCSE) to change the gap between layers and increase or diminish photon absorption by the material [3]. It is a well-known fact that this device, placed next to the optical sources, has many potential advantages and this is why it was considered for the XG-PON1 optic communication systems [3]. Among their key advantages are their low size, cost, chirp, and compatibility with monolithic integration.

The semi-conductor material composing the EAM is the same used to create the LD and, due to this fact, it can be built using the same substrate, creating a lower-cost integrated solution than the one of the MZM. In order to execute more multifaceted data modulation functions, EAM can be merged with lasers, semiconductor optical amplifiers and other EAMs [25]. Furthermore, contrary to the issues raised by the MZM, the size of the EAM can be quite small and they are easily integrated with the laser source, being a cost-effective solution to be employed in optical access networks.

Reviewing the overall specifications of the EAM, it was concluded that this device presents the advantages of being cheaper and smaller than the MZM.

Considering a XG-PON1 system, the distances are normally tens of kilometers, which open the possibility of using cheaper transmitters, such as the EAM.

2.3.2 XG-PON1 optical receiver

The optical receiver is responsible for the conversion of optic signals (coming from the optical fibre) to the electric domain. The photodetector converts the optic signal, which contains the coded information, into an electric signal. The photodetectors used in optic systems are photodiodes of semiconductors and so, the photodetectors used are the PIN or the APD.

The main characteristic of the PIN devices is their low internal noise, because they don't present internal gain. This fact influence the optical receivers using PIN to have their performance determined by the circuit noise rather then shot noise [5]. Therefore the PIN receivers present a worst performance than the receivers using APD. An important advantage of the PIN device it is their simpler structure, due to the inexistence of the structure part that supports the avalanche gain. This aspect makes these photodetectors much cheaper than the APD [5].

Considering the APD photodetectors, the existence of the internal gain implies that the performance is given not only by noise from the electrical part but also from the shot noise. In fact, as the shot noise power and the signal power depend on the mean gain of the APD, this can be conveniently designed so that the performance can be optimized [5]. The APD photodetector also presents more disadvantages, such as, more propriety sensitive in temperature variations, less reliability and the demand for higher bias voltages than the PIN to achieve the avalanche gain [5].

Considering the XG-PON1 recommendation G.987.2, there are some considerations regarding the optical receiver considering the downstream of 10 Gbit/s. The use of APD receivers is recommended when the minimum optical power at the receivers input is -28 dBm. If the minimum optical power at the receiver input is -21.5 dBm, a PIN receiver is recommended [7]. Considering the experimental demonstration that is performed in chapter 3 and 4, the photodetector used is the PIN because it was the only one available in the laboratory.

2.4 XG-PON1 Protocol Layer

In this section, a brief description of the XG-PON1 protocol layer is given. Alike the physical layer previously described, the protocol layer would also be based on the GPON system. However, this protocol, unlike GPON, was developed with much more care and was heavily structured in three distinct sublayers [18].

The first one was the physical adaptation sublayer (PAS), which takes care of the unique problems regarding the XG-PON1 physical layer. PAS also handles low level coding of the TC frame over the physical channel. In the physical layer, the feature of FEC is used in both communication directions and so much of the PAS work concerns FEC [18].

The second one was the framing sublayer (FS), which does the main work of TC, meaning, the control of the PON TDMA system, including activation and normal operation phases, as well as house keeping functions [18].

The third distinct sublayer was the client adaptation layer (CAS), which worked to carry user signals over the XG-PON1 system. This sublayer takes the user's data packets and formats them for transmission over the PON [18].

2.5 Conclusion

In this chapter, fundamental description of the NG-PON system was given. The XG-PON1 was described along its physical layer specifications. Topics like line rate, power budget and wavelength plan were addressed while describing the XG-PON1 physical layer. A brief notion of XG-PON2 and migration scenario was also given. A description of the XG-PON1 subsystems is made, along the types of transmitters and receivers to be used on this network. Types of modulators were also introduced and analyzed for the XG-PON1 system. Finally, a short description of the XG-PON1 protocol layer was reported.

Chapter 3

Electro-absorption Modulator Characterization

In this chapter, a characterization of the EAM device is performed. Some parameters are also presented, such as the chirp and dispersion parameter. In this chapter, a static and dynamic characterization of the modulator device is performed and presented in section 3.1 and 3.2, respectively. With static characterization of the EAM it is possible to study the optical output power of the modulator and to identify a reverse bias voltage test range in which the EAM presented a certain value for the extinction ratio. With dynamic characteristic of the EAM it is possible to study the amplitude response to a modulated signal. From this characteristic, it is also possible to measure the bandwidth of the EAM.

In section 3.3, a study of the dispersion and chirp parameter measurement when employing an EAM device into the system is realized.

As mentioned before, in the XG-PON1, external modulation was considered. External modulators are a part of the optical transmitter, as stated in section 2.3.1 of chapter 2 [5].

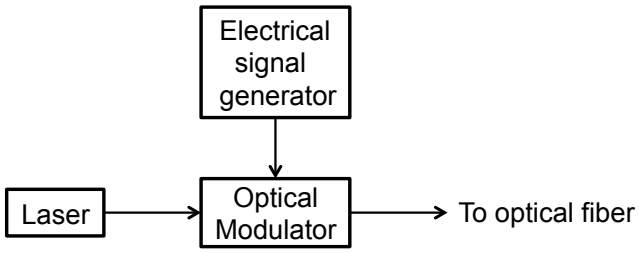

Figure 3.1 – Optical transmitter with external modulation

Figure 3.1 shows the block diagram of an optical transmitter with external modulation. The current applied to the laser is constant, and so, there is no change in carrier density in the active region of the laser and, therefore, there is no variation in the optical frequency of the laser. Consequently, the signal generated by the laser source has no chirp. In practice, external modulation, as presented in figure 3.1, there has been noticed small chirp levels. Considering direct modulation the typical values for the chirp parameter is between 5 and 7. Considering external modulation the values of the chirp parameters are lower or negative. The chirp parameter values considering external modulation can go between 0 and 2 [5]. Chirp is one of the most important characteristics of intensity modulators and directly modulated laser. For external modulators, it means residual phase modulation as the intensity varies. Chirp causes undesired frequency variation and may induce redundant optical sideband components in the spectrum of modulated light. Chirp effect may not be significant on signal quality in short distance, but the chromatic fiber dispersion can be diminished remarkably by reducing the chirp in long-haul propagation. EAMs are considered to have low-chirp performance [26]. Chirp parameter is defined to present the relation between phase modulation and intensity modulation of external modulators [26]. The positive chirp increases the dispersion effect and the negative chirp

helps to mitigate the dispersion effect [26]. In this experimental demonstration, the values for the chirp parameter generated by the EAM device are measured [25].

Remembering the specifications from chapter 2, the XG-PON1 has a downstream wavelength transmission window between 1575 and 1580 nm and a maximum reach of 40 km.

3.1 Static characterization of the EAM

The modulator used in this dissertation is the EAM available in the laboratory of the Optical Communications Group in IT-Lisboa, located at Instituto Superior Técnico.

The first step in this experimental demonstration is to make an accurate characterization of the EAM. Therefore, this characterization will start by measuring the static characteristic of the external modulator that is going to be used in this work.

The insertion loss of the EAM must be characterized as a function of the operating wavelength. This is obtained by the light emission from a tunable laser source into the EAM and monitoring the optical output power. This optical output power is measured as a function of bias voltage for several different wavelengths across the operating range of 1575 and 1580 nm, as indicated for the downstream direction [25]. With this measurement, it is possible to see the dependence of the optical output power to be applied to the optical fibre on the bias voltage applied to the EAM.

The setup for this measurement is shown in figure 3.2. The laser source emits an optical power between 0 and 7 dBm and the wavelengths used in this characterization were 1575, 1577 and 1579 nm. A direct current (DC) voltage signal is applied to the EAM and the output power is measured with the power meter. The bias voltage is between 0 and 4 V. The bias voltage was reversed at the DC source in order to present the output power results with a positive signal. This measurement is important to witness the impact that the EAM has on the optical power coming from the laser source.

The EAM used in the laboratory has a resistance. This resistance is used to control the temperature of the EAM through a DC power supply. This DC power supply, connected to the EAM resistance, is also linked to a multimeter to monitor the value of the resistance in the EAM, and so it is possible to control the temperature of the modulator.

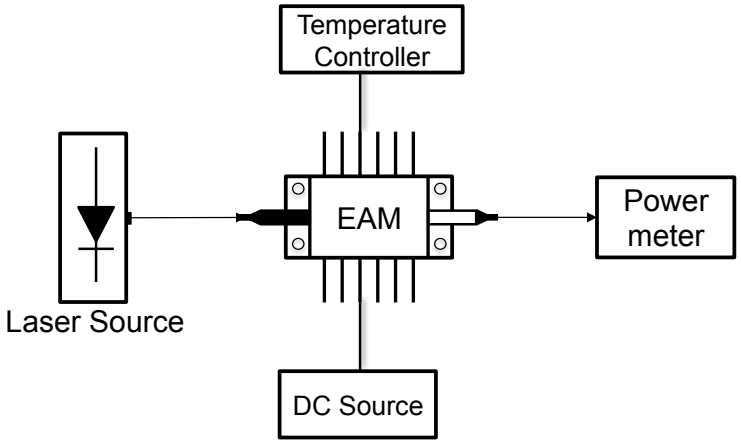

Figure 3.2 – Schematic for static characteristic measurement

The laser source shown in figure 3.2 is a Hewlett Packard, model 8168F tunable laser source. According to the vendor's specification, this laser model has a wavelength range of between 1450 and 1590 nm and a maximum output power of 8 dBm.

The setup shown in figure 3.2 is implemented to the laboratory. Before measuring the static characterization of the EAM, a first measurement is taken to confirm the information given in the vendor's specification of the EAM. The vendor's specification of the static characteristic of the EAM is presented in figure 3.3. The results of the optical power measured with the power meter are presented in dBm units. Therefore, the insertion losses of the EAM are calculated by the difference between the input optical power, coming from the laser source, and the optical output power value measured at the power meter located after the modulator device.

In the laboratory, a measurement was made at an operating wavelength of 1550 nm and 0 dBm of optical power applied to the tunable laser. The insertion loss of the EAM in order to validate the vendor's specification is presented in figure 3.3. Figure 3.3 presents an insertion loss that increases rapidly in slope before passing through an inflection point and finally saturating. As the value of reverse bias voltage increases, the insertion losses increases, or it is the same to say that the output optical power decreases. This means that the absorption is increasing whenever a constant optical input power is applied to the EAM. Figure 3.3 presents the insertion loss and not the optical power at the EAM output. The increasing absorption explains why figure 3.3 presents an increasing curve until reaching an inflection point and then decreasing. Therefore, all other figures for the static characterization of the EAM will present the same behavior.

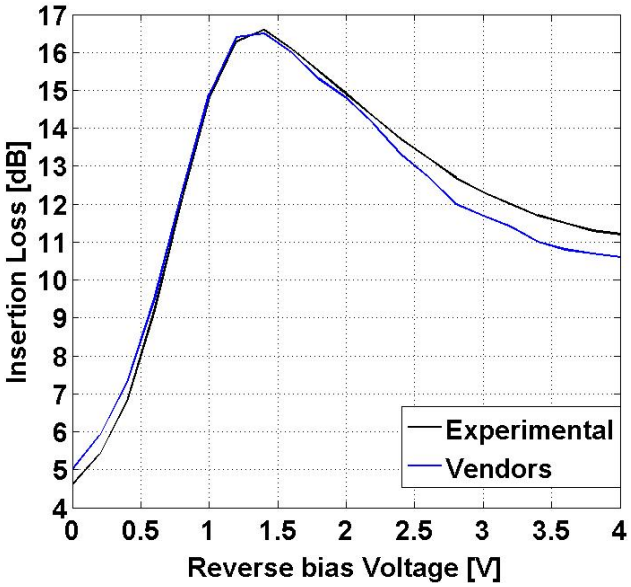

Figure 3.3 – Comparison between the vendor's specification of static characteristic of the EAM in the laboratory and the experimental static characteristic of the EAM at 1550 nm and 0 dBm of laser output power

Comparing the two curves of figure 3.3, it is possible to recognize their similarities. Despite the measurement made in the laboratory has 0 dBm (and not -1 dBm) of optical power at the laser output, the experimental curve presents very few differences to the vendor's information of the static characteristic of the EAM. It is possible to say, considering this measurement that the EAM available in the laboratory matches with the vendor's specification. The vendor specification of the EAM was only discovered later in the development of this dissertation. Therefore, the experimental

measurement of the static characteristic considering 1550 nm was not able to repeat for the laser output power of -1 dBm because the experimental setup could not be set again.

In order to mitigate the temperature effect on the modulator used for this dissertation, there were two measurements made using different voltage values for the EAM resistance. These different voltage values means that each measurement was made with a distinctive temperature. A lower voltage in DC power supply increases the temperature of the EAM device, and so, the modulator becomes hotter. To study the temperature effect on the output power of the EAM, it was considered a random wavelength value from the operating wavelength between 1575 and 1580 nm. The wavelength used in this study was 1577 nm. However, no difference was found in any other of the downstream wavelengths considered for this dissertation. The result of the measurement performed, in order to observe the temperature effect in the EAM, is presented in figure 3.4.

One measurement was realized with a temperature of approximately 19ºC and the other measurement was performed with nearly 30ºC. Figure 3.4 shows the result of this measurement.

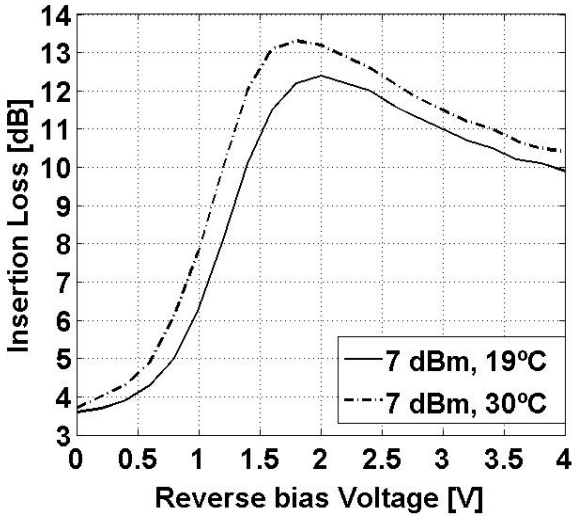

Figure 3.4 – Static characteristic of the EAM operating in two different temperatures

From figure 3.4 it is possible to see that, at different temperatures, the EAM has slightly different static characteristics. Figure 3.4 shows also that the maximum difference value between the two temperatures measured is approximately 1 dB seen around the reverse bias voltage of 1.5 V.

In order to maintain coherence in the all experimental measurements performed, the EAM was set to a temperature of approximately 19ºC.

The laser source was tuned to transmit at an operating wavelength value of 1575 nm. Regarding the optical power to be launched from the laser source, there are four output power levels used. The laser output power levels are 1, 3, 5 and 7 dBm.

The static characterization of the EAM considering the operating wavelength of 1575 nm is presented in figure 3.5. To acquire the information presented in figure 3.5 the laser source was tuned to transmit with the operating wavelength of 1575 nm. The output power of the laser source was set to 1, 3, 5 and 7 dBm. The laser source transmits the signal into the modulator device. The optic signal is then measured using the optical power meter located at the output of the EAM. Each reverse bias voltage corresponds to an optical output power value. Performing a sweep of all the reverse bias values produces the information presented in figure 3.5.

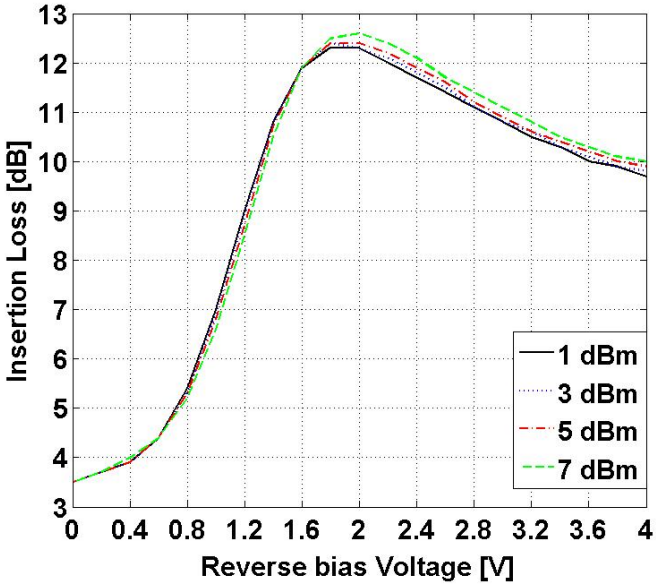

Figure 3.5 – Static characteristic of the EAM with 1575 nm of operating wavelength and four levels of optical power

Figure 3.5 shows the static characteristic of the modulator when operating with 1575 nm for several values of optical power. From figure 3.5, it is possible to see that there is not much of difference among the different laser output power levels. However, the output power of 7 dBm presents the higher insertion loss.

From inspection of figure 3.5, the insertion loss of the modulator operating at a wavelength of 1575 nm is between 3.5 and 12.5 dB, approximately. From figure 3.5, it is possible to see that the inflection point is around the bias voltage of 2 V and the saturation value for the insertion loss is approximately 9.5 dB.

The objective of the static characterization of the EAM is to measure the optical power at the EAM output. From these optical power levels it is possible to calculate the extinction ratio of the EAM. The extinction ratio is a parameter that presents relevance to this dissertation. The ITU-T recommendation for the XG-PON1 PMD presents the minimum value of the extinction ratio. As it was defined in the ITU-T G.957 standard, the extinction ratio results from the division of two optical power levels. In the case of this work, all optical power results are in dB units and, therefore, the extinction ratio results from the subtraction of the two optical power levels [5]. According to the ITU-T G.987.2 recommendation, the minimum value of extinction ratio is 8.2 dB [24]. Therefore this minimum extinction ratio value will be considered for this experimental demonstration. In order to achieve this extinction ratio value a bias voltage test range was considered. This test range is between 0 and 2 V. The reverse bias voltages between 2 and 4 V were not considered because the minimum extinction ratio value could not be achieved with these reverse bias voltages. The extinction ratio will be addressed in more detail in section 4.2 of chapter 4.

The static characterization of the EAM considering the operating wavelength of 1577 nm is presented in figure 3.6. The laser source used the optical power levels of 1, 3, 5 and 7 dBm.

Figure 3.6, shows the static characteristic of the EAM considering the operating wavelength of 1577 nm. By inspection of the figure 3.6, it is possible to see that insertion loss of the EAM for the

different power levels is very similar. However, the optical power of 7 dBm presents the higher value of insertion loss.

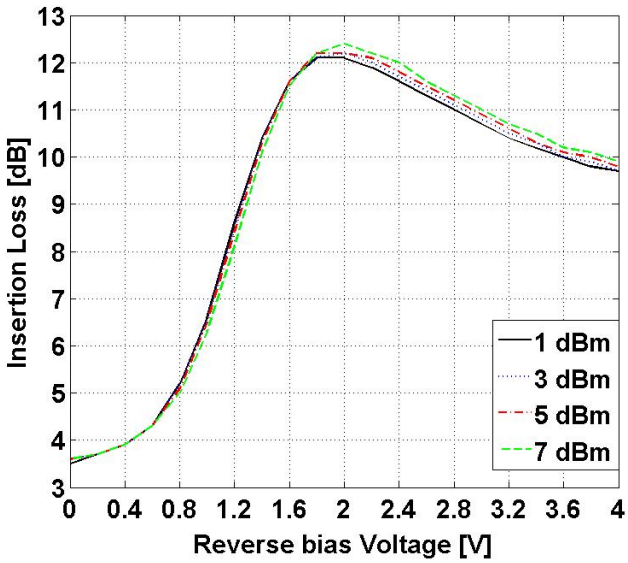

Figure 3.6 –Static characteristic of the EAM with 1577 nm of operating wavelength and four levels of optical power

The insertion loss of the modulator operating at a wavelength of 1577 nm is between 3.5 and 12.5 dB, approximately. From figure 3.6, it is possible to see that the inflection point is around the bias voltage of 2 V and the saturation value for the insertion loss is approximately 9.5 dB.

The static characterization of the EAM considering the operating wavelength of 1579 nm is presented in figure 3.8. For this operating wavelength the maximum output power of the laser source is 6.5 dBm. Therefore, the laser output power levels used for this experiment were 1, 3, 5 and 6.5 dBm.

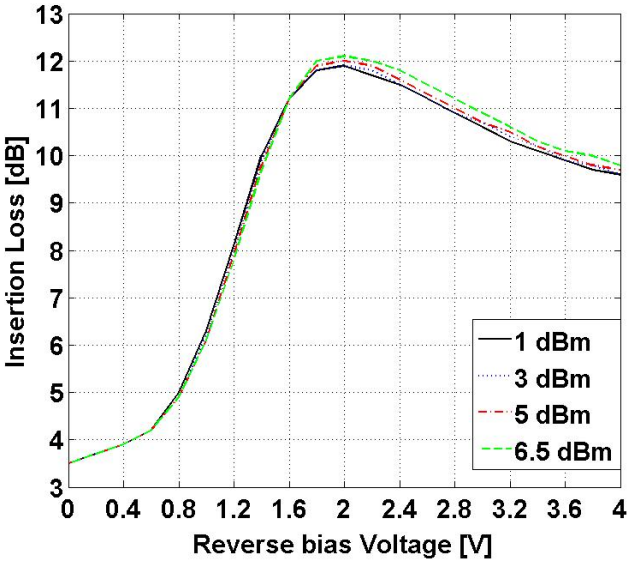

Figure 3.7 –Static characteristic of the EAM with 1579 nm of operating wavelength and four levels of optical power

Figure 3.7, shows the static characteristic of the EAM considering the operating wavelength of 1579 nm. By inspection of the figure 3.7, it is possible to see that insertion loss of the EAM for the

different power levels is very similar. However, the optical power of 6.5 dBm presents the higher value of insertion loss.

The insertion loss of the modulator operating at a wavelength of 1579 nm is between 3.5 and 12 dB, approximately. From figure 3.7, it is possible to see that the inflection point is around the bias voltage of 2 V and the saturation value for the insertion loss is approximately 9.5 dB.

Despite finishing all the measurements for the operating wavelength window determined for the downstream connection for the XG-PON1 (from 1575 to 1580 nm), another measurement was made for the 1581 nm wavelength to study the behavior of the EAM. The result of this measurement is presented in figure A.3, in section A.1 of Appendix A.

This last experiment finished the study and experimental measurement of the static characteristic of the EAM. With this study, it was possible to conclude that, for the wavelengths and the laser output power levels used the EAM presented similar behaviors.

It is now possible to present all the information obtained from the laboratory. The table A.1, in section A1 of Appendix A, presents all the values of optical power measured at the output of the EAM. These output power levels are important to obtain the extinction ratio.

In the section 3.2, a study of the dynamic characteristic of the optical modulator will be presented.

3.2 Dynamic characterization of the EAM

In this section a study dynamic characterization of the EAM is presented. A fundamental requirement of an EAM in a transmission system is that it has sufficient modulation bandwidth to allow the transmission and reception of the intended information. The bandwidth for an EAM is typically measured using a lightwave component analyzer or a vector network analyzer with a calibrated detector because these instruments are capable of measuring both the magnitude and the phase of the frequency response. However, in this experimental demonstration only the magnate of the EAM frequency response was measured [25].

A lightwave component analyzer is used to measure the small signal linear transmission and reflection characteristics of a device as a function of frequency. It operates by injecting a modulated signal into a test device and comparing the modulated input signal to the signal that is transmitted or reflected by the test device. For measuring an EAM a swept frequency RF source is applied to the device through the reverse bias test range found in section 3.1 [25].

The reverse bias enables a DC source to be applied to the device to control the operating point about which the RF voltage will swing. Light coupled through the device is modulated by this RF signal. The light is converted back into an electrical signal in a reference receiver, where it is compared to the initial modulation signal.

The dynamic characteristic of the EAM will be measured in the laboratory using a vector signal generator to generate the RF signal and an electric spectrum analyzer (ESA) to measure the EAM output signal

For this experimental study, it is necessary to rearrange the setup used for the static characteristic measurement used in section 3.1. The setup is presented in figure 3.8.

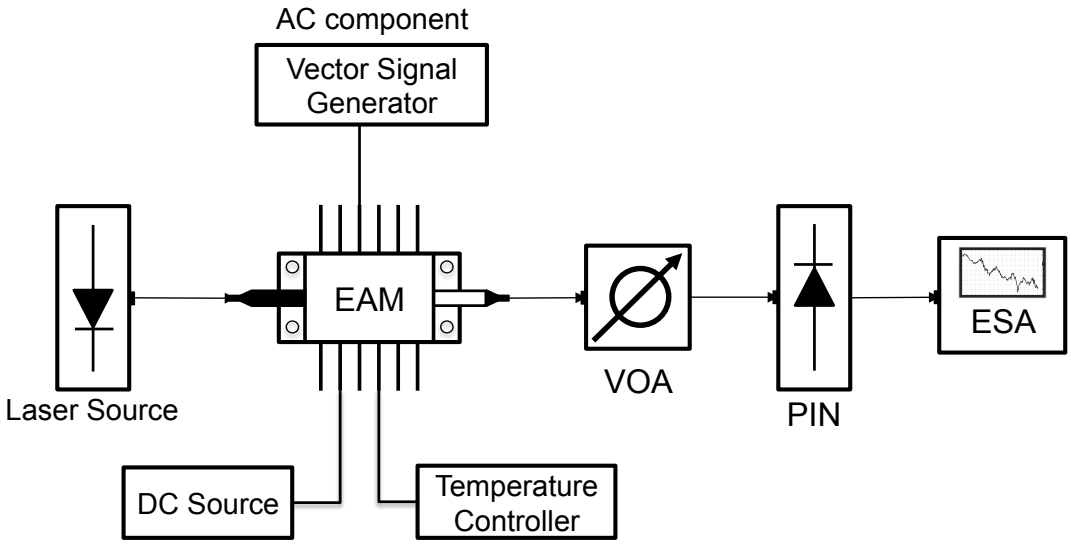

Figure 3.8 – Schematic for the dynamic characteristic measurement

In figure 3.8 it is possible to see a vector signal generator that is used to create an electric modulated signal at the EAM input. The vector signal generator used in the laboratory has frequency bandwidth between 250 kHz and 20 GHz and it was calibrated to transmit 170 samples. This sample number was considerable to be reasonable enough for the experimental demonstration.

This electrical signal is transmitted to the EAM. In this initial measurement stage, there is just a PIN after the modulator. The PIN enables the conversion of the optical signal to the electric domain and, therefore, allows the ESA to detect and study the spectrum of the electric signal. This dynamic measurement is important to study the amplitude response of the EAM measure the modulator bandwidth.

The PIN used in this experimental demonstration is a linear and versatile PIN equipped with a transimpedance amplifier (TIA). The PIN model is DSC-R401HG. The vendor's specification for the PIN photodetector indicated a RF bandwidth of 20 GHz, a linear gain to above +3 dBm optical input and a sensitivity of -15 dBm at a bit rate of 10 Gbit/s. For safety reasons the optical power at the PIN input was not above +1 dBm. An optical power value higher than 1 dBm could cause a malfunction to the photodetector. In section 3.1, the EAM output power levels were measured. These output powers are presented in table A.1 of section A.1 of Appendix A.

From inspection of table A.1, in section A.1 of Appendix A, it is possible to identify several optical power levels that exceeds +1dBm. In these identified cases of optical power above +1dBm, the use of a variable optical attenuator (VOA), as figure 3.8 shows, is needed and advised to attenuate the optical power level reaching the PIN input. The use of the VOA will assure that the safety condition of the photodetector is respected.

Before the measurement of the dynamic characteristic of the EAM, it is important to measure the implicit characteristic of the ESA used in this setup did not influence the final results. The ESA has a data of the filter that is implicit to the device. This means that the ESA presents behavior that must be studied. This study is important to assure that this ESA behavior does not influence the EAM

measurements. The behavior of the ESA is measured by a back-to-back setup between the ESA and the vector signal analyzer.

The frequency range used for the vector signal generator in all measurements that were taken was 0 to 17 GHz. Despite the frequency range used in the vector signal generator, the samples around 0 GHz were discarded because the ESA is not able to acquire measurements for frequencies near 0 GHz and so, the sample frequency range used was between approximately 100 kHz and 17 GHz.

The vector signal generator used was calibrated to transmit a modulated wave with the amplitude value of -10 dBm, which is represented by the AC component of the EAM shown in figure 3.8. This amplitude value was found to be enough to make sure that the non-linearity effects of the system do not influenced the measurement. These non-linear effects are cause by the PIN and the EAM that are in setup used for this measurement. There was a concern to use low values for amplitude of the modulated wave at the output of the vector signal generator. This concern was taken into account to make sure that in future setups, with the use of optical fibre, as it can be seen in section 3.3, the non-linear effects of the fibre were not detected. The ESA behavior was measured with the ESA directly connected to vector signal generator. The ESA behavior is presented in figure A.2 of section A.2 of Appendix A.

With this measurement, the ESA behavior is known and it can be subtracted to the measurements results of the EAM. This subtraction will assure that the ESA behavior does not influence the measurements performed to the EAM.

With the amplitude response resulting from back-to-back measurement between the ESA and vector signal generator, a normalization was made. This normalization was made in order to facilitate future data calculation with results obtained experimentally and it is presented in figure A.3 of section A.2 of Appendix A. The normalization used is explained by performing an average of the first fours values initial values measured by the ESA. These initial values will correspond to frequencies 100.7, 201.3, 301.9 and 402.56 kHz. This average will subtract to all the amplitude response measured by the ESA. The result of this subtraction is the internal behavior of the ESA. This data will be subtracted to all the measurements performed by the ESA.

After studying and observing the implicit behavior of the ESA, the setup of figure 3.8 is restored. In this measurement of the dynamic characteristic of the EAM, the reverse bias voltage values used were 0.2, 1.0, 1.2, 1.4 and 1.6 V. These reverse bias voltages were chosen because they are inside the reverse bias test range of the EAM, identified in the static characterization of the modulator, in section 3.1.

The operating wavelengths used in the measurement were 1575, 1577 and 1579 nm. The laser output power levels used were 1, 3, 5 and 7 dBm, except for the 1579 nm case, because the maximum optical power level is 6.5 dBm.

The amplitude response for the reverse bias voltage of 0.2 V, an operating wavelength of 1575 nm and the optical power of 1, 3, 5 and 7 dBm is presented in figure 3.9.

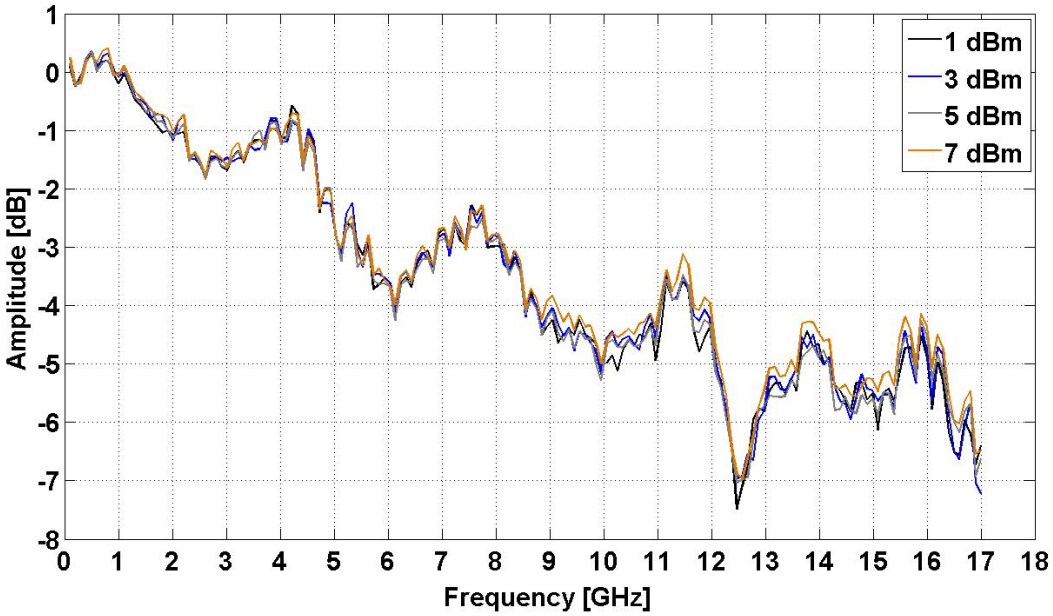

Figure 3.9 – Normalized amplitude response for different laser output power levels, 1575 nm of wavelength, reverse bias voltage of 0.2 V and frequency range of 100 kHz to 17 GHz

From figure 3.9, it can be seen that, the amplitude response in the wavelength of 1575 nm is increasing and becoming more negative. From figure 3.9 it is possible to see that, the amplitude response has two major notorious amplitude dips around frequency 6.1 and 12.5 GHz.

Figure 3.9 shows a normalized amplitude response of the electric power at the EAM output. The amplitude response in dB, $H_{dB}(f)$, is given by $H_{dB}(f)=20\log_{10}[H(f)]$, where H(f) is the amplitude response in linear units. The conversion of power to a dB scale is different from the conversion of voltage to a dB scale in factor of 2. Therefore, the voltage power level of 6 dB corresponds to a conversion of an optical power of 3 dB. Considering this fact, it is possible to state that the bandwidth of the EAM is around 12.3 GHz with an amplitude response of 6 dB.

This result shows that the EAM presented in the vendor's specification is not the same that is used in the laboratory, but it is very similar. The EAM of the vendor's specification has a bandwidth of 13.7 GHz.

The same measurement was performed for the operating wavelengths of 1577 and 1579 nm. The amplitude response of these wavelengths presented the same behavior and so, they are presented in section A.2 of Appendix A, in figures A.3 and A.4.

In addition to these last experiments, an additional measurement was made for the operating wavelength of 1581 nm. The amplitude response for this wavelength presents the same behavior for the wavelengths of 1575, 1577 and 1579 nm. The operating wavelength of 1581 nm has maximum optical power level for the optical source of 6.3 dBm. The measurement of is presented in figure A.5 in section A.2 of Appendix A.

All measurements performed for the reverse bias voltages of 1.0, 1.2, 1.4 and 1.6 V presented similar behavior, and so, they are presented in section A.2 of Appendix A.

This measurement of the dynamic characteristic of the modulator concluded that, for the different levels of optical power used, the dynamic characteristic of the EAM device presented reasonably similar results. Therefore, it is indifferent to use any laser output power level between 1 dBm and the maximum power value because they all present similar. The operating wavelengths used also presented the similar results.

Section 3.3 will present the study the chirp and dispersion parameter through experimental measurement performed in the laboratory.

3.3 Dispersion and chirp parameter measurement

In this section, the behavior of the EAM is studied and measured. Through this study, the fibre dispersion and the chirp parameters of the EAM employed in the laboratory are measured.

In the development of this dissertation, a measurement of these characteristics is performed. These measurements will give more information in order to properly identify the suitable values for reverse bias voltage that, applied to the EAM, will lead to a better performance.

The procedure that allows precise measuring of the chirp parameter (α) for an EAM device, can also measure the fibre dispersion [26]. This procedure can be described as a technique that uses a small-signal measure in the frequency domain to analyze the chirp features for the light propagation in the fibre transmission channel. The method is based on the fact that frequency chirp interacts with dispersion thereby limiting the link distance, which appears as frequency dips during detection. Considering the previous facts, Koyoma and Iga stated that these sharp resonance frequencies are originated from interferences between carrier and sideband wavelengths. Performing a more careful analysis of the frequencies at which those frequency dips occurred, it is possible to obtain precise and reproducible values for the chirp parameter of the transmitting source [25].

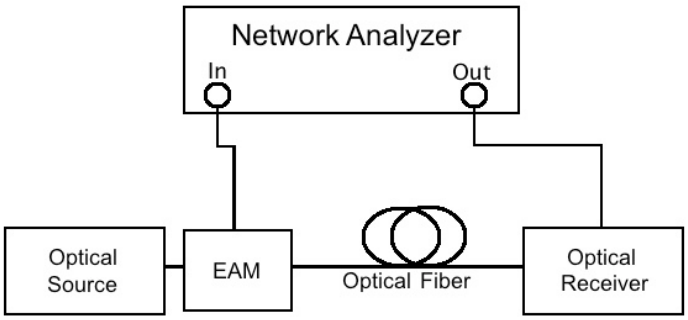

Figure 3.10 –Setup for measuring the amplitude response

The measurement is performed using a network analyzer with a calibrated optical receiver, the EAM to be measured, and a length of single mode optical fibre with a nonzero dispersion. The setup for this measurement is presented in figure 3.10. The length of fibre required depends on the dispersion of the fibre and the maximum frequency of the measuring system [25].

The chirp and dispersion parameters can be measured using the setup shown in figure 3.10. The optical fibre is placed, because in the absence of a dispersive device, the frequency or phase modulation that is found at the modulator's output is not detected.

The first step of this chirp parameter measurement is calibrating the amplitude response of the modulator and the photodetector. The calibration is realized by removing the optical fibre, meaning a back-to-back setup. The obtained result is to be used as a reference baseline. Subsequently, the optical fibre is then introduced and the measurement method is repeated. The amplitude response for the transmission through the dispersive fibre shows, as mentioned, a number of resonances, which appear as dips in the amplitude response [25].

With the implementation of the setup proposed in figure 3.10 in the laboratory, and adopting a more practical level of the setup, the corresponding schematic for measuring the dispersion parameter is presented in figure 3.11.

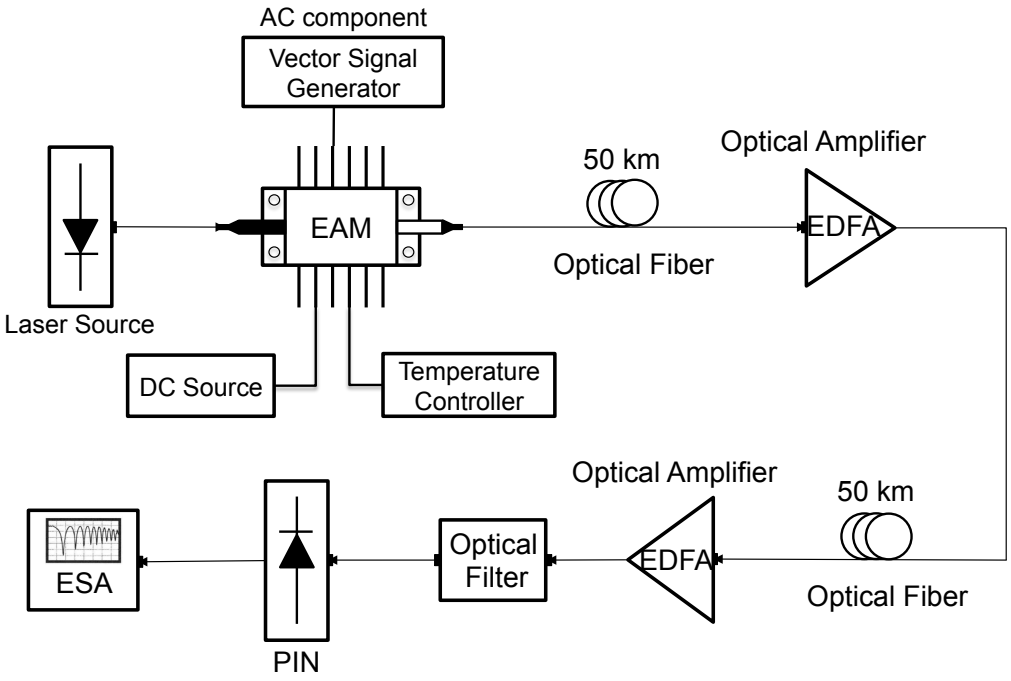

Figure 3.11 – Setup for the measurement of the dispersion parameter used in the laboratory

Figure 3.11 presents a detailed setup of all the components necessary to successfully measure the dispersion parameter. The optical signal is generated from the laser source and modulated by the EAM. The EAM has DC and an AC component, which can be controlled as presented in sections 3.1 and 3.2. The optical signal is then launched into an optical fibre with 50 km of length. At the end of the optical fibre, it is used an optical amplifier to amplify the optical signal coming from the fibre.

The optical amplifier used in this experimental demonstration is a JDSU multiple application platform controller. Two pre-amplifiers were used from the JDSU equipment. The two pre-amplifiers are characterized, by the vendor's specification with a saturation power 14 dBm and a noise figure of less 3.3 dB. Both amplifiers operate with wavelengths between 1528 to 1565 nm. These erbium doped fibre amplifiers (EDFA) are not suitable to work with the operating wavelength between 1575 and 1580 nm. All amplifiers in the laboratory work with the same operating wavelengths between 1528 to 1565 nm. This fact explains why the output powers of the EDFAs used in the laboratory are not the saturated power indicated by the vendor's specification.

The amplified output signal is then launched in another section of optical fibre with 50 km of length, as it is shown in figure 3.11. At the end of the second section of optical fibre, another optical

amplifier is used to amplify the optical signal coming from the fibre. This amplified optical signal is launched into a tunable optical filter in order to filter the noise generated from the amplification. The optical filter is located after the second section of optical fibre, because, there were few optical filters available in the laboratory. Using the filter after the second amplifier limits the optical noise resulting from both amplifiers. The optical filter used in this experimental demonstration is a Yenista Optics XTM-50 model and has a bandwidth of approximately 0.6 nm, meaning around 75 GHz.

The setup in figure 3.11 implemented in the laboratory has an optical fibre length of approximately 100 km. The type of all the optical fibre cables used in the laboratory is single mode fibre.

Figure 3.11 shows that, after the optical filter, the signal is launched into a PIN photodetector. This PIN device converts the optical signal at its input into an electrical one. This electric signal is then measured by the ESA, already presented section 3.2.

As it was presented in section 3.2, a measurement was performed to quantity the optical power level located at the PIN input. This measurement is realized, in order to verify the specification for the optical power level at the PIN's input already presented in section 3.2. The optical power levels reaching the photodiode are presented in table A.2, in section A.3 in Appendix A.

The losses of the optical fibres were measured in the laboratory using one random power level and measuring the power levels at each end of the optical fibre. The first section of optical fibre has approximately 10 dB of loss and the second one has a nearly 12.3 dB of loss.

The losses of the optical filter were also quantified by measuring the input-output power level. The tunable optical filter has approximately 4.3 dB of losses.

The setup shown in figure 3.11 was implemented in the laboratory. As it was concluded in section 3.2, it was experimentally verified that exists a similarity between the different operating wavelengths and laser output power levels. Therefore, the operating wavelengths used for this measurement were 1575 and 1579 nm. For the optical power level, the laser source was tuned for 3 and 7 dBm for the wavelength of 1575 nm and tuned for 3 and 6.5 dBm for the wavelength of 1579 nm.

The amplitude value for the modulated wave used for the AC component coming from the vector signal generator was -10 dBm for the bias voltage of 0.2, 0.4, 0.6, 0.8, 1.0, 1.2 and 1.4 V, except for the bias voltage of 1.6 V, which was -14 dBm. These amplitudes for the modulated signal of the AC component were carefully chosen through multiple measurements. This was done in order to not affect the measurements with the non-linear effects of the optical fibre.

The electric field can be represent by

$$E = \sqrt{I}\, e^{j\phi(I)} \tag{3}$$

and assume that the transmitted intensity is given by

$$I = I_0(1+m\ cos(2\,\pi\, f\, t)) \tag{4}$$

where f is the modulation frequency of light intensity, I_0 is the current and m the modulation depth, being less than 1 [25].

Through several calculations, an equation for the amplitude response was found [26]

$$I_f = I_0 m\sqrt{1+\alpha^2}\left|\cos\left(\frac{\pi\lambda^2 DLf^2}{c} + \arctan(\alpha)\right)\right| \quad (5)$$

where D is the dispersion parameter, L is the fibre length, c is the speed of light constant and α is the chirp parameter. The dispersion coefficient of the fibre D in equation (5) is commonly expressed in units of ps/(nm·km), its value depending on the wavelength of interest and the type of fibre used. For the fibre type used in the laboratory, which is a standard single-mode fibre, at 1550 nm wavelength, the dispersion coefficient is around +17 ps/(nm·km).

The result of the experimental measurement performed in the laboratory for the reverse bias voltage values of 0.2, 0.4, 0.6, 0.8, 1.0, 1.2, 1.4 and 1.6 V, a wavelength of 1575 nm, a laser output power level of 3 dBm is presented in figure 3.12. The reverse bias voltage values are within the test range identified in section 3.1.

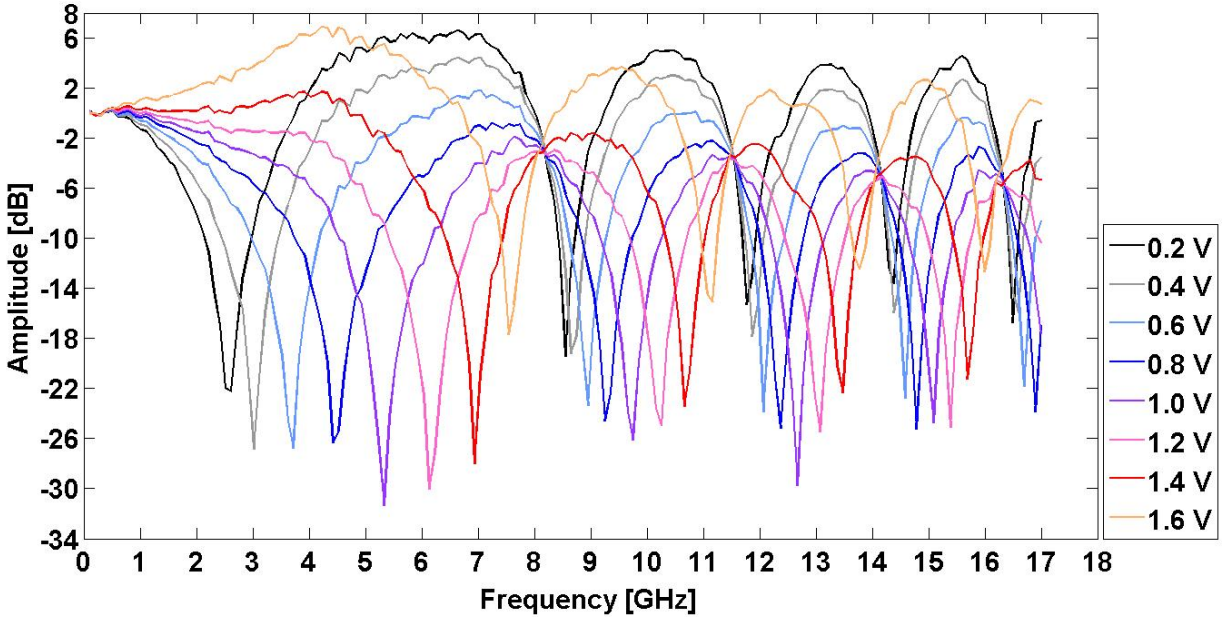

Figure 3.12 – Amplitude response after the photodetection with a fibre of 100 km of length, a wavelength of 1575 nm and a laser output power level of 3 dBm.

In figure 3.12, it can be seen that the frequency dips are well visible through the frequency sweep that was performed from the vector signal generator. Figure 3.12 also shows that the reverse bias voltages of 0.2, 0.4, 0.6 and 0.8 V present five sharp dips while the reverse bias voltages of 1.0, 1.2, 1.4 and 1.6 V only present four.

The amplitude response for the operating wavelength of 1575 nm and the maximum laser output power of 7 dBm shows the same characteristics to figure 3.12, and so, it is presented in figure A.22 of section A.3 of Appendix A. The amplitude response for the operating wavelength of 1579 nm, the minimum optical power of 3 dBm and the maximum of 6.5 dBm is also presented in section A.3 of Appendix A.

The sharp dips in amplitude response, or resonances located at frequencies f_u, correspond to the zeros of equation (5). The frequency sharp dips are calculated by equation (6)

$$f_u^2 L = \frac{c}{2D\lambda^2}\left(1 + 2u - \frac{2}{\pi}\arctan(\alpha)\right) \quad (6)$$

where the parameter 2*u* is twice the order of the resonance. The first sharp dip is the first resonance. The second sharp dip is the second resonance and so on. Plotting the f_u^2L parameter versus parameter 2*u*, it is possible to see a straight line whose slope and y-intercepts position yield the dispersion and the chirp parameter, respectively [26]. In order to confirm the linear behavior between the f_u^2L parameter and two times the resonance order predicted in equation (6), the solution was to create a linear regression over the frequency values of the sharp dips. A linear regression was performed between the f_u^2L parameter and the 2*u* parameter. This linear regression was realized for each reverse bias voltage value and laser output power levels, previously indicated. Figure 3.13 presents the result achieved through a linear regression for a reverse bias voltage of 0.2 V, an operating wavelength of 1575 nm and an optical power of 3 dBm [27].

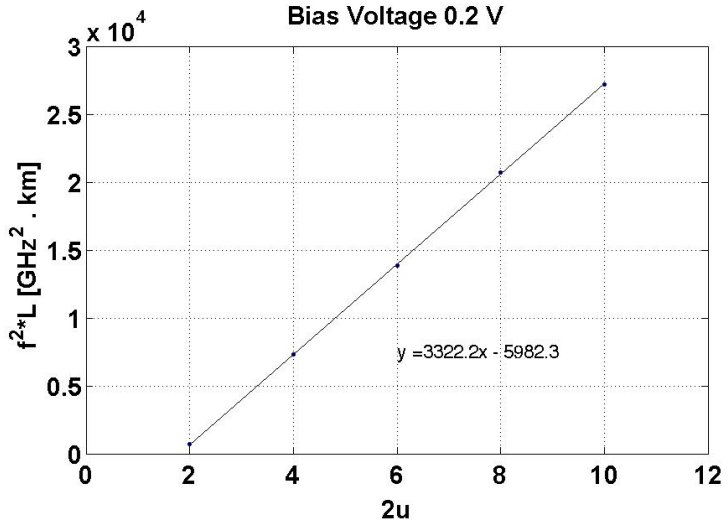

Figure 3.13 – Linear regression realized over the f_u^2L parameter versus two times the order of the resonance for the reverse bias voltage of 0.2 V, a wavelength of 1575 nm and a laser output power level of 3 dBm

Figure 3.13 shows that there is a fairly good agreement of the f_u^2L parameter acquired by the frequency sweep of the vector signal generator available in the laboratory. In figure 3.13, it can be confirmed that the amplitude response obtained in the practical measurement of figure 3.12 presents five sharp dips. This is proved by the five points, which were acquired from the linear regression.

The linear regression between the f_u^2L parameter and the 2u parameter considering the revere bias voltage values of 0.2, 0.4, 0.6, 0.8, 1.0, 1.2, 1.4 and 1.6 V is performed for the two operating wavelengths of 1575 and 1579 nm and the laser output power levels used for both these wavelengths is presented in section A.3 of Appendix A.

The form of the linear regression equation is

$$y = mx + b \tag{7}$$

where *m* is slope of the linear regression from which the dispersion parameter can be obtained, b is the value of the straight line that intersecting the *y* axis from which the chirp parameter can be obtained, *y* is represented by the f_u^2L parameter and *x* is two times the dip order. The dispersion parameter can be found from equation (6) and is given by

$$m = \frac{c}{2D\lambda^2} \Leftrightarrow D = \frac{c}{2m\lambda^2} \tag{8}$$

Exploiting equation (8) for the operating wavelength of λ = 1575 nm and λ = 1579 nm, a fibre length of L = 100 km and a frequency range of 100 kHz to 17 GHz, it was possible to measure the dispersion parameter value for a laser output power level of 3 dBm and a maximum of 7 dBm for 1575 nm or 6.5 dBm for 1579 nm and for all the reverse bias voltage of 0.2, 0.4, 0.6, 0.8, 1.0, 1.2, 1.4 and 1.6 V. Therefore, the resulting values for the dispersion parameter are presented in figure 3.14 and 3.15.

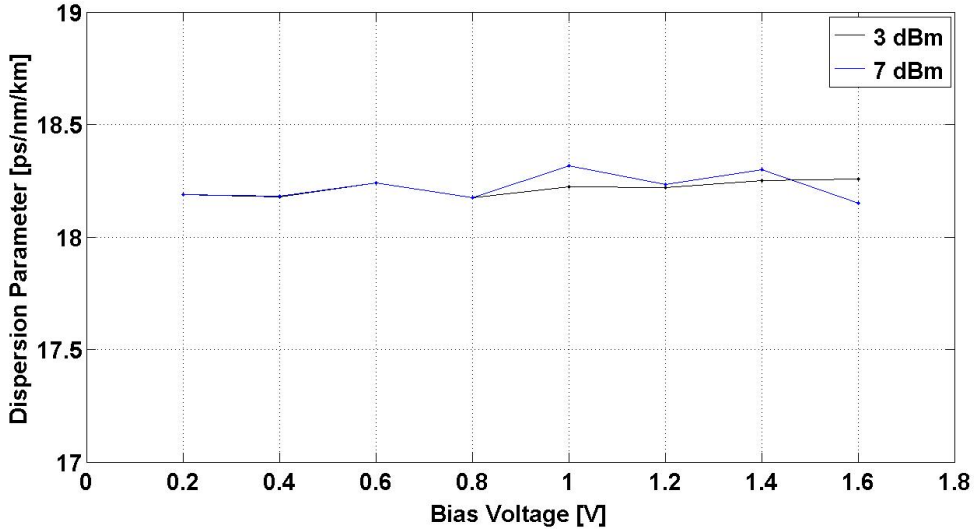

Figure 3.14 – Dispersion parameter for an operating wavelength of 1575 nm, a laser output power level of 3 and 7 dBm, a fibre length of 100 km, a frequency range of 100 kHz to17 GHz and all reverse bias voltage values

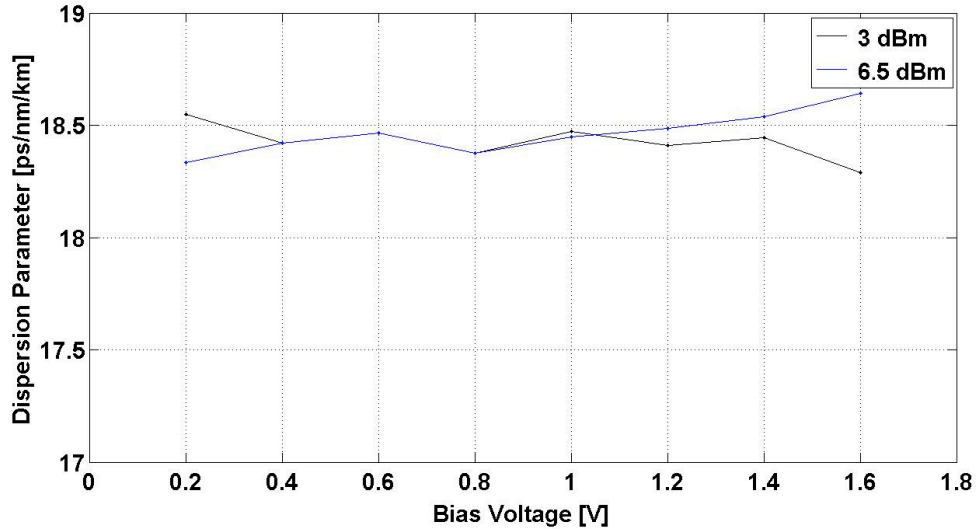

Figure 3.15 – Dispersion parameter for an operating wavelength of 1579 nm, a laser output power level of 3 and 6.5 dBm, a fibre length of 100 km, a frequency range of 100 kHz to17 GHz and all reverse bias voltage values

In a single mode fibre the dispersion parameter is approximately 17 or 18 ps/(nm.km). By inspection of figure 3.14 and 3.15, it is possible to affirm that the experimental measurement presents results that are closer to the dispersion parameter value in single mode fibres. The maximum difference between the different power levels is around 0.2 ps/(nm.km), which can be considered a reasonable fluctuation. These differences can be justified by measurement errors made while performing the experimental measurements.

For the chirp parameter the following equation is used

$$b = \frac{c}{D\lambda^2}\left(\frac{1}{2} - \frac{1}{\pi}arctan(\alpha)\right) \Leftrightarrow \alpha = tan\left[-\left(\frac{bD\lambda^2}{c} - \frac{1}{2}\right)\pi\right] \quad (9)$$

From equation (9) it was possible to calculate the chirp parameter considering an operating wavelength of λ = 1575 nm and λ = 1579 nm, a fibre length of L = 100 km, a frequency range of 100 kHz to 17 GHz, and a laser output power level of 3 dBm and a maximum of 7 dBm for 1575 nm or 6.5 dBm for 1579 nm and for all the reverse bias voltage of 0.2, 0.4, 0.6, 0.8, 1.0, 1.2, 1.4 and 1.6 V. The resulting values for the chirp parameter are presented in figure 3.16 and 3.17.

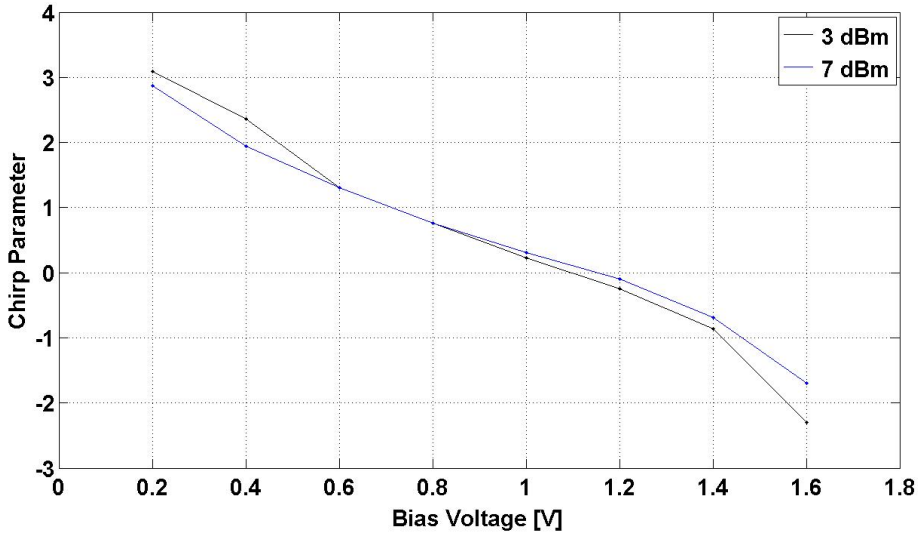

Figure 3.16 – Chirp parameter for an operating wavelength of 1575 nm, a laser output power level of 3 and 7 dBm, a fibre length of 100 km, a frequency range of 100 kHz to17 GHz and all reverse bias voltage values

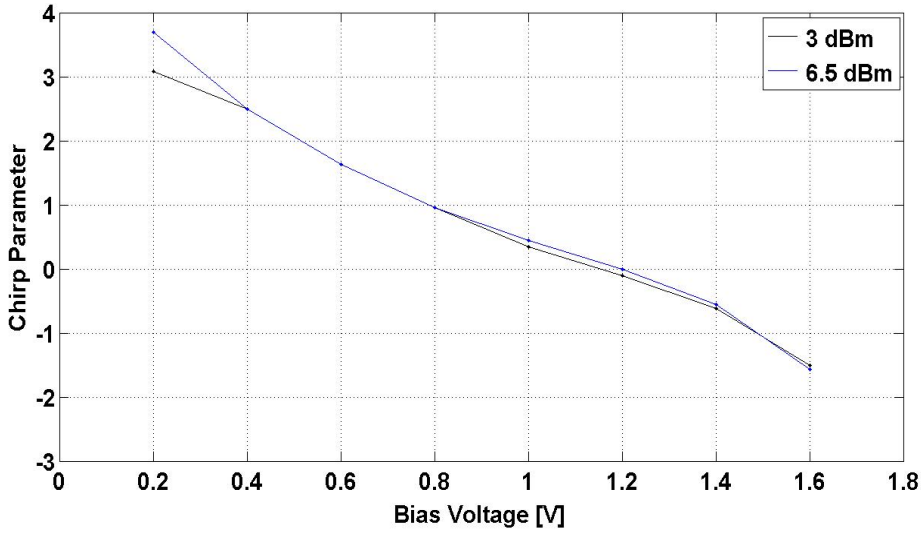

Figure 3.17 – Chirp parameter for an operating wavelength of 1579 nm, a laser output power level of 3 and 6.5 dBm, a fibre length of 100 km, a frequency range of 100 kHz to17 GHz and all reverse bias voltage values

From figure 3.16 and 3.17, it is possible to affirm that the experimental measurement can be assumed as a good approximation. From figure 3.17, it is possible to conclude that, for the reverse bias voltage values identified that presented a resonance peak in the frequency response will correspond to a negative value of chirp.

The few differences between the two laser output power levels used are justified by some measurement errors made while performing the experimental measurements

In order to confirm these experimental results obtained in the laboratory, a theoretical estimation of the dispersion and chirp parameter is made. In this estimation the values of chirp and dispersion parameters are used in equations (5) and (6).

In order to confirm the estimation through the simulation process, an amplitude response was generated through the Microsoft Office Excel tool. This estimation was made to compare with the results obtained in the laboratory. This comparison is presented in section A.4 of Appendix A.

3.4 Conclusion

In this chapter, a characterization of EAM has been presented. In section 3.1, the static characteristic of the EAM device has been performed. The setup to measure this characterization has been presented. The experimental results obtained in the laboratory have been also presented. In this section it has been concluded that for all the operating wavelengths and all laser output power levels used, the EAM presented similar characteristics for the output optical power.

In section 3.2, the study of the dynamic characteristic of the EAM device has been presented. The setup to acquire this characterization and experimental results obtained in the laboratory were presented. It was concluded that, for all the reverse bias voltage values, all the operating wavelengths and all laser output power levels used, the modulator presented similar behavior in its amplitude response.

In section 3.3, the setup and method to experimentally measure the dispersion and chirp parameter has been introduced. Experimental results obtained in the laboratory were presented and properly discussed. The chirp and dispersion parameter have been measured. It has been concluded that the chirp parameter of the EAM is between 3 and -2, approximately. The dispersion parameter has been measured and presented a value around 18 ps/(nm.km), which is a conventional value for single mode fibres.

Chapter 4

Experimental demonstration of a 10 Gbit/s signal in a downstream transmission employing an EAM

After the conclusion of the static and dynamic characterization of the EAM device in chapter 3, it is possible to continue to the next step of this work. In this chapter, an experimental demonstration of a 10 Gbit/s system using the EAM device is performed. This demonstration emulates the XG-PON1 downstream architecture by arranging the laboratory components in order to achieve the setup required for this network. With this setup, measurements are performed in order to evaluate the performance of 10 Gbit/s signals used in this experimental demonstration.

In section 4.1, the setup implemented for this experimental demonstration is presented and described in detail. The setup arrangement is also discussed.

In section 4.2, the extinction ratio scenarios of the EAM are presented and described. For each extinction ratio scenario, the BER parameter is measured. The method used order to measure the performance of a 10 Gbit/s signal transmitted in an optic link, which emulates the downstream direction of a PON. In this section, conclusions about the extinction ratio scenario that presents lower BER results, resulting in a better performance, is also drawn.

In section 4.3, the performance of a signal transmitted in an optic link, which emulates the downstream direction of a PON using FEC is evaluated. This performance evaluation is explained and some experimental measures are performed to support it.

In section 4.4, an additional experimental measurement of the BER is performed without optical cables. This measurement is performed in order to study the dispersion effect of the optical fibre in the performance of the 10 Gbit/s downstream signal.

In section 4.5 a theoretical BER is calculated using the expressions of the literature and some experimental results. This theoretical BER calculation is performed to validate the experimental results obtained in the experiments.

4.1 Experimental setup

The schematic used in section 3.3, presented in chapter 3, is re-arranged in this chapter into the schematic shown in figure 4.1. With this experimental setup it is possible to measure the performance of a 10 Gbit/s signal transmitted in an optic link, which emulates the downstream direction of a XG-PON1 architecture. The system performance is measured by the BER parameter. The BER parameter is a commonly used performance metric which describes the probability of error in terms of number of

erroneous bits received per bit transmitted, and gives a simple one-to-one binary decision as to whether a bit is erroneous or not [28].

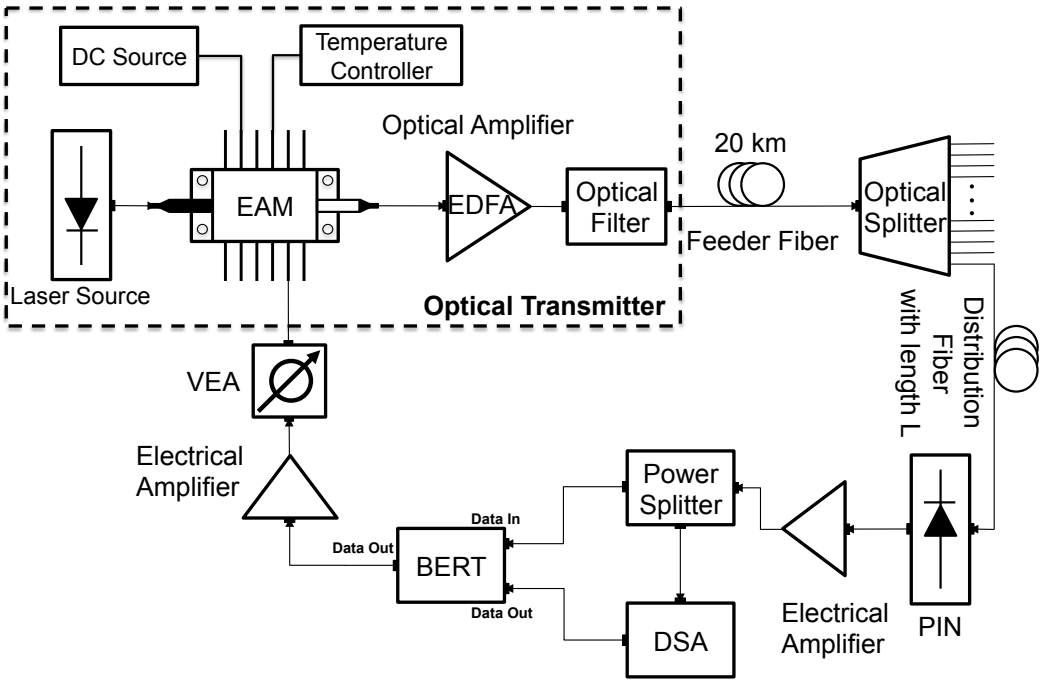

Figure 4.1 – Experimental demonstration setup for measurement of the 10 Gbit/s signals used in the laboratory

By visualization of figure 4.1 it is possible to conclude that, the optical transmitter used in this experimental demonstration is composed by the tunable laser source, the EAM, the optical amplifier and the optical filter.

Some of the components such as the laser source, the EAM device, the optical filter and the PIN used in the experimental setup shown in figure 4.1 were already introduced and analyzed in section 3.1 and section 3.3 in chapter 3.

In section 3.2, in chapter 3, a vector signal generator was applied to the EAM device, which modulates the EAM with a sinusoidal wave. In the schematic presented in figure 4.1, the bit error ratio tester (BERT) generates a voltage, which is applied to the EAM. The BERT device used in the laboratory for this experimental demonstration is an Agilent Technologies N4906B model and it has line rate of a maximum of 12.5 Gbit/s. It is also equipped with a pattern generator and an error detector with several bit rate setups.

The BERT device generates a random sequence of bits that are sent to the modulator with a bit rate of 9.985328 Gbit/s, recommended by the standard of the XG-PON1 [24]. These sequence of bits are carried in a waveform with a certain amplitude level. More details about the random sequence of the BERT are presented in section 4.2. The BERT generates a certain voltage level, and therefore, to control the voltage values described in the presented scenarios for extinction ratio, some electric components were used. After the BERT, an electric amplifier is applied to increase the voltage levels coming from the equipment. This amplifier has a bandwidth between 700 MHz and 18 GHz, a gain of 26 dB and works with DC voltages of +15 V and -15 V. This is a Super Ultra Wideband Amplifier ZVA-183+.

After increasing the voltage level it is was necessary to make sure that an adequate voltage level is applied to the EAM device. Thus, a variable electric attenuator (VEA) is used to control the voltage level. The use of this attenuator will be addressed later in this section.

In the setup of figure 4.1, it can be seen an optical amplifier and an optical filter connected to the EAM device. This is the same optical amplifier and filter that was used in section 3.3 of chapter 4, to measure the dispersion and the chirp parameters.

The optical amplifier used in this experimental demonstration is a Constelex Hydra series 14-20 EDFA. This equipment has two optical amplifiers. Only one optical amplifier was used and it is characterized, by the vendor's specification with an input power of above -10 dBm, a saturation power of 20 dBm, a small signal gain of above 30 dB and a noise figure of less 4 dB with an operating wavelength of 1555 nm. This optical amplifier, used in the experimental demonstration, amplifies the input optical power to the optical power level of around 16 dBm independently to the optical power at the amplifier input. This EDFA is operated in the saturation but is working outside its wavelength range of 1530 to 1565 nm. The output power of 16 and not 20 dBm is explained by this fact.

As stated in section 2.2.3 of chapter 2, the optical reach of the XG-PON1 is comprehended between two fibre distances. These two fibre distances have a maximum value of 20 km and 40 km [24]. The distance of 20 km is the fibre reach for the GPON system. Therefore the distance of 20 km is considered as the minimum distance in this experimental demonstration. The feeder fibre of 20 km introduces a loss value of approximately 5 dB in the optical power.

The new optical components used in this experimental demonstration are the optical splitters. There were two types of optical splitter used in this work, the 1/16 and the 1/2 optical splitter. The 1/16 optical splitter has a loss value of approximately 12.5 dB and the 1/2 optical splitter has a loss value of approximately 3.2 dB. The splitting factors that will be used in this system are the 1/16, 1/32 and 1/64. The splitting factor of 1/32 is obtained by combining an optical splitter of 1/16 and 1/2 and the splitting factor of 1/64 is obtained by combining an optical splitter of 1/16 and two of 1/2.

After the optical splitters a distribution fibre is implemented. The length of this distribution fibre will vary. Sections of 5 km from 0 to 35 km are added along the experimental demonstration. The maximum length for the distribution fibre used in the experimental demonstration is 35 km. The maximum optical fibre length is 55 km (35 km of the distribution fibre plus the 20 km of feeder fiber), which is higher than 40 km, as it was specified for the XG-PON1. The additional length was used to test how far we can go in the laboratory.

Considering the ITU-T G.987.2 recommendation, it is possible to identify the right ODN class based on the mean launched optical power. The minimum and maximum optical power was measured with a power meter at the optical filter output. The minimum optical power measured was approximately 5.4 dBm and the maximum was around 10.1 dBm. These optical power levels are result of using different wavelengths and optical power levels at the laser source. Contemplating these optical powers, the ODN class identified to this experimental demonstration was the 'Nominal2' (N2) class [24].

Remembering the loss values found in the feeder fibre and the optical splitter used in this experimental demonstration, it is possible to identify the class of attenuation range presented in the

ITU-T G.987.2 recommendation [24]. The minimum attenuation range is found by adding the loss value of the feeder fibre to the loss value of the optical splitter of 1/16. The loss value is 17.5 dB. The maximum attenuation value is 23.9 dB, which is given by the feeder fibre and one optical splitter of 1/16 and two optical splitters of 1/2. The path loss class that is defined between the 17.5 and 23.9 dB loss values is the N2 class, which has an attenuation value between 16 and 31 dB.

After the PIN device, another electrical amplifier is used to increase the electrical levels at the PIN output. This electrical amplifier has a bandwidth of between 2.5 kHz and 10 GHz, a gain of 26 dB and it is recommended, by the manufacturer, to work with a DC voltage of +8.25 V and -5.25 V. The electric amplifier is a Picosecond 10 GHz Electric Linear Amplifier model 5866.

From figure 4.1, it can be seen that, after the electrical amplifier, an electrical power splitter was placed because the electrical signal had to be connected to the BERT and to the digital serial analyzer (DSA). The amplifier was used to amplify the electric signal at the PIN output. This amplifier is also useful to compensate the losses of the power splitter. The power splitter has a bandwidth of 18 GHz.

The DSA is used to measure the electrical power at the BERT output and the electrical power coming from the PIN device. The DSA allowed the visualization of the eye diagram of the signal at the BERT output and the signal received in at PIN output. The DSA device used in this work is a Tektronix DSA8200 model and it has a bandwidth of 30 GHz, a 40 Gbit/s sampling rate and two electrical modules with 30 GHz of bandwidth each.

After the description of the setup used for the measurement of the performance of 10 Gbit/s signals, it is important to better describe the BERT. The extinction ratio of the EAM is controlled by the signal that is transmitted by the BERT. As stated in section 3.1 of chapter 3 the minimum extinction ratio scenario is 8.2 dB. From the conclusions presented in Appendix B, it is possible to identify two different scenarios regarding the extinction ratio. One scenario uses the maximum extinction of the EAM with a value of 9.1 dB. This value is obtained when considering the reverse bias variation between 0 and 2 V. The maximum extinction ratio scenario is achieved considering the EAM static characterization performed in section 3.1 of chapter 3. The second scenario uses the minimum value of 8.2 dB for the extinction ratio, recommended by the standard, and it is obtained when considering the reverse bias voltage variation between 0.6 and 2 V. The two scenarios are studied in this dissertation.

The attenuation value of the VEA indicates which extinction ratio scenario is applied to the EAM. The scenario of minimum extinction ratio uses an attenuation value of 7 dB and 4 dB for the scenario of maximum of extinction ratio.

Some photographs taken from the setup implemented in the laboratory are presented in section B.2 of Appendix B.

Finally, with all the components of the setup of figure 4.1 explained, it is possible to move on into the experimental demonstration realized in the laboratory.

4.2 Experimental measurement of BER with a 10 Gbit/s system in a downstream transmission

The operational wavelengths used in this experimental demonstration, as introduced in chapter 3, are 1575 and 1579 nm, and the optical power at the laser source output is 7 dBm for 1575 nm and 6.5 dBm for 1579 nm. The laboratory demonstration was initiated with the minimum extinction ratio scenario and the operating wavelength of 1575 nm.

The starting point of the experimental demonstration, after bringing the components all together, was the inspection the experimental waveform at the BERT output. Figure 4.2 shows the waveform of the 10 Gbit/s signal, represented by the eye diagram, at the output of the BERT.

All graphical waveforms are generated by the DSA device and the visualization setup of the analyzer is the same for every waveform taken and presented in this work, except the vertical scale, which had to change for some cases due to adequate visualization purposes. The horizontal scale of the DSA is 20 ps per division and it is represented in figure 4.2.

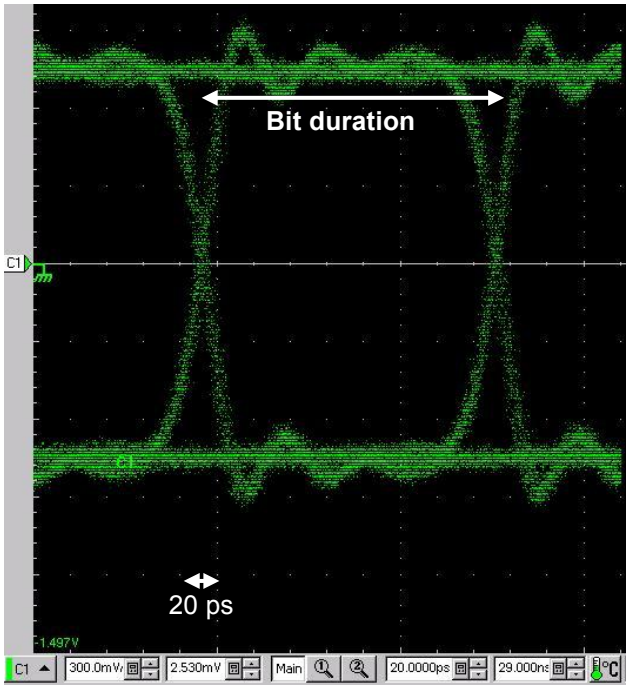

Figure 4.2 – Waveform of the 10 Gbit/s signal at the output of the BERT

Ideally, the waveform shown in figure 4.2 would be a rectangle. The fluctuations of the waveform are explained by the frequency limitations of the BERT. This same frequency limitation is also visible on the transitions between the “0” and the “1” bit and vice-versa.

This system has a bit rate of 9.985328 Gbit/s. This bit rate corresponds to a bit duration of approximately 100 ps. From figure 4.2, it is possible to see that, the bit duration has approximately 100 ps. Figure 4.2 shows also that the distortion has little influence in the amplitude of the waveform. This fact can be explained because the eye aperture is clearly opened.

The BER measurement performed in this experimental demonstration considering the two extinction ratio scenarios is presented in subsection 4.2.1 and 4.2.2, respectively.

4.2.1 BER measurement considering a minimum extinction ratio scenario

In this subsection a BER measurement is performed to the 10 Gbit/s system considering a minimum extinction ratio scenario of 8.2 dB, as it was stated in section 3.1 of chapter 3.

The BERT generates a –A to A voltage. This means that the device does not present a 0 to A voltage level, and so, some basic calculations had to be made in order to establish the adequate voltage value for the working scenarios.

As explained in section 3.1 of chapter 3, the extinction ratio is calculated by a subtraction of two optical powers in dB units. The minimum extinction ratio scenario of 8.2 dB is calculated considered the reverse bias voltage of 2 and 0.6 V. The subtraction of the two optical powers at the EAM output for these reverse bias voltages is 8.2 dB. The voltage variation needed of these two reverse bias voltages is 1.4 V. The voltage applied to the EAM device must be 1.4 V, and to achieve and control the electrical value at the EAM input, the VEA is placed between the electrical amplifier and the EAM. Considering that the BERT has a –A to A voltage, the middle point of the voltage variation of 1.4 V is 0.7 V. Therefore, the DC source must be tuned to the value of 1.3 V (0.7 plus 0.6 V of the reverse bias voltage), because it is the middle value for the reverse bias variation of 0.6 and 2 V. The VEA was set to an attenuation value of 7 dB in order to achieve the desired electric voltage values.

The waveform of the 10 Gbit/s signal reaching the EAM device is presented in figure 4.3. In figure 4.3, it is possible to view the waveform at the input of the EAM device and the waveform at the output of the BERT device.

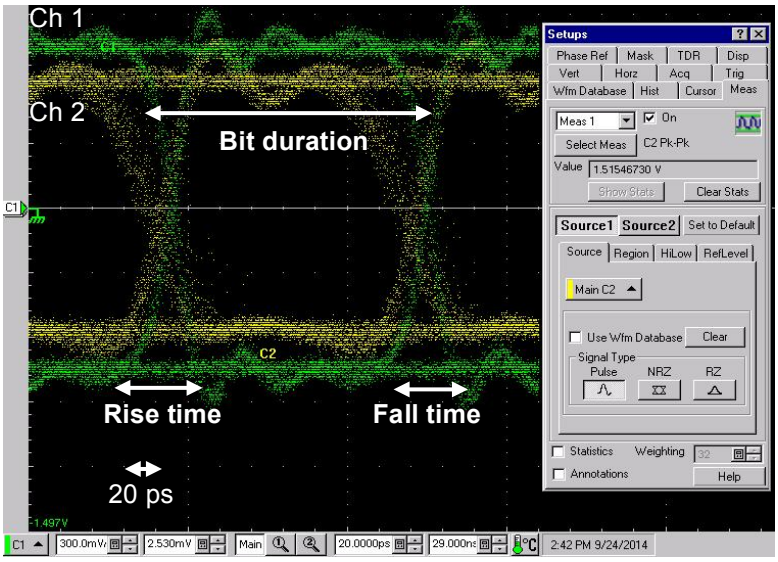

Figure 4.3 – Waveform of the 10 Gbit/s signal at the output of the BERT and the waveform received at the EAM input considering the minimum extinction ratio scenario

In figure 4.3, the waveform of the 10 Gbit/s signal at the output of the BERT is represented by channel 1 and in the green color. This waveform remains the same through all the experimental demonstration. The waveform of the 10 Gbit/s signal reaching the EAM input is represented by channel 2 and it is showed as the yellow waveform. In figure 4.3, it is possible to visualize the setup dialogue of the DSA. This information indicates the voltage that is applied to the EAM input. With the use of the VEA with 7 dB of attenuation, the actual peak-to-peak amplitude value measured at the

EAM input is around 1.5 V. This value can be explained by the lack of flexibility in the VEA. The VEA can only add or subtract a minimum of 1 dB of attenuation. This means that, with a higher loss value of 8 dB, the waveform generated by the BERT would have a voltage value below 1.3 V at the EAM input. This fact would lead to an extinction ratio of 8.1 dB, which did not represent a minimum extinction ratio scenario. In figure 4.3 it can be seen that, the electric amplifier introduces very little noise to the signal. This noise can be seen by the little amplitude distortion in waveform of channel 2.

The green waveform shown in figure 4.3 is the same in figure 4.2. Comparing the two waveforms of figure 4.3, it is possible to see that there is a significant attenuation in the waveform that is reaching the EAM input. This attenuation effect is visible by the closure of the eye pattern in the yellow waveform. The distortion is cause by the VEA placed before the EAM. From figure 4.3, it is possible to see that the bit duration is still approximately 100 ps. The rise time is a measure of the mean transition time of the data on the upward slope of an eye diagram. The fall time is measure of the mean transition time of the data on the downward of an eye diagram. These measurements are typically made at the 20 and 80 percent or 10 and 90% levels of the slope. The rise and fall time are approximately 30 ps.

After configuring the DC source and the peak-to-peak amplitude of the BERT output 10 Gbit/s signal considering the minimum extinction ratio scenario, it is possible to proceed to the first BER measurement. In order to see the dispersion effect of the optical fibre, the feeder fibre of 20 km is removed and an attenuator is placed. As it was stated in section 4.1, the loss value of the feeder fibre is approximately 5 dB. This value is placed in the attenuator and the waveform at the PIN output is presented in figure 4.4.

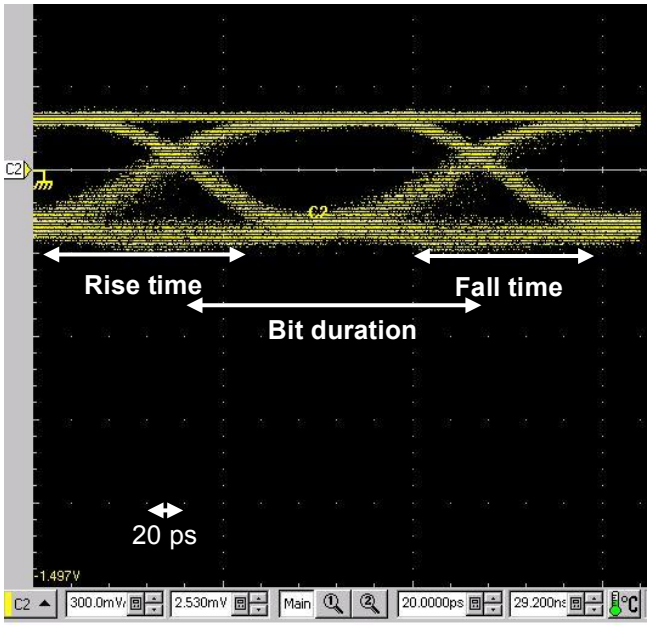

Figure 4.4 – Waveform of the 10 Gbit/s signal at the PIN output for 1575 nm of wavelength, considering the minimum extinction ratio scenario, 0 km of feeder and distribution fibre, an attenuator with 5 dB of loss and an optical splitter of 1/16.

Comparing figure 4.3 to 4.4, it is possible to observe a major difference in the eye aperture. This eye closing is due to the distortion and noise imposed to the signal. This distortion and noise are imposed by the different network elements, such as, the optical amplifier, the attenuator and the

optical splitter. The optical filter mitigates the noise effect from the amplifier but does not erase it completely. From figure 4.4 it is also possible to see a dispersion effect due to intersymbol interference and the use of the optical amplifier. The dispersion effect caused by the optical amplifier is visible on the bit transitions. The transitions take more time than the ones shown in figure 4.3. The noise is also present in the amplitude of the waveform. The attenuator is removed and the feeder fibre of 20 km is restored. In figure 4.4 it is possible to see that the bit duration is still approximately 100 ps. However the rise time and fall time are longer than the ones shown in figure 4.3. The rise and fall time is around 80 ps.

The measurement of the waveform of the 10 Gbit/s signal at the PIN output was performed with an optical splitter of 1/16 and a starting point of 0 km of feeder and distribution fibre.

The eye diagram of the waveform after the photodetection is presented in figure 4.5.

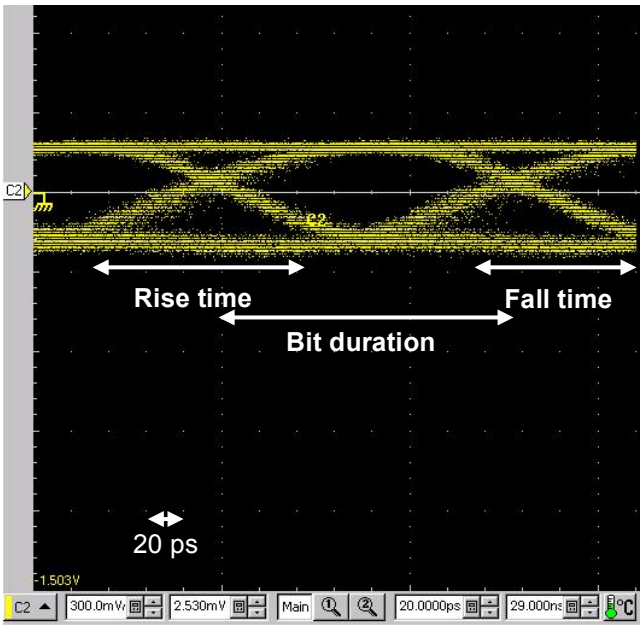

Figure 4.5 – Waveform of the 10 Gbit/s signal at the PIN output for 1575 nm of wavelength, considering the minimum extinction ratio scenario, 0 km of distribution fibre and an optical splitter of 1/16.

Figure 4.5 shows that the eye diagram of this waveform is well defined. It is possible to state that the eye in this diagram is opened. However, the eye aperture is not the same as it is in figure 4.4. The dispersion effect, after placing the optical fibre, is also much more visible in this waveform than in figure 4.4. The bit transitions are even longer with the feeder fibre of 20 km. The rise and fall time is around 90 ps. The bit duration is still around 100 ps but the rise and fall times are longer in comparison with figure 4.4.

This experimental setup configuration results in a BER measurement of lower than 10^{-12}. This information is presented in figure 4.6.

Figure 4.6 presents a snapshot of the BERT when realizing the measurement of this first experimental demonstration. It is possible to see that the BERT indicates a count of 0 errors for a period of around 16 minutes, which represents a bit count of around 10^{13} bits.

In order to support the BER measurements realized, a confidence interval was considered. It is conventionally acceptable in experimental demonstrations that a good BER measurement is obtained

when the number of errors is 100, at least. The bit sequence has the length of 10^{13} bits, which means that a BER measurement of 10^{-11} is considered to be a robust result.

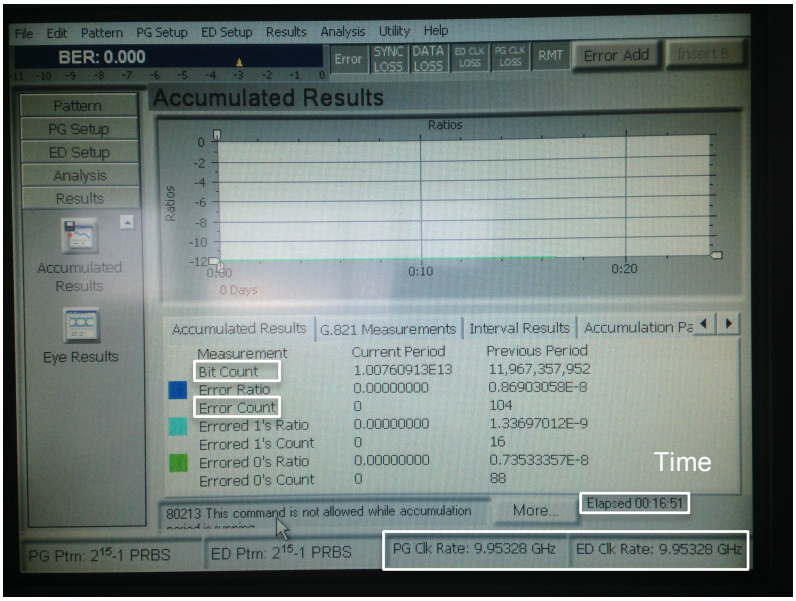

Figure 4.6 – Snapshot of the BERT measurement

The error ratio of 0 means that the BERT cannot measure the actual BER ratio. This happens because the device has a lower limit of 10^{-12}. From figure 4.6, it is also possible to visualize that the pattern generate and error detection clock rates (on the lower right corner of figure 4.6) are 9.95328 GHz, as the ITU-T G.987.1 recommendation indicates [20].

The result of all the waveforms at the PIN output considering a minimum extinction ratio scenario, all splitting factors, an operating wavelength of 1575 nm, and all fibre sections used are presented in figure B.13, B.14 and B.15 of section B.3 of Appendix B.

For the next BER measurements performed the distribution fibre was increased in sections of 5 km, from 0 to 35 km, and the splitting factors applied to the system also increased from 1/16 to 1/32 and 1/64. There is no section of 20 km of distribution fibre because a second span with this fibre length is not available in the IT laboratory.

Table 4.1 presents the results of all the measurements taken, considering the minimum extinction ratio scenario and a wavelength of 1575 nm.

	Fiber Length [km]						
Splitter	**0**	**5**	**10**	**15**	**25**	**30**	**35**
1/16	<-12.0	<-12.0	<-12.0	<-12.0	<-12	-9.6	-4.4
1/32	<-12.0	<-12.0	-10.1	-8.0	-5.9	-4.0	X
1/64	-11.0	-7.3	X	X	X	X	X

Table 4.1 – $\log_{10}$ BER for the experimental demonstration of the 10 Gbit/s signal considering the minimum extinction ratio scenario and with 1575 nm of wavelength

By looking at table 4.1, it is possible to conclude that the measured BER values are increasing when fibre sections are added to the system or when the splitting factor increases. This makes sense because by increasing the distribution fibre and the splitting factor, the optical power level reaching the

PIN decreases. As the optical power at the PIN photodetector decreases the values of BER parameter increases. The symbol 'X', presented on table 4.1, represents the cases in which it was impossible to measure the BER because the BERT has a top limit of 10^{-3} of BER.

The optical power levels, in dBm, at the PIN input are presented in table 4.2.

	Fiber Length [km]						
Splitter	**0**	**5**	**10**	**15**	**25**	**30**	**35**
1/16	-7.5	-8.7	-10.5	-11.3	-12.7	-14.4	-16.1
1/32	-10.6	-11.7	-14.0	-14.6	-15.8	-16.8	-
1/64	-13.7	-14.9	-	-	-	-	-

Table 4.2 – Optical power levels, in dBm, at the PIN input considering the minimum extinction ratio scenario and with 1575 nm of wavelength

When realizing the measurements for table 4.1 and 4.2, it was possible to observe that the PIN device has a limitation (presented in section 3.2 of chapter 3) when the optical power level approaches the value of approximately -15 dBm. Around this value it is extremely difficult to measure the BER because the BERT is constantly losing synchronization. The symbol '-' in table 4.2 represents the cases in which it was impossible to measure the BER with the BERT.

From inspection of tables 4.1 and 4.2, it is possible to say that, the system has a very good performance when using a splitting factor of 1/16 until 25 km of distribution fibre. The more distance, the less optical power it implies, which leads to a higher value of BER. This lower optical power is due to more dispersion caused by the addition of fibre sections. With a splitting factor of 1/32 and a distribution fibre of 10 km, the optical power at the PIN output is around -15 dBm, which begins to increase the BER. This continues to happen until the distribution fibre reaches the 35 km, when it is impossible to measure the BER ratio because it is above 10^{-3}. The same situation occurs with the splitting factor of 1/64 that starts with no distribution fibre with an optical power of approximately -14 dBm, until 10 km of distribution fibre. With a fibre length of above 10 km it is not possible to measure the BER because it is higher than 10^{-3}.

After the measurements performed for the minimum extinction ratio scenario for an operating wavelength of 1575 nm, the operating wavelength was changed to 1579 nm. The laser source was modified to transmit at 1579 nm of wavelength and the optical filter tuned with the wavelength of 1579 nm. The results of this measurement are presented in table 4.3 and 4.4. All the eye patterns for the of the 10 Gbit/s signal measured at the PIN output considering a minimum extinction ratio scenario, all splitting factors, an operating wavelength of 1579 nm, and all fibre sections used are presented in figure B.16, B.17 and B.18 of section B.3 of Appendix B.

Upon inspection of tables 4.3 and 4.4, it is possible to conclude that the BER has a lower performance when operating at 1579 nm, rather than 1575 nm, considering every splitting factor. This fact is explained by the lower optical power reaching the PIN device when operating at 1579 nm. In comparison with the previous case of 1575 nm, the optical power at the PIN input with a splitting factor of 1/16 and no sections of distribution fibre is -9.2 dBm, while with 1575 nm is -7.5 dBm. This difference in optical power between the two operating wavelengths is justified by the two optical powers at the output of the laser source.

	Fiber Length [km]						
Splitter	**0**	**5**	**10**	**15**	**25**	**30**	**35**
1/16	<-12.0	<-12.0	<-12.0	-10.3	-4.8	-3.4	X
1/32	<-12.0	-9.6	-6.1	X	X	X	X
1/64	-6.3	-3.8	X	X	X	X	X

Table 4.3 – $\log_{10}$ BER for the experimental demonstration of the 10 Gbit/s signal considering the minimum extinction ratio scenario and with 1579 nm of wavelength

	Fiber Length [km]						
Splitter	**0**	**5**	**10**	**15**	**25**	**30**	**35**
1/16	-9.2	-10.7	-12.5	-13.5	-15.2	-16.6	-
1/32	-12.5	-13.5	-15.5	-16.8	-	-	-
1/64	-15.5	-16.5	-	-	-	-	-

Table 4.4 – Optical power levels, in dBm, at the PIN input considering the minimum extinction ratio scenario and with 1579 nm of wavelength

As it was mentioned earlier, with the operating wavelength of 1579 nm the output optical power of the laser source is 6.5 dBm. When using this operating wavelength of 1579 nm, the optical power launched to the fibre is lower comparing with the one using the operating wavelength of 1575 nm. As it was stated in section 3.1 of chapter 3, the maximum output power of the laser source with the operating wavelength of 1579 nm is 6.5 dBm. In addition, the optical amplifier is not working within the operating wavelength range of 1530 to 1565 nm, which can explain the lower optical. The optical power launch to the feeder fiber considering an operating wavelength of 1575 nm was 10.1 dBm and 8.2 dBm for the 1579 nm. This fact is important to explain why the optical power at the PIN input is lower than -7.5 dB. The difference between these two scenarios allows explaining the lower performance with this operating wavelength, once there is a relation between the optical power and the BER. This relation is observed and verified throughout the entire experimental demonstration.

After comparison between the BER and optical power tables concerning the two operating wavelengths, it is clear that the wavelength of 1575 nm presents a better and higher performance for the downstream signal. Therefore, the operating wavelength of 1579 nm is discarded from the experimental demonstration.

The best operating wavelength of 1575 nm for this work was identified, thus, in the next section the experimental measurement of the 10 Gbit/s signal continued to the next scenario of extinction ratio.

4.2.2 BER measurement considering a maximum extinction ratio scenario

In this subsection, the BER measurement is performed to the 10 Gbit/s system considering a maximum extinction ratio scenario of 9.1 dB. This is the maximum value of the extinction ratio with EAM considering the modulator output power in the static characterization.

Considering the maximum extinction ratio scenario of 9.1 dB, the voltage variation needed is 2 V. This value is the range of the interval between 0 and 2 V. The subtraction of the two optical powers at the EAM output for these reverse bias voltages is 9.1 dB. The voltage applied to the EAM device must be 2 V, and to achieve and control the electrical value at the EAM input, the VEA is placed between the electrical amplifier and the EAM. Considering that the BERT has a –A to A voltage, the middle point of the voltage variation of 2 V is 1 V. Therefore, the DC source must be tuned to the value of 1 V, because it is the middle value for the reverse bias variation of 1 and 2 V. The VEA was set to an attenuation value of 4 dB in order to achieve the desired electric voltage values.

The waveform of the 10 Gbit/s signal at the BERT output versus the waveform at the EAM input is presented in figure 4.7.

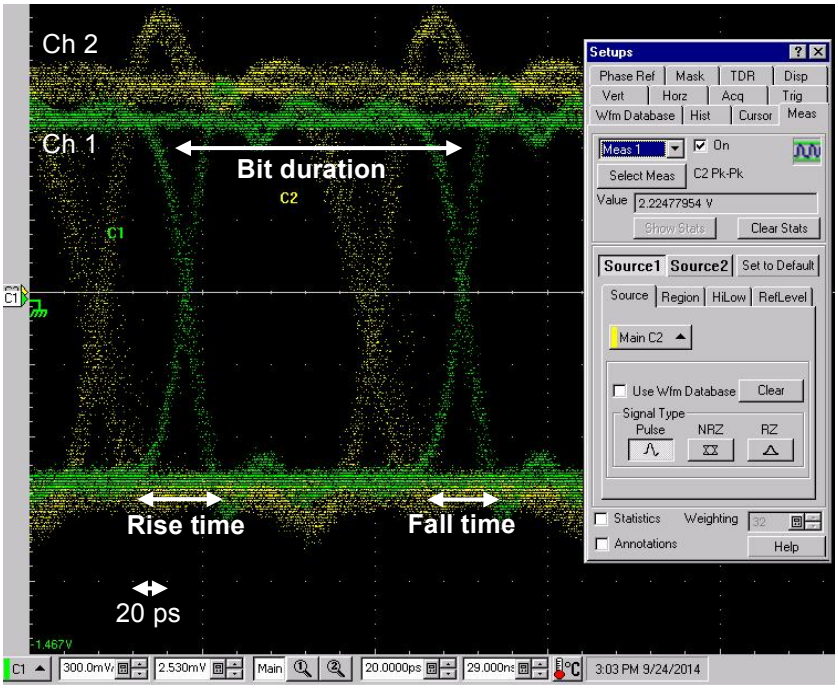

Figure 4.7 – Waveform of the 10 Gbit/s signal at the output of the BERT versus the waveform received at the EAM input considering the maximum extinction ratio scenario

In figure 4.7, the waveform of the 10 Gbit/s signal at the output of the BERT is represented by channel 1 and in the green color. This waveform remains the same through all the experimental demonstration. The waveform of the 10 Gbit/s signal reaching the EAM input is represented by channel 2 and it is showed as the yellow waveform. By inspection of figure 4.7, it is possible to see that the yellow waveform is the result of the amplification of the waveform at the BERT output.

The information in figure 4.7 indicates the voltage that is applied to the EAM input. With the use of the VEA with 4 dB of attenuation, the actual peak-to-peak amplitude value measured at the EAM

input is around 2.2 V. This value can be explained by the lack of flexibility in the VEA. This means that, with a higher loss value of 5 dB, the waveform generated by the BERT would have a voltage value below 2 V at the EAM input. This fact would lead to an extinction ratio of 9 dB, which did not represent the minimum extinction ratio scenario. In figure 4.7 it can be seen that, the electric amplifier introduces little noise to the signal. This noise can be seen by the little amplitude distortion in waveform of channel 2.

The attenuation of the VEA in figure 4.7 is not so visible as it was presented in figure 4.3 because the attenuation value is lower and the resulting waveform has higher amplitude than the waveform in channel 1. The bit duration, the rise and fall time considering this extinction ratio scenario is the same of section 4.2.1. The delay between the two waveforms presented in figure 4.7 is due to an offset that was accidently added.

After configuring the DC source and the peak-to-peak amplitude of the BERT output 10 Gbit/s signal considering the maximum extinction ratio scenario, it is possible to proceed to the BER measurement. The experimental measurement considering the maximum extinction ratio scenario was performed with an optical splitter of 1/16 and a starting point of 20 km of feeder fibre and 0 km of distribution fibre. The eye diagram of the waveform after the photodetection of the PIN photodetector is presented in figure 4.8.

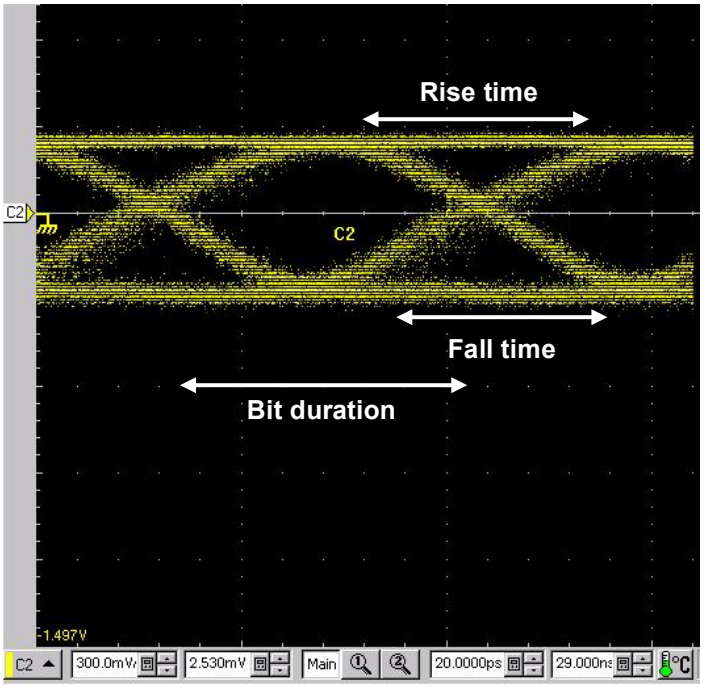

Figure 4.8 – Waveform of the 10 Gbit/s signal at the PIN output for 1575 nm of wavelength, considering the maximum extinction ratio scenario, 20 km of feeder fibre, 0 km of distribution fibre and an optical splitter of 1/16.

Comparing figure 4.8 to 4.7, it is possible to observe the same conclusions the comparison considering the minimum extinction ratio of section 4.2.1. From figure 4.8, it is possible to state that the eye in this diagram is opened. However, the eye aperture is not the same as it is in figure 4.7. The dispersion effect, after placing the optical fibre and the optical amplifier, is much more visible in this waveform than in figure 4.8. The bit transitions are even longer with the feeder fibre of 20 km. The bit duration is still around 100 ps but the rise and fall times are much longer in comparison with figure 4.7.

The result of all the waveforms of the 10 Gbit/s signal at the PIN output considering a maximum extinction ratio scenario, all splitting factors, an operating wavelength of 1575 nm, and all fibre sections used are presented in figure B.19, B.20 and B.21 of section B.3 of Appendix B.

The BER considering the maximum extinction ratio scenario and an operating wavelength of 1575 nm are presented in table 4.5.

	Fiber Length [km]						
Splitter	**0**	**5**	**10**	**15**	**25**	**30**	**35**
1/16	<-12.0	<-12.0	<-12.0	-10.4	-9.3	-7.5	-4.2
1/32	<-12.0	<-12.0	-8.9	-7.1	-5.0	X	X
1/64	-10.1	-6.0	X	X	X	X	X

Table 4.5 – $\log_{10}$BER for the experimental demonstration considering the maximum extinction ratio scenario and with 1575 nm of wavelength

The optical power at the PIN photodetector input is presented in table 4.6.

	Fiber Length [km]						
Splitter	**0**	**5**	**10**	**15**	**25**	**30**	**35**
1/16	-7.0	-8.2	-10.3	-11.2	-12.3	-13.8	-15.9
1/32	-10.2	-11.3	-13.9	-14.7	-15.6	-	-
1/64	-13.3	-14.7	-	-	-	-	-

Table 4.6 – Optical power levels, in dBm, at the PIN input considering the maximum extinction ratio scenario and with 1575 nm of wavelength

By inspection of table 4.5, it is also possible to conclude that the measured BER values are increasing when fibre sections are added to the system or when the splitting factor increases.

From inspection of table 4.5 and 4.6, it is possible to state that the system has a very good performance when using a splitting factor of 1/16 until 15 km of distribution fibre. In this extinction ratio scenario, it is also possible to observe that more distance in the distribution fibre implies less optical power, which leads to a higher value of BER ratio. With a splitting factor of 1/32 and a distribution fibre of 10 km, the optical power at the PIN output is around -14 dBm, which begins to increase the BER ratio. This continues to happen until the distribution fibre reaches the 30 km, when it is impossible to measure the BER because it is above 10^{-3}. The same happens with the splitting factor of 1/64 that starts with no distribution fibre with an optical power of approximately -13.3 dBm, until 10 km of distribution fibre.

With the two extinction ratio scenarios measured, it is now possible to realize a comparison in the BER values from tables 4.1 and 4.5. Comparing the two tables, it is possible to state that, despite, the optical power values at the PIN input are very similar in both extinction ratio scenarios, the minimum extinction ratio scenario presents lower values for the BER. These lower values of BER indicate a better performance of the system. A lower BER value indicates a detection of lower incorrect bits, This superior performance comparison is verified through all the splitting factors. With this assessment, it is possible to, finally, conclude that the minimum extinction ratio scenario has a

better performance. Therefore, the minimum extinction ratio scenario is the chosen one to be applied in this downstream connection.

4.3 Experimental measurement of BER with a 10 Gbit/s system in a downstream transmission using FEC

As it was concluded in section 4.2, the best extinction ratio scenario to use in order to achieve the better performance in this experimental demonstration is the minimum extinction ratio scenario. In order to improve the results of the measurements performed in the laboratory, it is necessary to implement a FEC technique. The BER results considering longer distribution fibre sections are higher then the ones with less distance in distribution fibre. Therefore the use of a FEC decoder can improve the BER. For instance, a BER of approximately of 10^{-4} can be improved with a FEC decoder.

The use of FEC improves the effective sensitivity and overload characteristics of the optical receiver by introducing redundancy in the transmitted bit stream and allowing the receiver to operate at a higher BER level. FEC introduces redundancy in the transmitted data and so, allows the decoder to detect and correct certain transmission errors. In an XG-PON1 system, FEC encoding is based on Reed-Solomon (RS) codes [29].

This FEC technique is frequently used in data transmission for controlling errors and correcting error in sent bits. From ITU-T G-Supplement 39 recommendation, the FEC techniques are specified in standard G.709 (reference [30]) [31]. From ITU-T G.709 recommendation it is identified that the FEC technique implements the Read-Solomon (RS) (255,239). The number of symbols per codeword is 255 bytes and the number of information symbols per codeword is 239 bytes [30].

The use of FEC implies a coding gain in essence. In the case of the recommended RS code, it generates a bit rate gain overhead of around 7%. This fact will result in a bit rate of approximately 10.7092 Gbit/s.

The performance of a 10.7092 Gbit/s transmitting in an optic link, which emulates the downstream direction of a PON is evaluated. The BERT has a setup for this FEC implementation according to the ITU-T G-Supplement 39 recommendation [30]. The pattern generator and error detector of the BERT has a setup option of the bit rate applied to the pattern generator and error detector modules of 10.7092 GHz with the reference to the ITU-T G.709 recommendation. The Preset option is applied to the BERT. The measurement of the 10.7092 Gbit/s signal was realized only for the splitting factor of 1/32, because, it is the one with more results to test this new bit rate measurement. The result of the FEC implementation is presented in table 4.7.

	Fiber Length [km]						
Splitter	**0**	**5**	**10**	**15**	**25**	**30**	**35**
1/32	<-12.0	-10.6	-7.5	-6.9	-5.5	-4.4	X

Table 4.7 – $\log_{10}$ BER for the experimental demonstration considering the bit rate of 10.7092 Gbit/s

ITU-T G-Supplement 39 recommendation indicates that, for a BER reference level of 10^{-12}, an output BER ratio of $1.8x10^{-4}$ (-3.7 in Log_{10} BER) will result in a BER higher than of 10^{-12} after the FEC decoder [31].

From the BER results acquired for this measurement, presented in table 4.7, and from ITU-T G-Supplement 39 recommendation, it is possible to conclude that, for the BER values measured for the fibre sections of 10, 15, 25 and 30 km, the FEC technique will result in a BER ratio value not worse than 10^{-12}. All BER values measured are lower than $10^{-3.7}$, therefore after the application of the FEC decoder, the resulting BER values will be lower than 10^{-12}.

4.4 Experimental measurement of BER with a 10 Gbit/s system in a downstream transmission without optical fibre

In order to study the effect of the fibre dispersion on the experiment of the BER measurement was performed again but this time all optical fibre cables of the distribution fibre and feeder fibre sections were removed. Instead of the optical fibre cables, a VOA is placed after the optical filter to simulate the attenuation of the optical fibre. These attenuation values are inserted in the VOA, in order to get the same optical power values that were measured at the PIN input with optical fibre. This measurement is performed considering the minimum extinction ratio scenario and an operating wavelength of 1575 nm. The eye patterns of the 10 Gbit/s signal resulting from this measurement are presented in section B.4, of Appendix B.

The waveforms of the 10 Gbit/s signal at the PIN input considering the maximum extinction ratio scenario were also measured and are presented in section B.5 of Appendix B. The attenuation values that were inserted by the VOA are presented in table 4.8. These attenuation values were used to make sure that the same optical power is present at the PIN input.

	Fiber Length [km]						
Splitter	**0**	**5**	**10**	**15**	**25**	**30**	**35**
1/16	4.8	6.0	7.8	8.6	10.0	11.6	13.3
1/32	4.6	5.3	7.3	8.3	9.3	10.5	-
1/64	4.6	5.8	-	-	-	-	-

Table 4.8 – Attenuation values, in dB, inserted by the VOA for the minimum extinction ratio scenario

The BER measurements results with the VOA replacing the optical fibre are presented in table 4.9.

From the results presented in table 4.9 and in table 4.1 of section 4.2.1, it is possible to realize a comparison between the BER ratio measured with and without the optical fibre cables. This comparison was performed with the splitting factor of 1/32 because this splitting ratio is the one with more experimental BER results with lower values than 10^{-12}. The other splitting ratios only presented one or two BER results of lower than 10^{-12}

	Fiber Length [km]						
Splitter	**0**	**5**	**10**	**15**	**25**	**30**	**35**
1/16	<-12.0	<-12.0	<-12.0	<-12.0	<-12.0	-9.2	-6.1
1/32	<-12.0	<-12.0	-10.8	-8.5	-6.6	-4.7	X
1/64	-9.8	-7.2	X	X	X	X	X

Table 4.9 – $\log_{10}$ BER measured considering the optical fibres replaced by the VOA and considering the minimum extinction ratio scenario

Figure 4.9 shows the result of this comparison considering all the fiber distance.

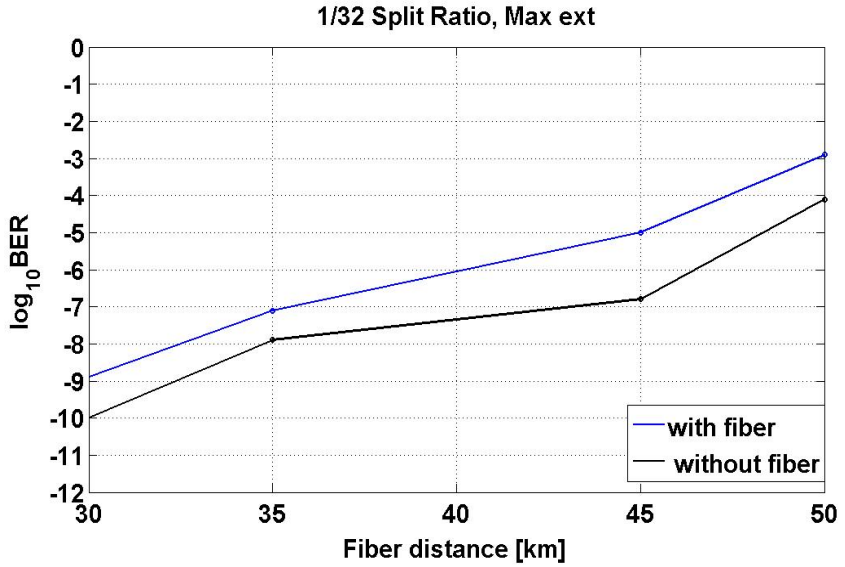

Figure 4.9 – $\log_{10}$ BER measurement comparison between the minimum extinction ratio scenario considering optical fibre and the VOA replacing the optical fibre for the splitting factor of 1/32

In figure 4.9, it can be seen that the BER measurement realized for the system with no fibre cables results in better BER values than the one measured with fibre cables. From the result shown in figure 4.9, one may conclude that the dispersion present in the system, with the use of fibre cables, results in higher values for the BER parameter. Before the fiber distance of 30 km it was not possible to measure the BER because it was below 10^{-12}.

4.6 Theoretical calculation of BER

In this section, a theoretical calculation of the BER parameter considering the minimum extinction ratio scenario, a wavelength of 1575 nm and the optical power measured at the PIN input is performed. A theoretical calculation of the BER parameter is important to validate and authenticate the results achieved with the experimental demonstration performed in the laboratory. The theoretical BER results will then be compared to the one found in section 4.2.1. This calculation is achieved by the theoretical expressions that relate the BER parameter with the optical power at the PIN input. This BER calculation was only performed considering the best extinction ratio scenario found.

The BER is achieved by

$$BER = \frac{1}{2} \cdot \text{erfc}\left(\frac{Q}{\sqrt{2}}\right) \quad (10)$$

where Q is the Q parameter and the erfc is the complementary error function. The Q parameter is related to the optical power at the receiver input. In the case of this work, the Q parameter is related to the optical power at the PIN photodiode input. This relation is given by

$$\overline{p}_i = \frac{1 + r}{1 - r} \cdot \frac{Q\sqrt{\sigma_c^2}}{R_\lambda} \quad (11)$$

where r is the inverse of the extinction ratio, $\overline{p}_i$ is the optical power at the PIN input (in W), σ_c^2 is variance of the noise current and R_λ is the responsivity [5]. Considering equations (10) and (11), the relation between the BER and the optical power at the PIN input is found through the Q parameter.

In order to perform this BER calculation, some experimental values of BER and optical power levels measured at the receiver input are used. The values used are the ones measured for the splitting ratio of 1/32. It is only possible to use the values that indicate a BER higher than 10^{-12} because the BERT is not able to measured BER values lower than 10^{-12}. This BER calculation is performed considering the slipping factor of 1/32, because this splitting ratio is the one with more experimental BER values with lower values than 10^{-12}.

The variance of the noise current and the responsivity did not change between BER measurements. Therefore, they are considered as a constant. According to this fact, from the experimental BER values and optical power levels, the ratio between the circuit noise and the responsivity was calculated. The ratio is approximately 4.74 μW. With this ratio value it is now possible to calculate every Q parameter from the experimental optical power levels received at the PIN input. Using equations (11) and (12), the theoretical BER considering the experimental optical power levels at the receiver input are presented in table 4.10.

	Fiber Length [km]						
Splitter	**0**	**5**	**10**	**15**	**25**	**30**	**35**
1/32	-46.5	-28.5	-10.6	-8.2	-5.2	-3.6	X

Table 4.10 – $\log_{10}$ BER calculation using equation (10) and (11) considering the minimum extinction ratio scenario and the optical power at the PIN input with a splitting ratio of 1/32

By inspection of table 4.10 and comparing it to table 4.1, from section 4.2.1, it is possible to state that the results this theoretical BER are similar to the results found considering the minimum extinction ratio. Without considering the BER results lower than 10^{-12}, all other BER results are similar in comparison with to the ones measured and presented in section 4.2.1.

From these results it is possible to conclude that the experimental results present a good measure of the BER parameter.

The graphical result of this theoretical approach is presented in figure 4.10.

From inspection of figure 4.10, it can be seen that the theoretical BER calculation is extremely close to the one measured from the experimental demonstration. The difference identified between these sets of BER results can be explained by measurement errors while performing the experimental measurements. Before the fiber distance of 30 km it was not possible to measure the BER because it was below 10^{-12}.

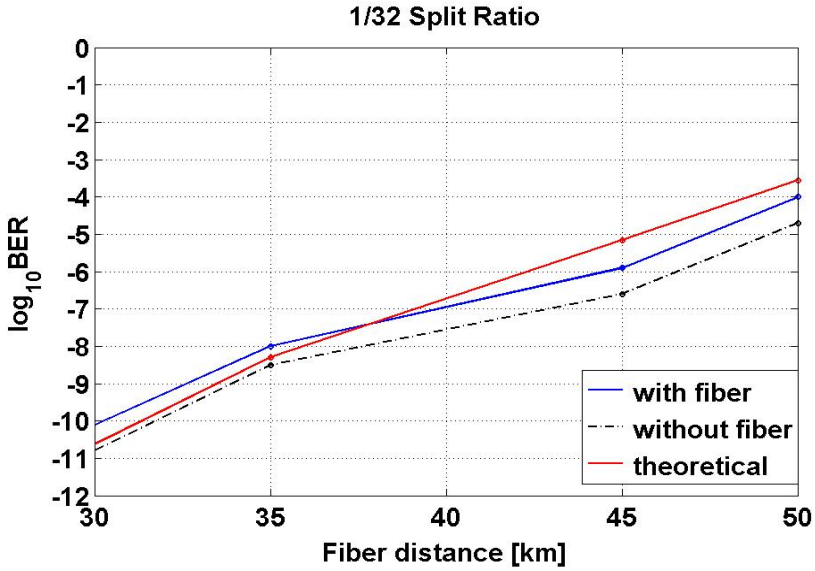

Figure 4.10 – $\log_{10}$ BER comparison between the minimum extinction ratio scenario considering optical fibre, considering optical fibre and the VOA replacing the optical fibre and the theoretical approach for the splitting factor of 1/32

4.5 Conclusion

In this chapter, the experimental demonstration realized in the laboratory of the IT has been presented. The performance evaluation is presented and experimentally measured in order to study the performance of the 10 Gbit/s signal emulating the XG-PON1 system.

In section 4.1, the experimental setup has been introduced and thoroughly explained. The new components to the setup have been described and characterized according to its vendor specification. The configuration setup of the optical laser source, optical amplifier, optical filter, DSA, BERT and electric amplifiers was also explained.

In section 4.2, the waveforms obtained from the BERT device have been presented. Subsections 4.2.1 and 4.2.2 are presented in order to measure the BER parameter for each extinction ratio scenario. The optical power at the PIN input has been also measured. It has been concluded that the minimum extinction ratio scenario presented better performance.

In section 4.3, the performance of a signal transmitted in an optic link, which emulates the downstream direction of a PON using FEC has been evaluated. The bit rate for considering FEC is 10.7092 Gbit/s.

In section 4.4, the optical fibre cables have been removed. With the introduction of a VOA to replace the attenuation introduced by the fibre, it has been possible to simulate the optical power levels of the fibre cable and performed a BER measurement to observe the effect of the fibre dispersion. The result of this BER measurement concludes that, with the fibre dispersion presented in the optical fibre cables, the system indicates a lower performance. This fact is explained by the lower BER results experimentally measured with no fibre cables.

In section 4.5 a theoretical BER calculation has been performed using the theoretical expressions for calculating the BER parameter through the relation between the *Q* parameter and the

optical power at the PIN input. The result of this BER calculation is very similar to the results achieved in the experimental demonstration. This fact helps to validate and authenticate the experimental results obtained.

Chapter 5

Conclusion

In this chapter, the final conclusions of the work developed in this report are presented.

5.1 Final conclusions

In this dissertation, an experimental demonstration of an XG-PON1 downstream signal is realized, using an EAM. The performance of this laboratory experiment is evaluated in detail with several laboratory components that allowed practical measurements. An introduction of the PON and previous networks were presented.

In chapter 1, the characterization of the PON communication system was made, along with historical perspective to the PON system until the legacy GPON.

In chapter 2, the fundamentals of NG-PON configurations were explained. A general description was made and as the focus of this report is the physical layer of the NG-PON system, a more careful approach to its physical infrastructure and sub systems was taken. Afterwards, the NG-PON2 system and some migration scenarios of the next evolution PON were defined and considered. XG-PON1 main components such as the optical transmitter and receiver are presented and explained.

In chapter 3, a static characterization of the EAM device is performed and clarified. The setup used for this practical measurement is also presented. From the static characteristic it was possible to measure the optical power at the EAM output and from the dynamic characteristic it was possible to study the amplitude response of the modulator. Through the study of the amplitude response of experimental setup employing 100 km of fibre, the chirp and dispersion parameter were measured. The chirp parameter of the EAM is between 3 and -2, approximately. The dispersion parameter has been measured and presented a value around 18 ps/(nm.km), which is a conventional value for single mode fibres.

In chapter 4, experimental demonstration in order to evaluate the performance of a 10 Gbit/s signal transmitted in an optic link, which emulates the downstream direction of a XG-PON1 architecture is presented. From this experimental demonstration it has been concluded that the minimum extinction ratio scenario operating with a wavelength of 1575 nm presented the best performance. After these measurements, a BER measurement in order to evaluate the performance of a 10.7092 Gbit/s signal transmitted in an optic link, which emulates the downstream direction of a XG-PON1 architecture is presented. This bitrate is presented considering a FEC scenario.

In this chapter another measurement is performed to study the effect of the fibre dispersion. All optical fibre cables are removed and a VOA is used to add attenuation to the optical power in order to simulate the optical fibre path loss. This measurement concluded that the optical fibre introduces dispersion to the system affecting the BER.

5.2 Future work

Following the conclusions presented in section 5.1, some work topics for future investigation are suggested in order to complement or continue the work accomplished in this dissertation:

- Study the performance measurement of the XG-PON1 system with the APD photodetector
- Study the experimental demonstration performed with another optical amplifier and optical filter. It would be interesting to study the experimental demonstration with these other equipment's. The optical amplifier is not working with a wavelength range between 1575 and 1580 nm. The optical power at the amplifier output is lower than the saturated power. It would be interesting to change this equipment's in order to increase the optical power at the receiver input. With the optical power increase, study the performance of the system.

References

[1] FiberOptics.info, Applications in the Real World, 2008. [Online]. Available at: http://www.fibre-optics.info/history/P3/. [Accessed: 20-Sep-2013].

[2] R. Ramaswami, K. Sivarajan, and G. Sasaki, “Optical Networks A Practical Perspective”, *Second Edition*, *Elsevier*, *Morgan Kaufmann Publishers*, USA, 2010.

[3] C. Lam, “Passive Optical Networks: Principles and Practice, ”*Academic Press*, San Diego, California, USA, 2007.

[4] A. Cartaxo, “Transmissão por Fibra Óptica”, Departamento de Engenharia Electrotécnica e de Computadores, Instituto Superior Técnico, 2003.

[5] Nngroup.com, Nielson’s Law, 2008. [Online]. Available at: http://nngroup.com/articles/law-of-bandwidth/. [Accessed: 16-Oct-2013].

[6] A. Cartaxo, “Chapter 5 - Optical Access Networks”, *Sistemas de Telecomunicações por Fibra Óptica*, Departamento de Engenharia Electrotécnica e de Computadores, Instituto Superior Técnico, 2013.

[7] F. Bourgart, “Optical access transmission: XG-PON system aspects”, *FTTH Conference 2010, ITU-T Standardization: from G-PON to 10G XG-PON,* Lisbon, 25 February 2010.

[8] J. Pires, “Capitulo 7 – Redes de Acesso”, *Redes de Telecomunicações*, Instituto Superior Técnico, 2013.

[9] F. Effenberger, “Tutorial: XG-PON”, Optical Fiber Communication, collocated in *National Fiber Optic Engineers Conference*, pp. 1-37, March 2010.

[10] I. Cale, A. Salihovic and M. Ivekovic, "Gigabit passive optical network-GPON", *Proceedings of the ITI 2007 29th Int. Conf. on Information Technology Interfaces*, pp. 679-684, Cavtat, Croatia, June 25-28, 2007. doi: 10.1109/ITI.2007.4283853.

[11] FSAN, “Broadband optical access systems based on Passive Optical Networks”, *ITU-T G983.1 Recommendation*, 2005.

[12] FSAN, “A broadband optical access system with increased service capability by wavelength allocation”, *ITU-T G.983.3 Recommendation*, 2001.

[13] FSAN, “A broadband optical access system with increased service capability using dynamic bandwidth assignment*”, ITU-T G.983.4 Recommendation*, 2001.

[14] G. Kramer, "Ethernet passive optical network (EPON): building a next-generation optical access network", *IEEE Communication Magazine*, vol. 40, nº 2, pp. 66– 73, February 2002. doi10.1109/35.983910.

[15] ITU-T, Recommendation G.984 series, “Gigabit-capable passive optical networks (G-PON)”, 2008.

[16] B. Batagelj, V. Erzen, J. Tratnik, L. Naglic, V. Bagan, Y. Ignatov and M. Antonenko, “Optical access network migration from GPON to XG-PON”, *The Third International Conference on Access Networks*, pp 62-67, 2012.

[17] S. Jain, F. Effenberger, A. Szabo, Z. Feng, A. Forcucci, W. Guo, Y. Luo, R. Mapes, Y. Zhang and V. O'Byrne, "World's First XG-PON Field Trial", *IEEE/OSA Journal of Lightwave Technology*, vol. 29, nº 4, pp. 524-528, January 2011. doi 10.1109/JLT.2010.2104313.

[18] F. Effenberger, "The XG-PON system: cost effective 10 Gb/s access", *IEEE/OSA Journal of Lightwave Technology*, vol. 29, nº 4, pp. 403-409, February 15, 2011. doi 10.1109/JLT.2010.2084989.

[19] ITU-T G.984.5 Recommendation, "Gigabit-capable passive optical networks (GPON): enhancement band", 2007.

[20] ITU-T, Recommendation G.987.1 series, "10-Gigabit-capable passive optical network (XG-PON) systems: General requirements", July 2010.

[21] Huawei Technologies Co., LTD., "Next-Generation PON Evolution", White Paper, October 2010.

[22] J. Kani, F. Bougart, A. Cui, A. Rafel, M. Campbell and S. Rodrigues, "Next-generation PON – part I: technology roadmap and general requirements", *IEEE, Communications Magazine*, vol. 47, nº11, pp. 43-49, November 2009. doi 10.1109/MCOM.2009.5307465.

[23] ITU-T, Recommendation G.989.1 series, "40-Gigabit-capable passive optical network (NG-PON2) systems: General requirements", March 2013.

[24] ITU-T G.987.2 Recommendation, "10-Gigabit-capable passive optical networks (XG-PON): Physical media dependent (PMD) layer specification", March 2011.

[25] T. Mason, "Electroabsorption modulators", from A. K. Dutta, N. K. Dutta, and M. Fujiwara, *WDM Technologies: Active Optical Components*, Eds San Diego, CA: Academic, 2002

[26] F. Koyama and K. Iga, "Frequency chirping in external modulators" *IEEE/OSA Journal of Lightwave Technology*, vol. 6, nº 1, pp. 87-93, January 1998. doi 10.1109/50.3969.

[27] F. Devaux, Y. Sorel and J. Kerdiles, "Simple measurement of fibre dispersion and of chirp parameter of intensity modulated light emitter" *IEEE/OSA Journal of Lightwave Technology*, vol. 11, nº 12, pp. 1937-1940, December 1993. doi 10.1109/50.257953.

[28] R. Shafik, S. Rahman, and R. Islam, "On the extended relationships among EVM, BER and SNR as performance metrics" International Conference on Electrical and Computer Engineering, pp. 408-411, December 2006.

[29] ITU-T G.987.3 Recommendation, "10-Gigabit-capable passive optical networks (XG-PON): Transmission convergence (TC) layer specification", July 2014.

[30] ITU-T G.709 Recommendation, "Interfaces for the optical transport network", February 2012

[31] ITU-T G-Supplement 39 Recommendation, "Optical system design and engineering considerations", March 2013"

Appendix A

Additional information and validation of the EAM characterization

In this appendix, additional information of the EAM characteristics are presented. In section A.1, additional information of the EAM static characteristic is presented. This section shows the static characteristic for the EAM device for an operating wavelength of 1581 nm and a table that presents the different optical output power levels for all the wavelengths and input optical power values.

In section A.2, additional information of the EAM dynamic characteristic is presented.

In section A.3, additional information for the chirp and dispersion parameters measurement is presented. This section shows the optical power levels reaching the PIN photodetector with the operating wavelengths of 1575 and 1579 nm, the reverse bias voltages between 0.2 and 1.6 V, the amplitude response after the photodetection of an EAM with a fiber of 100 km of length, all the operating wavelengths and all laser output power levels and all the reverse bias voltage used. This section also presents the linear regression realized for all the operating wavelengths, all laser output power levels and all the reverse bias voltages used for this measurement.

A.1 Additional information on the EAM static characteristic

When realizing the measurement of the static characteristic for an operating wavelength of 1581 nm in the laboratory, it was discovered that the laser source has a limitation on the optical power of value 7 dBm for this wavelength value. Consequently, the laser output power levels used for this experiment were 1, 3, 5 and 6.3 dBm.

The result is presented in figure A.1.

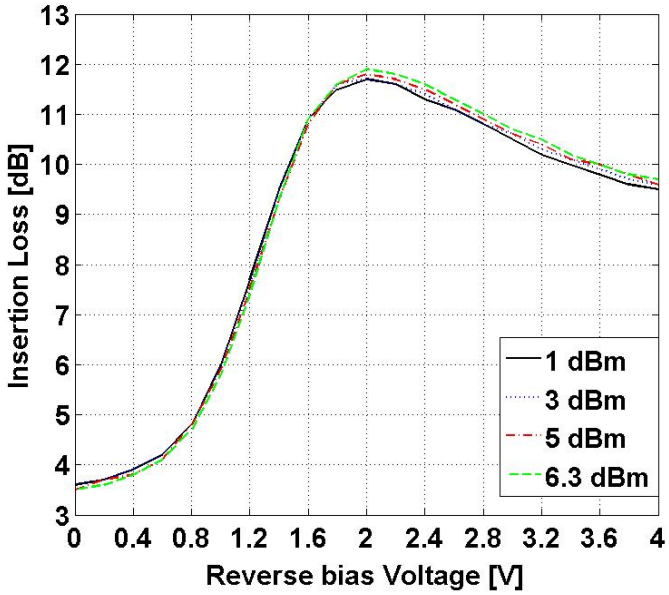

Figure A.1 – Static characteristic of the EAM device with 1581 nm of operating wavelength and four levels of optical power

After gathering the information for figure A.1, it can be concluded that the external modulator still presents the same characteristics for an operating wavelength around the window of 1575 and 1580 nm. Figure A.1 shows the static characteristic of the EAM device when operating with 1581 nm for the levels of optical power of 1, 3, 5 and 6.3 dBm.

By inspection of figure A.1, it is possible to comment that there is not a major difference between the different laser output power levels with this operating wavelength. However, the optical power of 6.5 dBm presents the higher value of insertion loss.

The insertion losses of the modulator device operating at a wavelength of 1581 nm are comprehended between 3.5 and 12 dBm, approximately.

Looking at figure A.1, it is possible to identify a linear region on the EAM device between 0.5 V and around 2 V of the reverse bias voltage. This linear region is the one that should be used to work with the modulator device if this wavelength was recommend for the XG-PON1.

Table A.1 illustrates the values of optical power measured at the output of the EAM device. This table is presented as function of the reverse bias voltage of the modulator device used in the laboratory for this work.

	Operating Wavelength [nm] / Optical Power transmitted from Laser Source [dBm]											
Reverse bias Voltage [V]	**1575**				**1577**				**1579**			
	1	**3**	**5**	**7**	**1**	**3**	**5**	**7**	**1**	**3**	**5**	**6.5**
0.0	-2.5	-0.5	1.5	3.5	-2.5	-0.6	1.4	3.4	-2.5	-0.5	1.5	3.0
0.2	-2.7	-0.7	1.3	3.3	-2.7	-0.7	1.3	3.3	-2.7	-0.7	1.3	2.8
0.4	-2.9	-0.9	1.1	3.0	-2.9	-0.9	1.1	3.1	-2.9	-0.9	1.1	2.6
0.6	-3.4	-1.4	0.6	2.6	-3.3	-1.3	0.7	2.7	-3.2	-1.2	0.8	2.3
0.8	-4.4	-2.3	-0.3	1.8	-4.2	-2.2	-0.1	2.0	-4.0	-1.9	0.1	1.6
1.0	-6.0	-3.9	-1.8	0.4	-5.6	-3.6	-1.5	0.7	-5.3	-3.2	-1.1	0.4
1.2	-8.0	-5.9	-3.7	-1.5	-7.6	-5.5	-3.4	-1.1	-7.1	-5.0	-2.9	-1.3
1.4	-9.8	-7.8	-5.7	-3.5	-9.4	-7.4	-5.3	-3.1	-9.0	-6.9	-4.8	-3.2
1.6	-10.9	-8.9	-6.9	-4.9	-10.6	-8.6	-6.6	-4.5	-10.2	-8.2	-6.2	-4.7
1.8	-11.3	-9.4	-7.4	-5.5	-11.1	-9.1	-7.2	-5.2	-10.8	-8.8	-6.9	-5.5
2.0	-11.3	-9.3	-7.4	-5.6	-11.1	-9.2	-7.2	-5.4	-10.9	-8.9	-7.0	-5.6
2.2	-11.0	-9.1	-7.2	-5.4	-10.9	-9.0	-7.1	-5.2	-10.7	-8.8	-6.9	-5.5
2.4	-10.7	-8.8	-6.9	-5.1	-10.6	-8.7	-6.8	-5.0	-10.5	-8.5	-6.6	-5.3
2.6	-10.4	-8.5	-6.6	-4.7	-10.3	-8.4	-6.5	-4.6	-10.2	-8.2	-6.3	-5.0
2.8	-10.1	-8.1	-6.2	-4.4	-10.0	-8.1	-6.2	-4.3	-9.9	-7.9	-6.0	-4.7
3.0	-9.8	-7.8	-5.9	-4.1	-9.7	-7.8	-5.9	-4.0	-9.6	-7.7	-5.7	-4.4
3.2	-9.5	-7.6	-5.6	-3.8	-9.4	-7.5	-5.6	-3.7	-9.3	-7.4	-5.5	-4.1
3.4	-9.3	-7.3	-5.4	-3.5	-9.2	-7.3	-5.3	-3.5	-9.1	-7.2	-5.2	-3.8
3.6	-9.0	-7.1	-5.2	-3.3	-9.0	-7.0	-5.1	-3.2	-8.9	-6.9	-5.0	-3.6

3.8	-8.9	-6.9	-5.0	-3.1	-8.8	-6.9	-5.0	-3.1	-8.7	-6.8	-4.8	-3.5
4.0	-8.7	-6.8	-4.9	-3.0	-8.7	-6.7	-4.8	-2.9	-8.6	-6.6	-4.7	-3.3

Table A.1 – Optical output power levels of the EAM of all the operating wavelengths and optical input power values

A.2 Additional information on the EAM dynamic characteristic

The signal at the PIN output is measured by the ESA and it is presented in figure A.2.

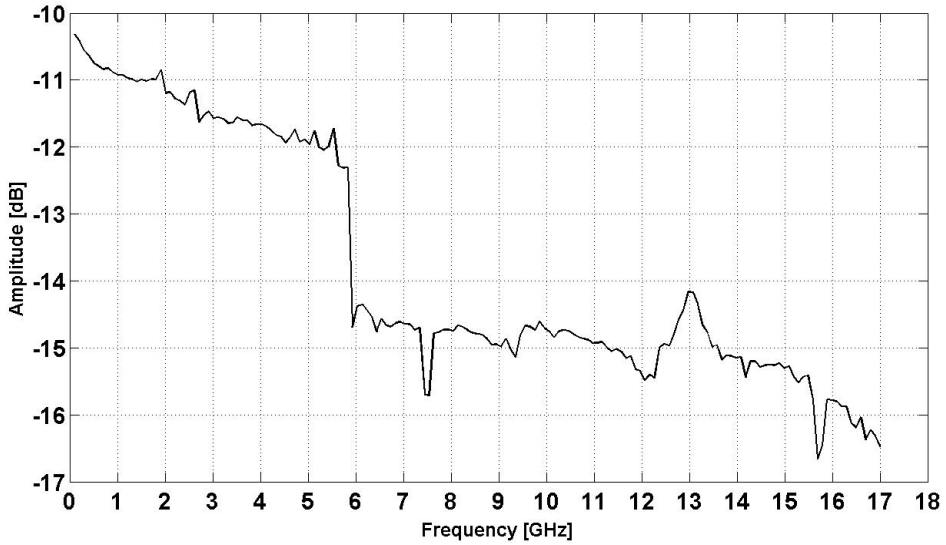

Figure A.2– Amplitude response of the ESA behavior for a frequency range of 100 kHz to 17 GHz

In figure A.2, is possible to see an abrupt drop around 6 GHz. It is also possible to notice a small amplitude dip around 7.5 and 15.7 GHz.

After the normalization explained in section 3.2 of chapter 3, the ESA behavior is presented in figure A.3.

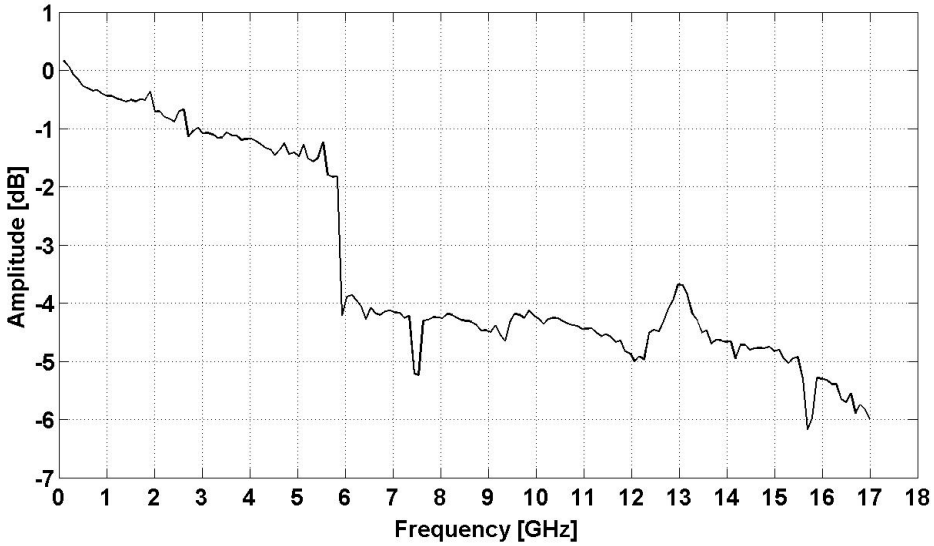

Figure A.3 – Normalized amplitude response of the ESA behavior for a and frequency range of 100 kHz to 17 GHz

As it was expected, the same amplitude dips in figure A.2 are also present in figure A.3 because the normalization can be translated as a simple change in the amplitude axis.

The ESA measurement for the signal at the PIN output considering the reverse bias voltage of 0.2 V, an operating wavelength of 1577 and 1579 nm and laser output power levels of 1, 3, 5 and 7 dBm are presented in figures A.4 and A.5

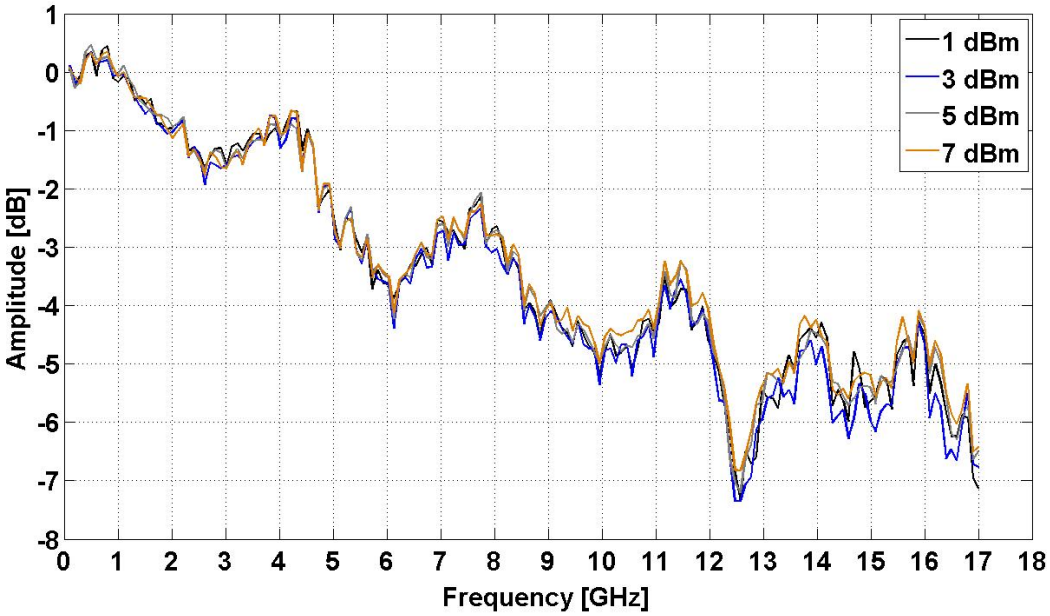

Figure A.4 – Normalized amplitude response for different laser output power levels, 1577 nm of wavelength, reverse bias voltage of 0.2 V and frequency range of 100 kHz to 17 GHz

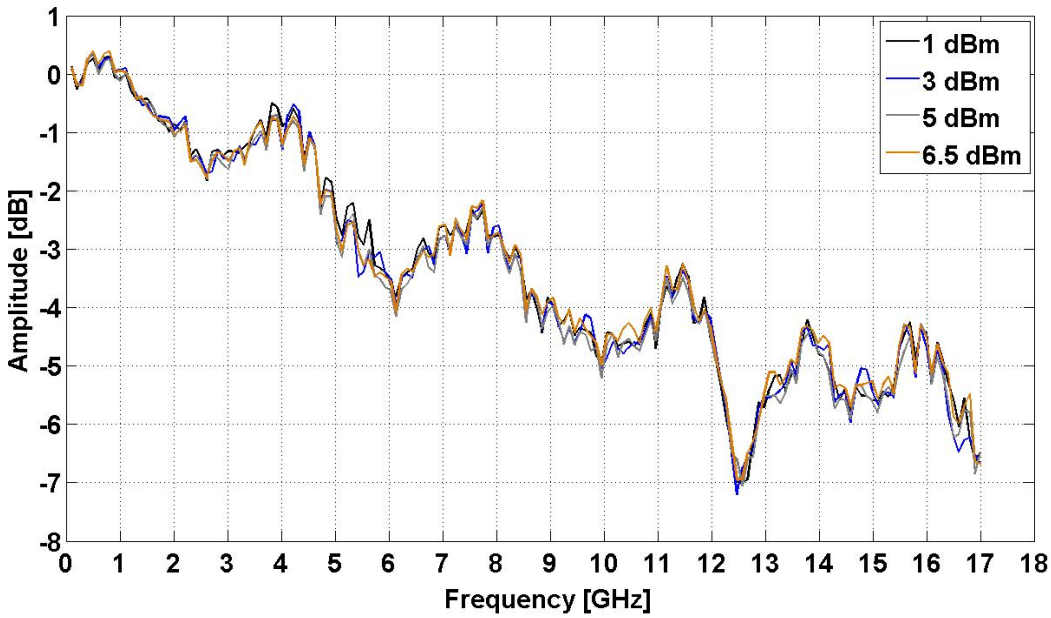

Figure A.5 – Normalized amplitude response for different laser output power levels, 1579 nm of wavelength, reverse bias voltage of 0.2 V and frequency range of 100 kHz to 17 GHz

In figures A.4 and A.5 shows equal behavior to the one presented in section 3.2 of chapter 3.

The amplitude response for the reverse bias voltage of 0.2 V, an operating wavelength of 1581 nm and laser output power levels of 1, 3, 5 and 6.3 dBm are presented in figures A.6.

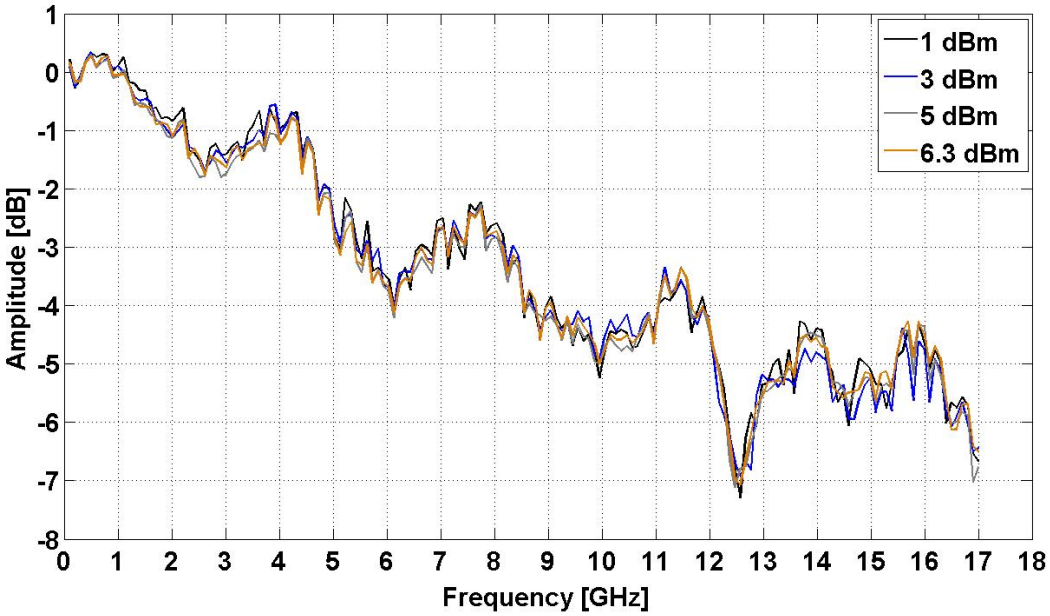

Figure A.6 – Normalized amplitude response for different laser output power levels, 1581 nm of wavelength, reverse bias voltage of 0.2 V and frequency range of 100 kHz to 17 GHz

As figure A.6 shows, the operating wavelength of 1581 nm still verifies the same features that the previous wavelengths presented in section 3.2 of chapter 3. Concluded this measurement for the reverse bias voltage of 0.2 V, the next measurement was realized for the reverse bias voltage of 1.0 V.

The operating wavelengths used in the measurement were 1575, 1577 and 1579 nm. The lser output power levels used were 1, 3, 5 and 7 dBm, except for the 1579 case, because the maximum optical power of the laser source for this wavelength is 6.5 dBm.

The amplitude response for the reverse bias voltage of 1.0 V, an operating wavelength of 1575, 1577 and 1579 nm and the referred laser output power levels are presented in figures A.7, A.8 and A.9.

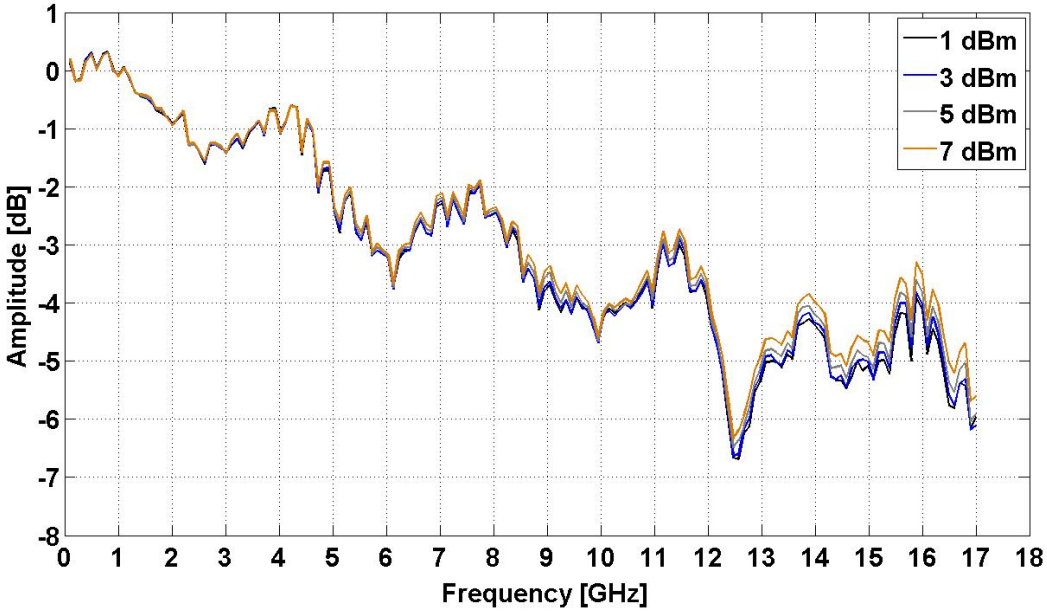

Figure A.7 – Normalized amplitude response for different laser output power levels, 1575 nm of wavelength, reverse bias voltage of 1.0 V and a frequency range of 100 kHz to 17 GHz

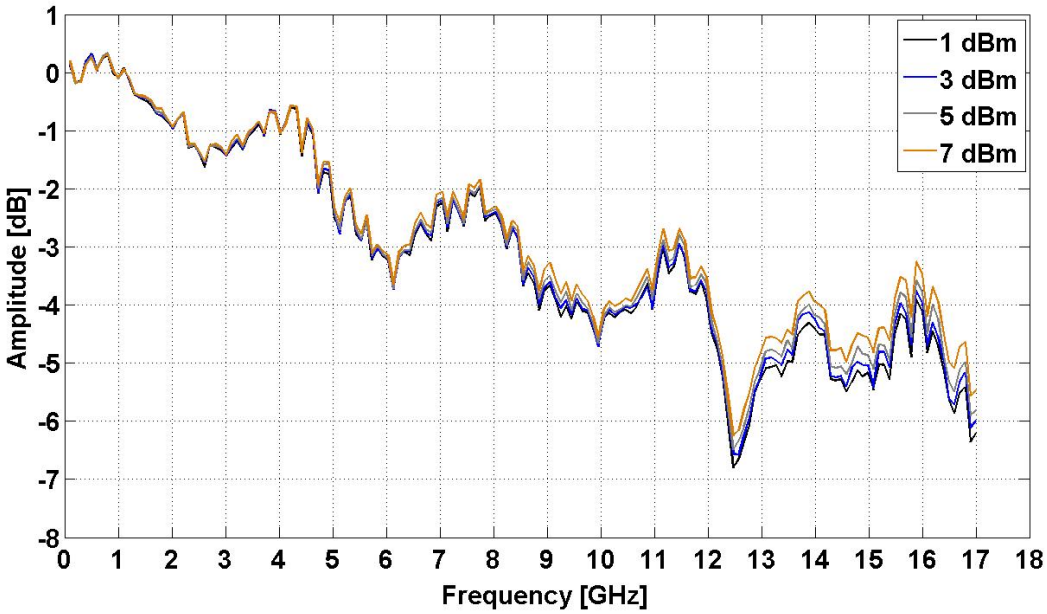

Figure A.8 – Normalized amplitude response for different laser output power levels, 1577 nm of wavelength, reverse bias voltage of 1.0 V and 0-17 GHz frequency range

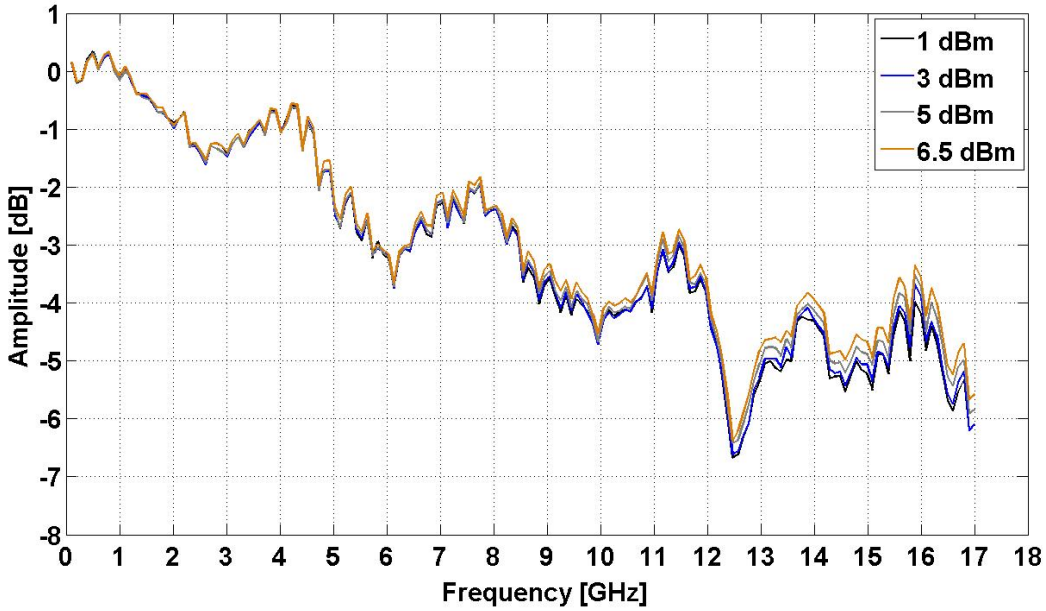

Figure A.9 – Normalized amplitude response for different laser output power levels, 1579 nm of wavelength, reverse bias voltage of 1.0 V and 0-17 GHz frequency range

By inspection of figures A.7, A.8 and A.9, it is possible to comment that the amplitude response in all three operating wavelengths is descending and has three major notorious amplitude dips around frequencies 6.1 and 12.5 GHz, same as the reverse bias voltage of 0.2 V, presented in section 3.2 of chapter 3.

In addition to these last experiments, another measurement was made for the operating wavelength of 1581 nm in order to observe if this present behavior of amplitude response is also witness. This operating wavelength has maximum optical power level for the optical source of 6.3 dBm. The measurement is presented in figure A.10.

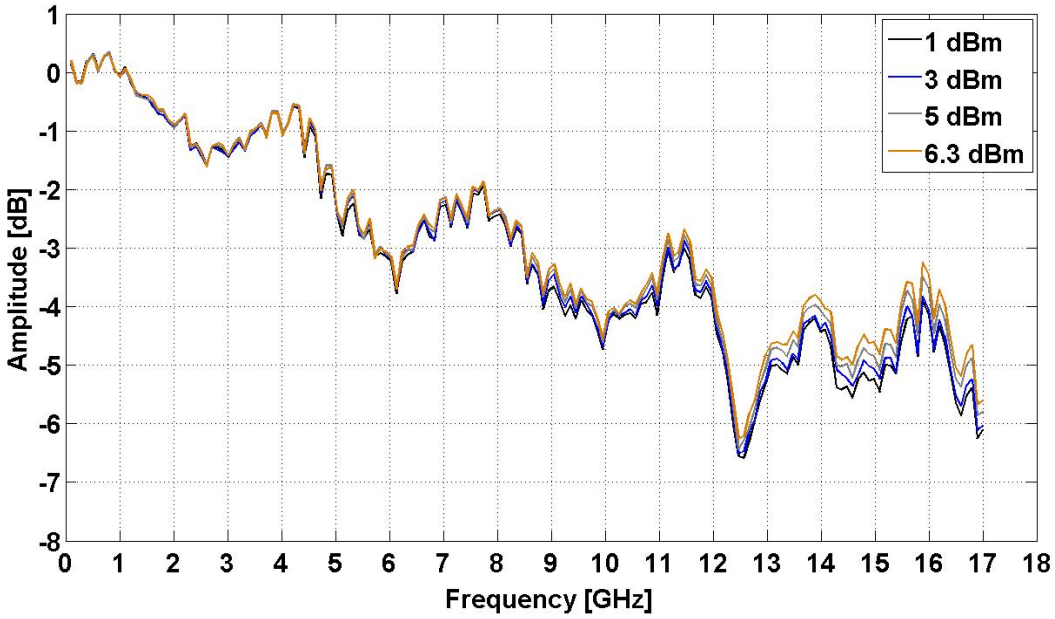

Figure A.10 – Normalized amplitude response for different laser output power levels, 1581 nm of wavelength, reverse bias voltage of 1.0 V and 0-17 GHz frequency range

As figure A.10 shows, the operating wavelength of 1581 nm still verifies the same features that the previous wavelengths presented. Concluded this measurement for the bias value of 1.0 V of reverse bias voltage, the next measurement was realized for the reverse bias voltage of 1.2 V.

The operating wavelengths used in the measurement were 1575, 1577 and 1579 nm. The laser output power levels used were 1, 3, 5 and 7 dBm, except for the 1579 case, because the maximum optical power of the laser source for this wavelength is 6.5 dBm.

The amplitude response for the reverse bias voltage of 1.2 V, an operating wavelength of 1575, 1577 and 1579 nm and the referred laser output power levels are presented in figures A.11, A.12 and A.13.

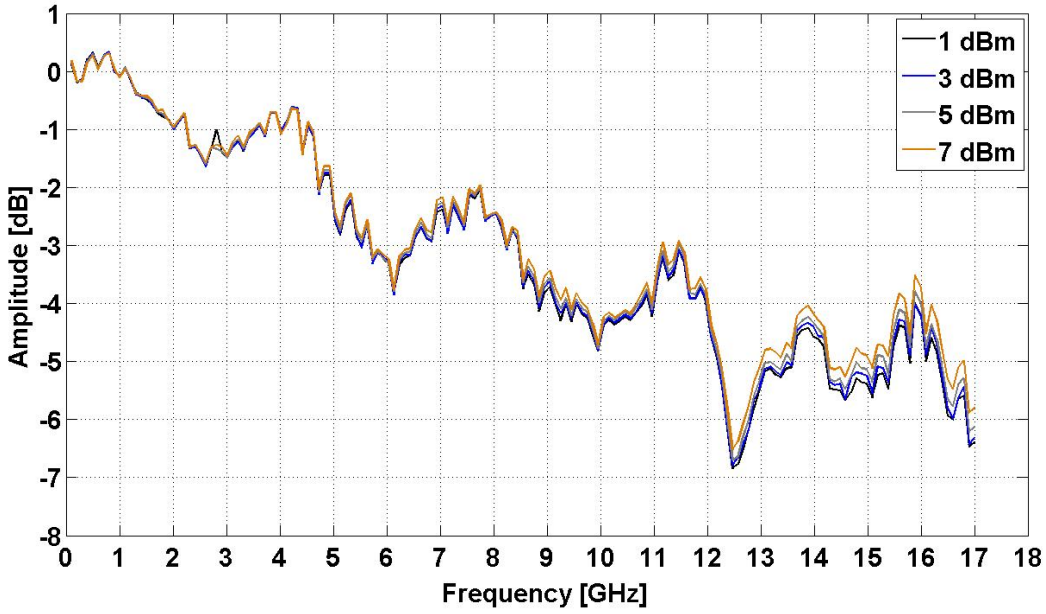

Figure A.11 – Normalized amplitude response for different laser output power levels, 1575 nm of wavelength, reverse bias voltage of 1.2 V and 0-17 GHz frequency range

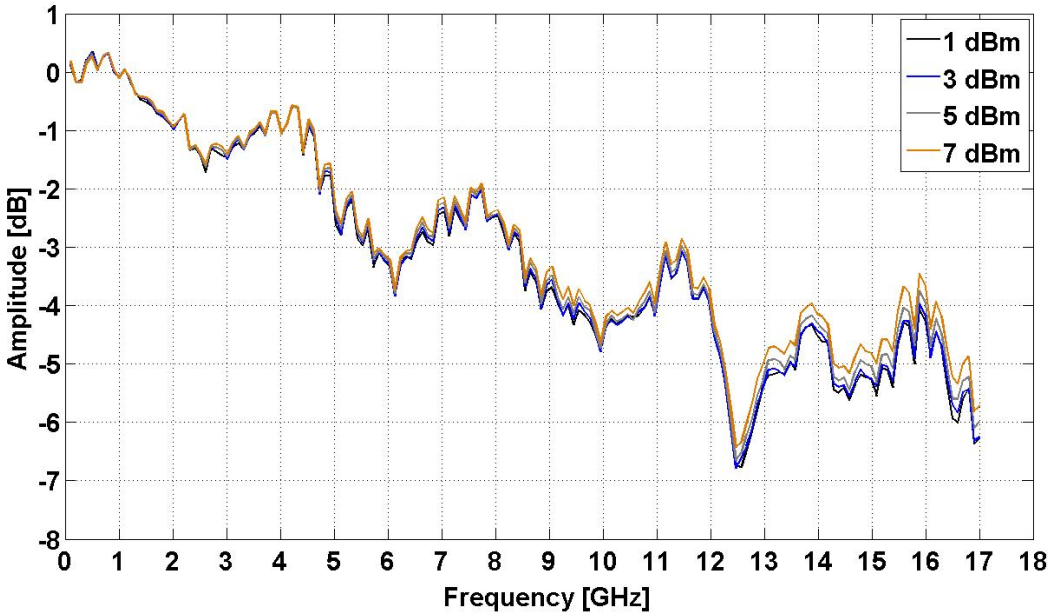

Figure A.12 – Normalized amplitude response for different laser output power levels, 1577 nm of wavelength, reverse bias voltage of 1.2 V and 0-17 GHz frequency range

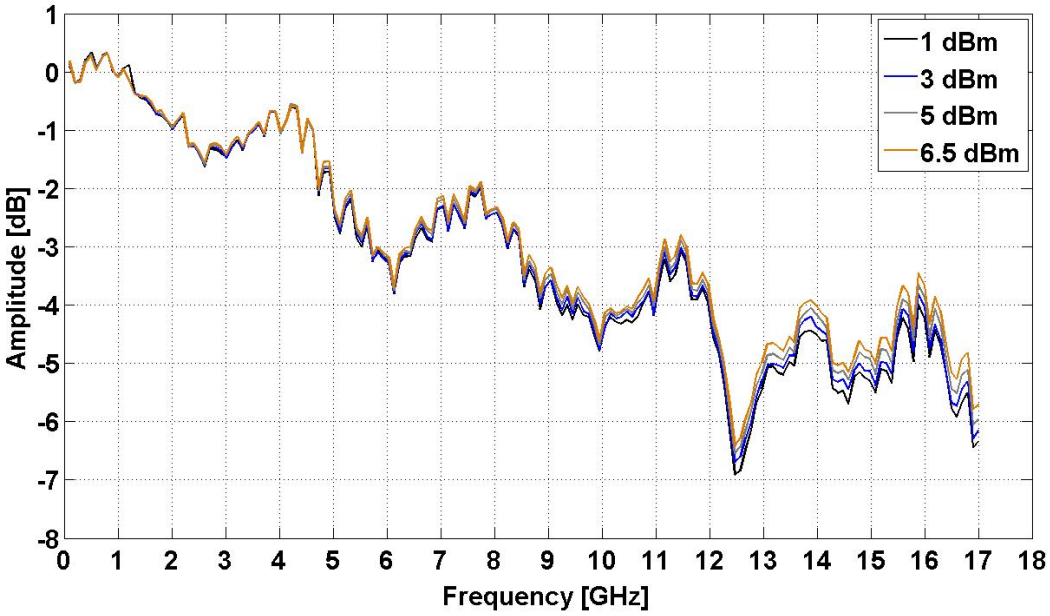

Figure A.13 – Normalized amplitude response for different laser output power levels, 1579 nm of wavelength, reverse bias voltage of 1.2 V and 0-17 GHz frequency range

By inspection of figures A.11, A.12 and A.13 it is possible to comment that the amplitude response in all three operating wavelengths is descending and has three major notorious amplitude dips around frequency 6.1 and 12.5 GHz, same as the reverse bias voltage of 1.0 V, presented in section 3.2 of chapter 3.

In addition to these last experiments, another measurement was made for the operating wavelength of 1581 nm in order to observe if this present behavior of amplitude response is also witness. This operating wavelength has maximum optical power level for the optical source of 6.3 dBm. The measurement is presented in figure A.14.

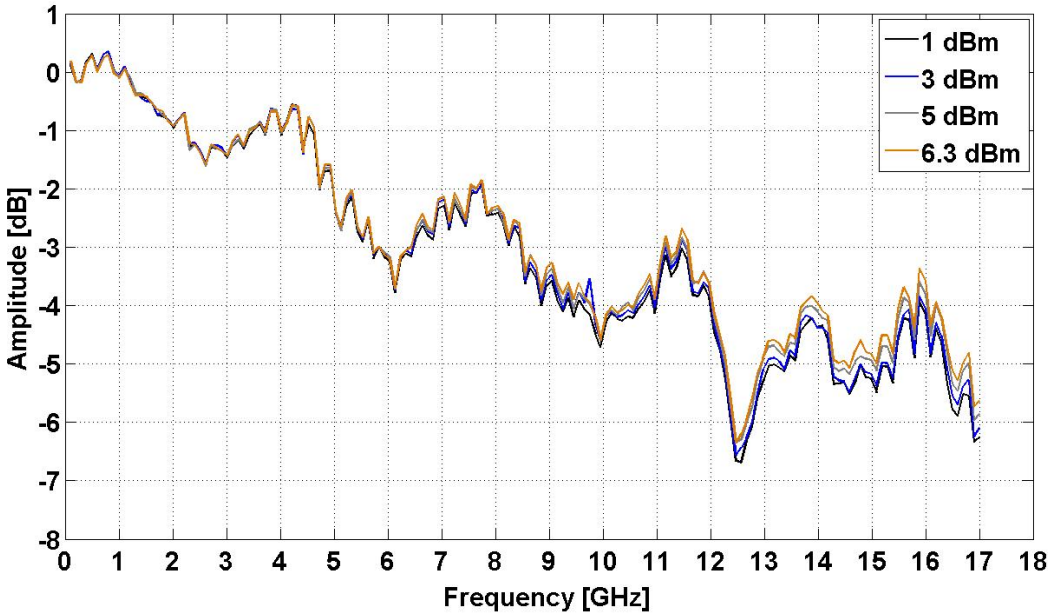

Figure A.14 – Normalized amplitude response for different laser output power levels, 1581 nm of wavelength, reverse bias voltage of 1.2 V and a frequency range of 100 kHz to 17 GHz

As figure A.14 shows, the operating wavelength of 1581 nm still verifies the same features that the previous wavelengths presented. Concluded this measurement for the bias value of 1.2 V of reverse bias voltage, the next measurement was realized for the reverse bias voltage of 1.4 V.

The operating wavelengths used in the measurement were 1575, 1577 and 1579 nm. The laser output power levels used were 1, 3, 5 and 7 dBm, except for the 1579 case, because the maximum optical power of the laser source for this wavelength is 6.5 dBm.

The amplitude response for the reverse bias voltage of 1.4 V, an operating wavelength of 1575, 1577 and 1579 nm and the referred laser output power levels are presented in figures A.15, A.16 and A.17.

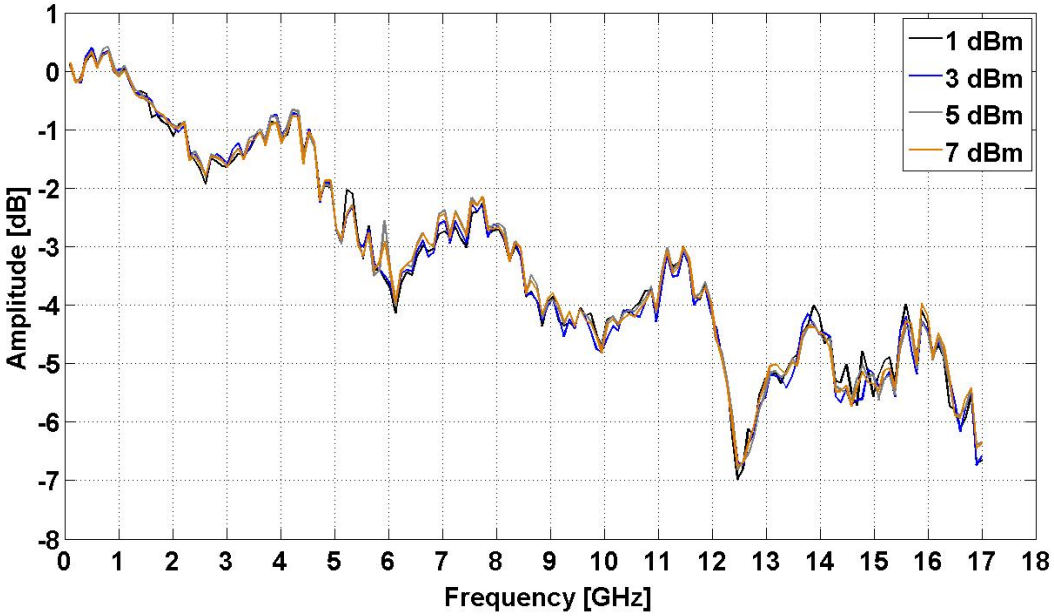

Figure A.15 – Normalized amplitude response for different laser output power levels, 1575 nm of wavelength, reverse bias voltage of 1.4 V and a frequency range of 100 kHz to 17 GHz

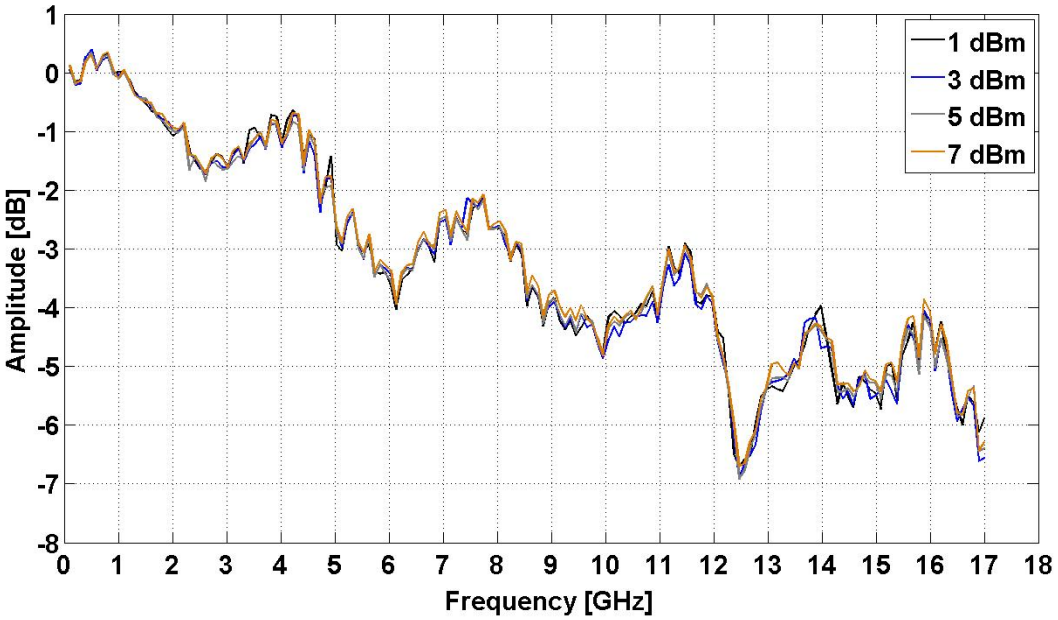

Figure A.16 – Normalized amplitude response for different laser output power levels, 1577 nm of wavelength, reverse bias voltage of 1.4 V and a frequency range of 100 kHz to 17 GHz

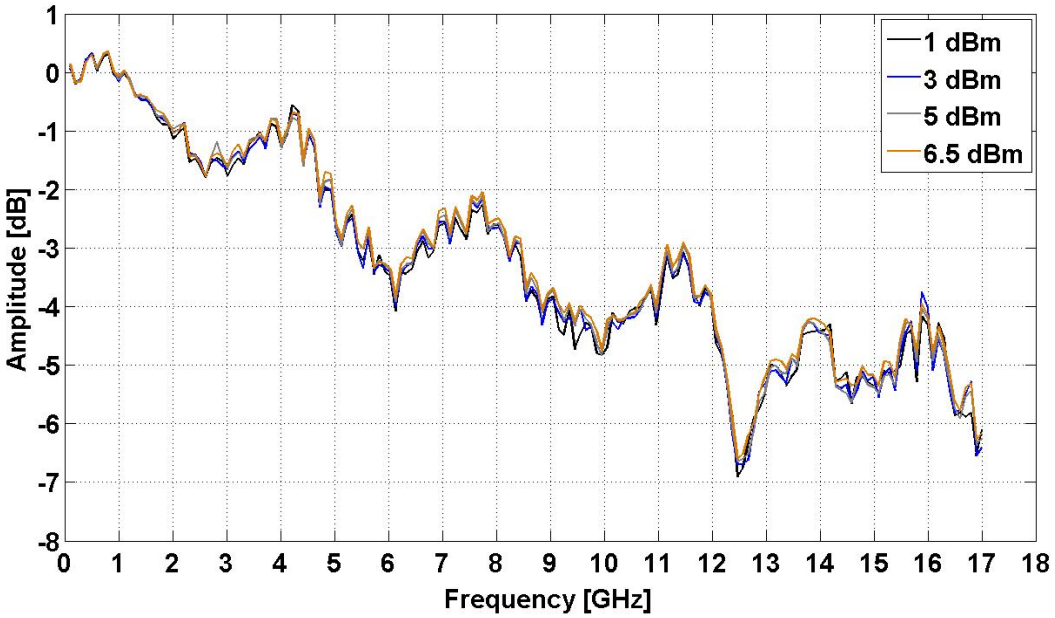

Figure A.17 – Normalized amplitude response for different laser output power levels, 1579 nm of wavelength, reverse bias voltage of 1.4 V and a frequency range of 100 kHz to 17 GHz

By inspection of figures A.15, A.16 and A.17 it is possible to comment that the amplitude response in all three operating wavelengths is descending and has three major notorious amplitude dips around frequencies 6.1 and 12.5 GHz, same as the reverse bias voltage of 1.0 and 1.2 V, presented in section 3.2 of chapter 3.

In addition to these last experiments, another measurement was made for the operating wavelength of 1581 nm in order to observe if this present behavior of amplitude response is also witness. This operating wavelength has maximum optical power level for the optical source of 6.3 dBm. The measurement is presented in figure A.18.

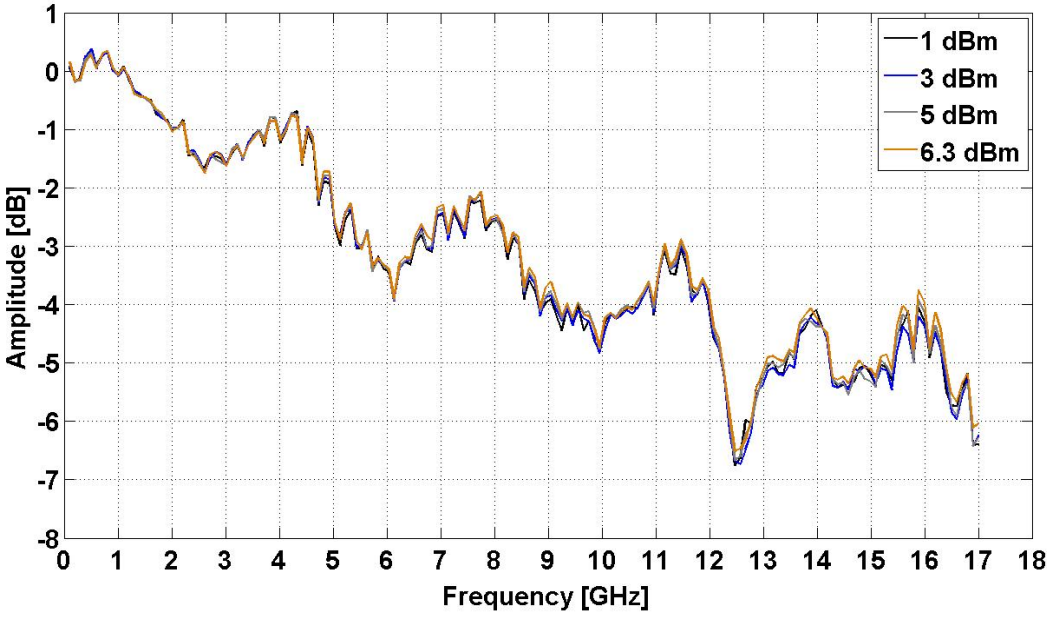

Figure A.18 – Normalized amplitude response for different laser output power levels, 1581 nm of wavelength, reverse bias voltage of 1.4 V and a frequency range of 100 kHz to 17 GHz

As figure A.18 shows, the operating wavelength of 1581 nm still verifies the same features that the previous wavelengths presented.

The last reverse bias voltage of 1.6 V is relevant to present, in order to perceive it's different behavior. This last reverse bias voltage is approaching the end of the linear region, identified in the static characteristic of the EAM device, located in section 3.1 of chapter 3.

The operating wavelengths used in the measurement of the bias voltage of 1.6 V were 1575, 1577 and 1579 nm. The laser output power levels used were 1, 3, 5 and 7 dBm, except for the 1579 case, because the maximum optical power is 6.5 dBm. The different amplitude response with the reverse bias voltage of 1.6 V, an operating wavelength of 1575, 1577 and 1579 nm and the referred laser output power levels are presented in figures A.19, A.20 and A.21.

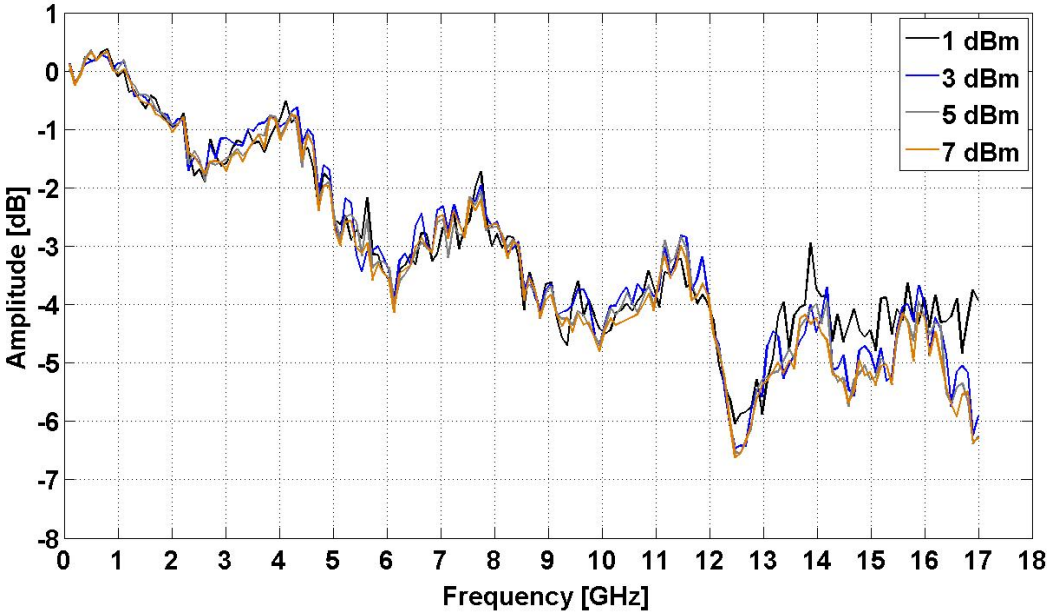

Figure A.19 – Normalized amplitude response for different laser output power levels, 1575 nm of wavelength, reverse bias voltage of 1.6 V and a frequency range of 100 kHz to 17 GHz

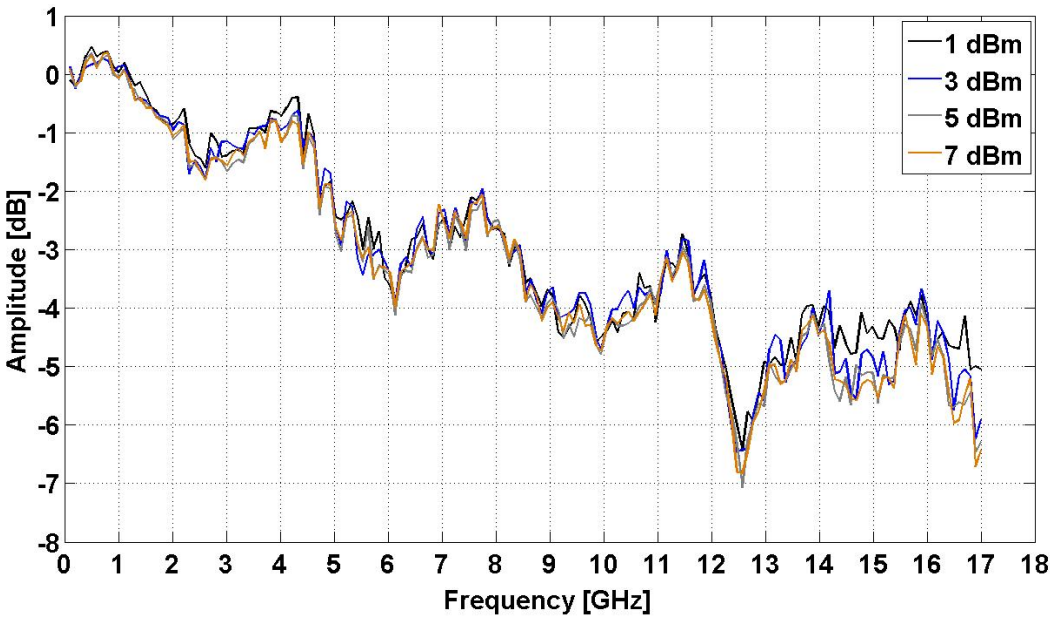

Figure A.20 – Normalized amplitude response for different laser output power levels, 1577 nm of wavelength, reverse bias voltage of 1.6 V and a frequency range of 100 kHz to 17 GHz

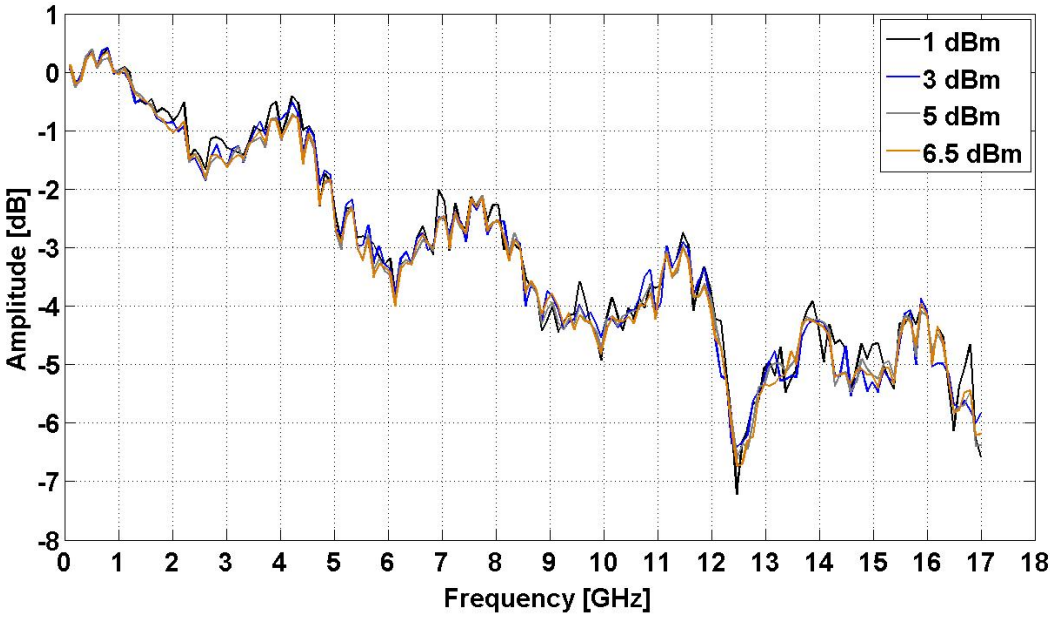

Figure A.21 – Normalized amplitude response for different laser output power levels, 1579 nm of wavelength, reverse bias voltage of 1.6 V and a frequency range of 100 kHz to 17 GHz

From inspection of figures A.19, A.20 and A.21 it is possible to comment that the amplitude response in all three operating wavelengths is descending and has three major notorious amplitude dips around frequencies 6.1 and 12.5 GHz, same as the previous bias voltage presented. In figures A.19, a 31 and A.21, which represent the dynamic characterization of the EAM device with a reverse bias voltage of 1.6 V, it is possible to watch the non-similarities between the different laser output power levels, which were seen in the bias voltage of 0.2 V. The reverse bias voltage of 1.6 V is located, remembering the static characteristics of the EAM device showed in figures 3.5, 3.6 and 3.7 of section 3.1 of chapter 3, in the end of the linear region and approaching a maximum curve. This fact, explains the lack of similarity to the other reverse bias voltage used, which presented a more similar amplitude response.

In addition to these last experiments, another measurement was made for the operating wavelength of 1581 nm in order to see if this present behavior of amplitude response is also witness. This operating wavelength has maximum optical power level, for the laser source, of 6.3 dBm. The measurement is presented in figure A.22.

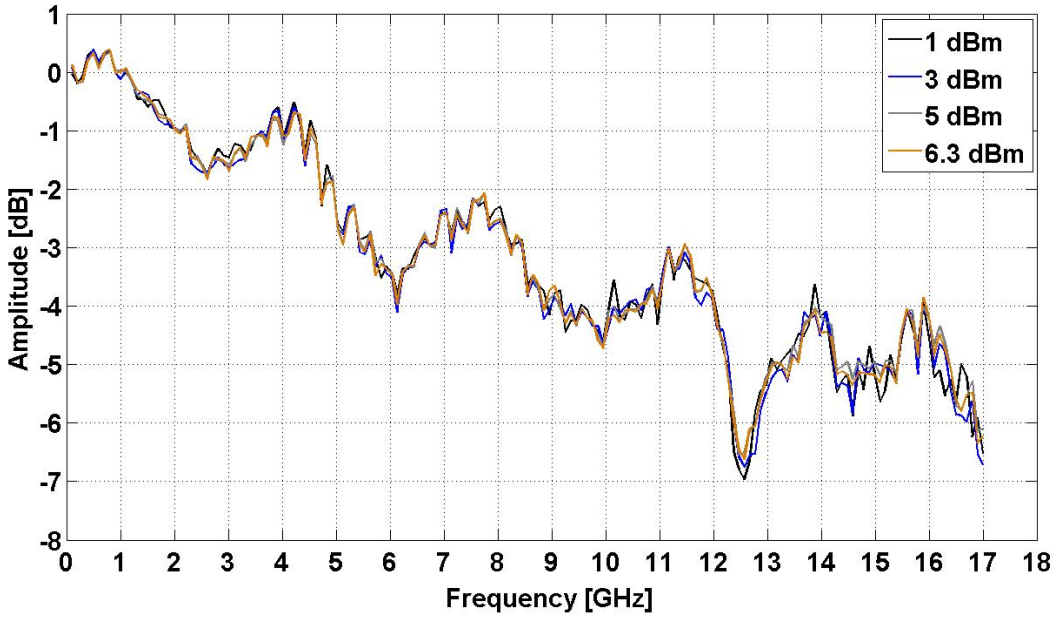

Figure A.22 – Normalized amplitude response for different laser output power levels, 1581 nm of wavelength, reverse bias voltage of 1.6 V and a frequency range of 100 kHz to 17 GHz

As figure A.22 shows, the operating wavelength of 1581 nm still verifies the same features that the previous wavelengths presented. Figure A.22 also presents the same non-similarities to the other reverse bias voltage values.

A.3 Additional information on the chirp and dispersion parameter measurement

Before preforming the measurement for the chirp and dispersion parameter, it is necessary to measure the optical power level reaching the photodetector, in order to check if that level of power is acceptable for the PIN specifications. Similar to the information presented in table A.1, table A.2 will show the optical power level reaching to the PIN, after travelling through the two optical fiber sections, the two optical amplifiers and the optical filter right before the photodetector, according to figure 3.11, located in section 3.3 of chapter 3. In this table, it will only be presented the information for the operating wavelength of 1575 and 1579 nm, the reverse bias voltage values between 0.2 and 1.6 V and a frequency range of 100 KHz to 17 GHz. The other reverse bias voltages values are not comprehended in the linear region identified in the EAM static characteristics, in section 3.1 of chapter 3.

Reverse bias voltage [V]	Operating Wavelength [nm] / Optical Power transmitted from Laser Source [dBm]			
	1575		1579	
	3	7	3	6.5
0.2	-4.1	-2.4	-6.9	-4.6
0.4	-4.2	-2.5	-7.1	-4.7
0.6	-4.5	-2.6	-7.4	-4.9
0.8	-5.2	-3.0	-8.1	-5.4
1.0	-6.4	-3.7	-9.3	-6.3
1.2	-8.2	-4.8	-11.1	-7.7
1.4	-9.9	-6.4	-12.8	-9.3
1.6	-11.0	-7.5	-14.0	-10.6

Table A.2 – Optical power levels reaching the PIN photodetector with the operating wavelengths of 1575 and 1579 nm and reverse bias voltage values between 0.2 and 1.6 V

In table A.3, the optical power levels launched at the fiber section are presented. Table 4.3 presents the optical power considering the operating wavelengths of 1575 and 1579 nm, the reverse bias voltages of 0.2, 0.4, 0.6, 0.8, 1.0, 1.2, 1.4 and 1.6 V, the laser output power levels of 3 and 7 dBm for 1575 nm and 3 and 6.5 dBm for 1579 nm.

The result of the experimental measurement performed in the laboratory for all the reverse bias voltage values, a wavelength of 1575 and a laser output power level of 7 dBm is presented in figure A.23.

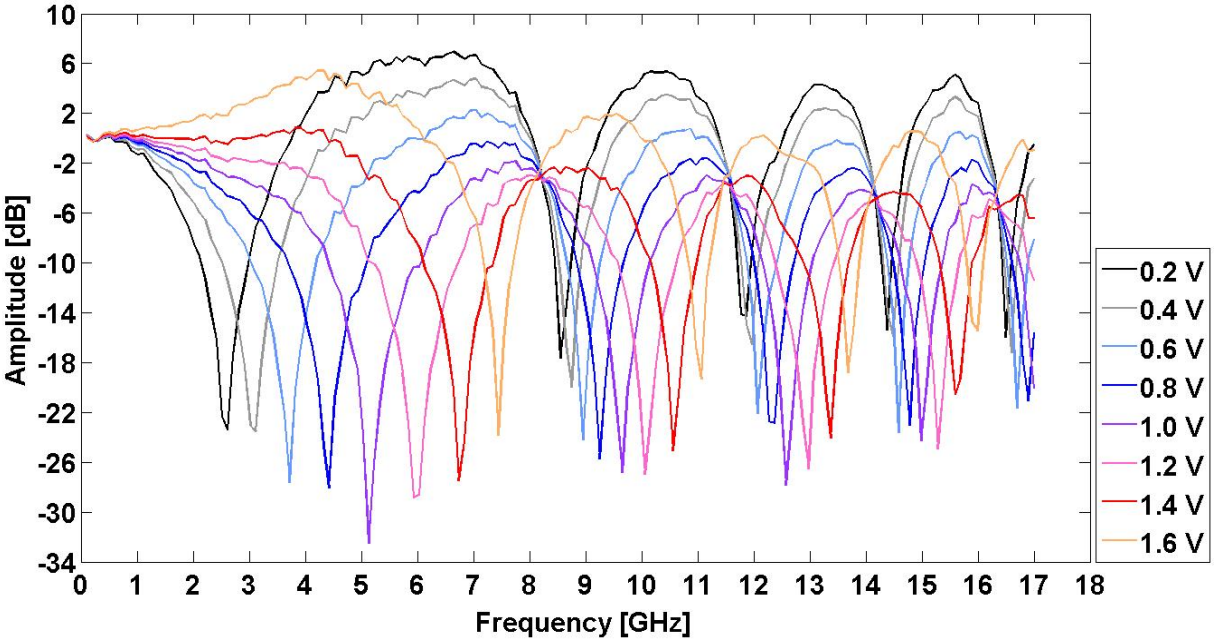

Figure A.23 – Amplitude response after the photodetection with a fiber of 100 km of length, a wavelength of 1575 nm and a laser output power level of 7 dBm for all the reverse bias voltage values

In comparison with figure 3.12 of section 3.3 of chapter 3, figure A.23 presents the same behavior.

Comparing to the amplitude response from figure A.23 to figure 3.12, in section 3.3 of chapter 3, there is no major difference in the amplitude response considering the laser output power levels of 3 or 7 dBm.

The practical measurement for the amplitude response considering an operating wavelength of 1579 nm, a laser output power level of 3 dBm and a maximum of 6.5 dBm are presented in figures A.24 and A.25.

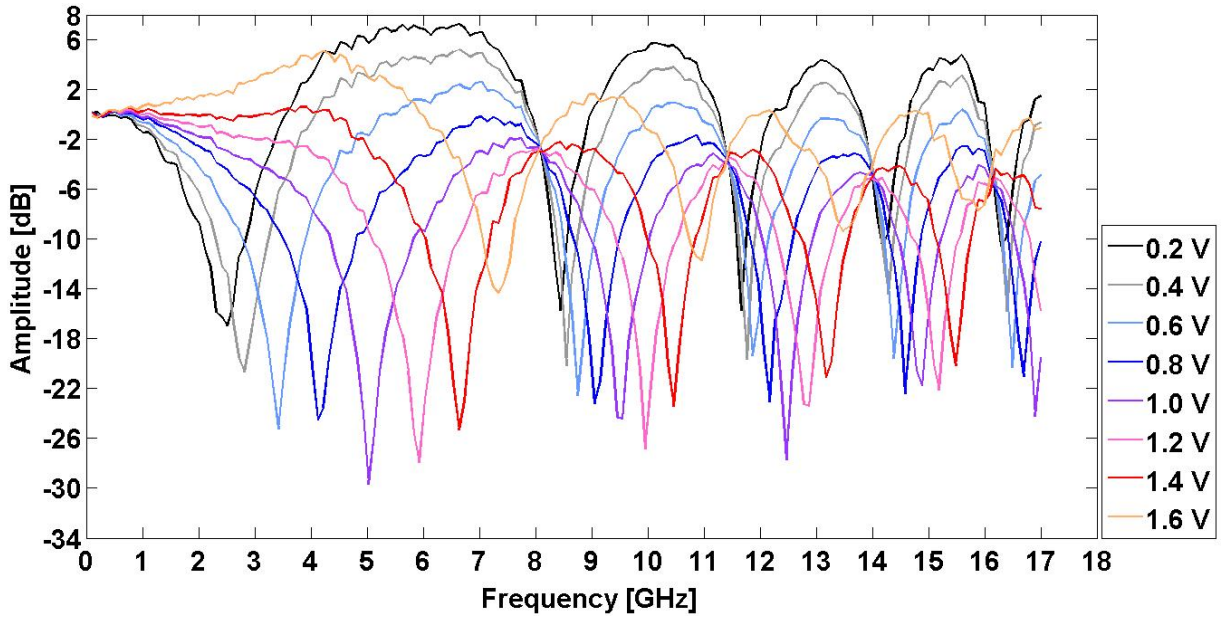

Figure A.24 – Amplitude response after the photodetection with a fiber of 100 km of length, a wavelength of 1579 nm and a laser output power level of 3 dBm for all the reverse bias voltage values

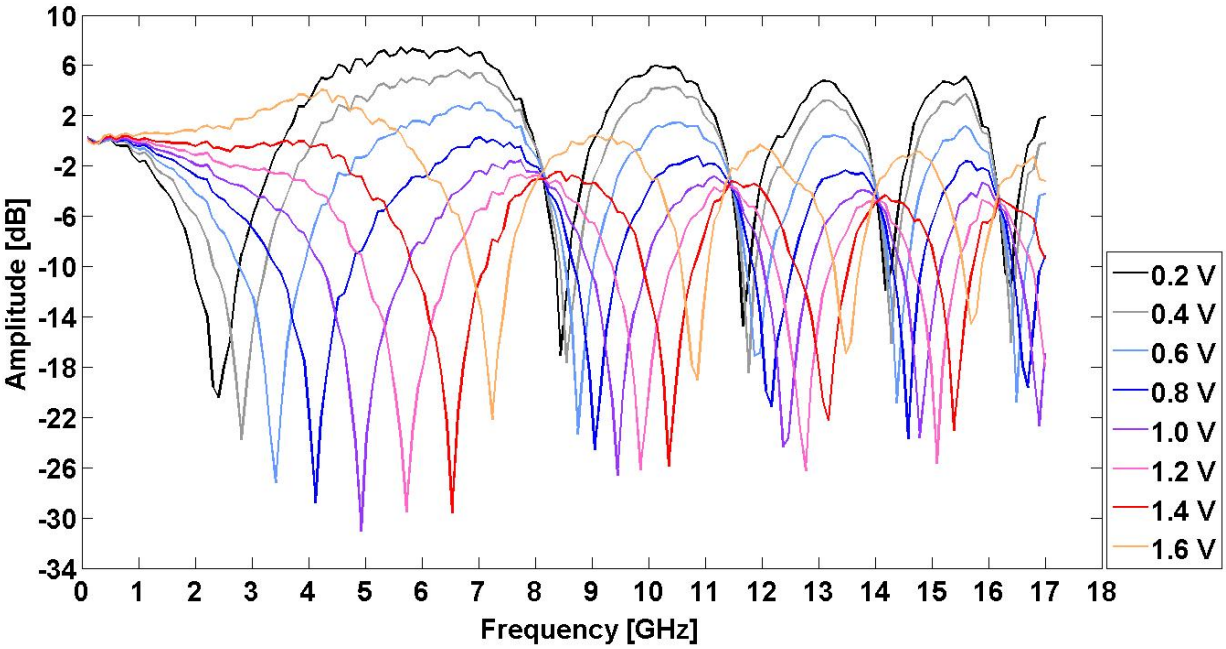

Figure A.25 – Amplitude response after the photodetection with a fiber of 100 km of length, a wavelength of 1579 nm and a laser output power level of 6.5 dBm for all the reerse bias voltage values

In figure A.24, it can be seen that, the frequency dips are well visible through the frequency sweep that was performed from the vector signal generator. Figure A.24 also shows that, the reverse bias voltages of 0.2, 0.4, 0.6, 0.8 and 1.0 V presents five sharp peeks while the reverse bias voltages

of 1.2, 1.4 and 1.6 V only present four. It can be seen from figure A.24 that, the reverse bias voltage of 1.6 V presents a resonance peak when comparing to the other reverse bias voltages values.

The amplitude response for the operating wavelength of 1579 nm and the minimum optical power of 3 dBm presents the same characteristics that figure A.25. Comparing to the amplitude response from figure A.24 to figure A.25, there is no major difference in the amplitude response considering the laser output power levels of 3 or 6.5 dBm.

Figure A.26 to A.33 presents the result achieved through a linear regression for all the reverse bias voltage values, a wavelength of 1575 and 1579 nm, a laser output power level of 3 dBm and the maximum of 7 dBm for 1575 nm or 6.5 dBm for 1579 nm.

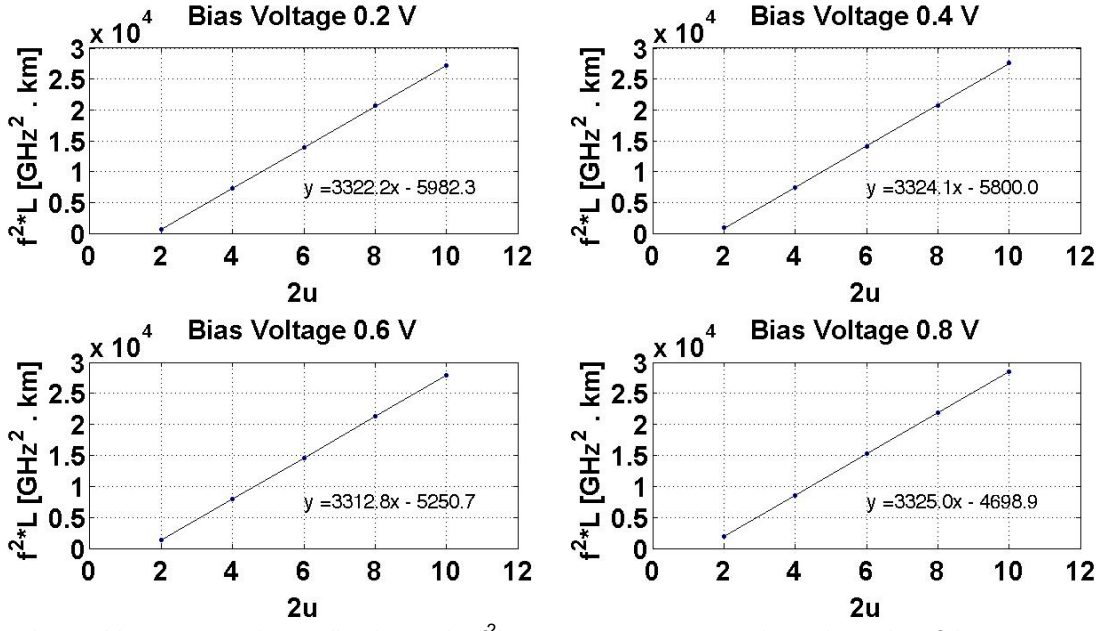

Figure A.26 – Linear regression realized over the f_u^2L parameter versus two times the order of the resonance for a wavelength of 1575 nm, a laser output power level of 3 dBm and the reverse bias voltage of 0.2 to 0.8 V

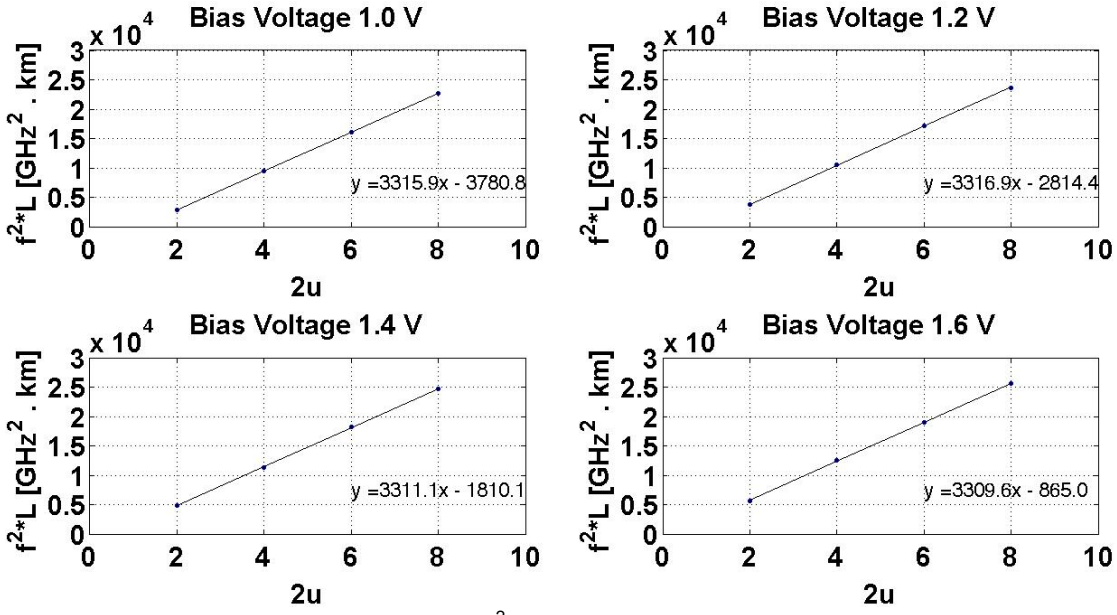

Figure A.27 – Linear regression realized over the f_u^2L parameter versus two times the order of the resonance for a wavelength of 1575 nm, a laser output power level of 3 dBm and the reverse bias voltage of 1.0 to 1.6 V

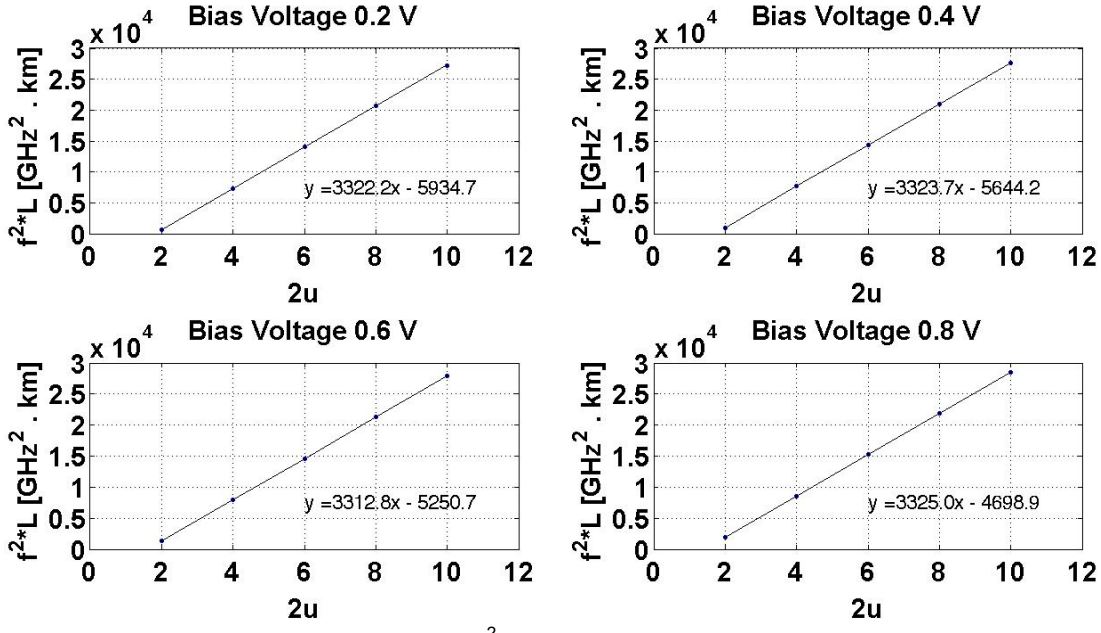

Figure A.28 – Linear regression realized over the f_u^2L parameter versus two times the order of the resonance for a wavelength of 1575 nm, a laser output power level of 7 dBm and the reverse bias voltage of 0.2 to 0.8 V

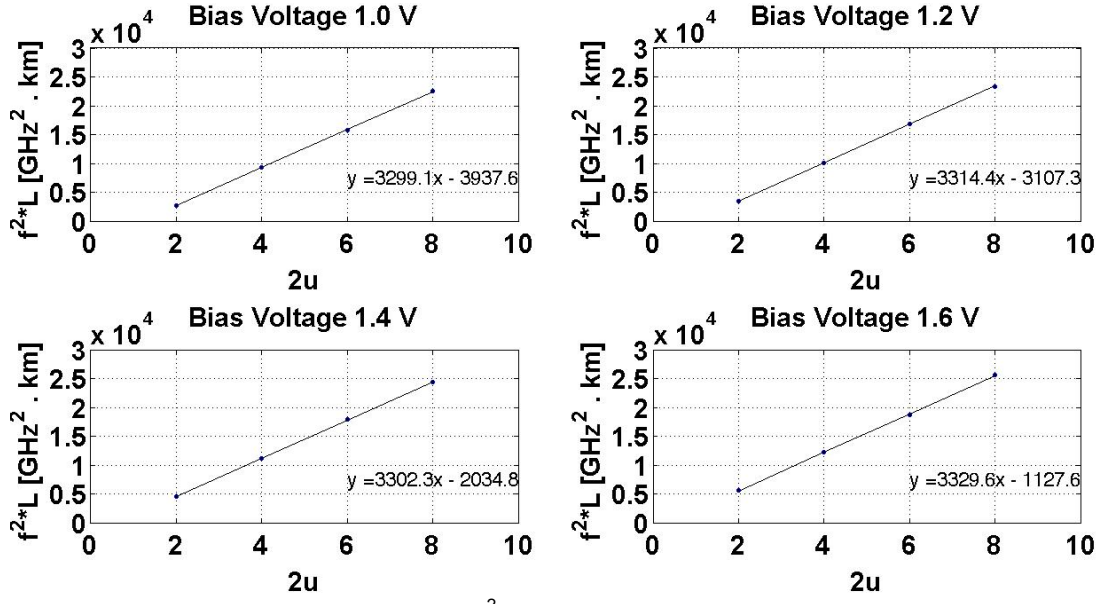

Figure A.29 – Linear regression realized over the f_u^2L parameter versus two times the order of the resonance for a wavelength of 1575 nm, a laser output power level of 7 dBm and the reverse bias voltage of 1.0 to 1.6 V

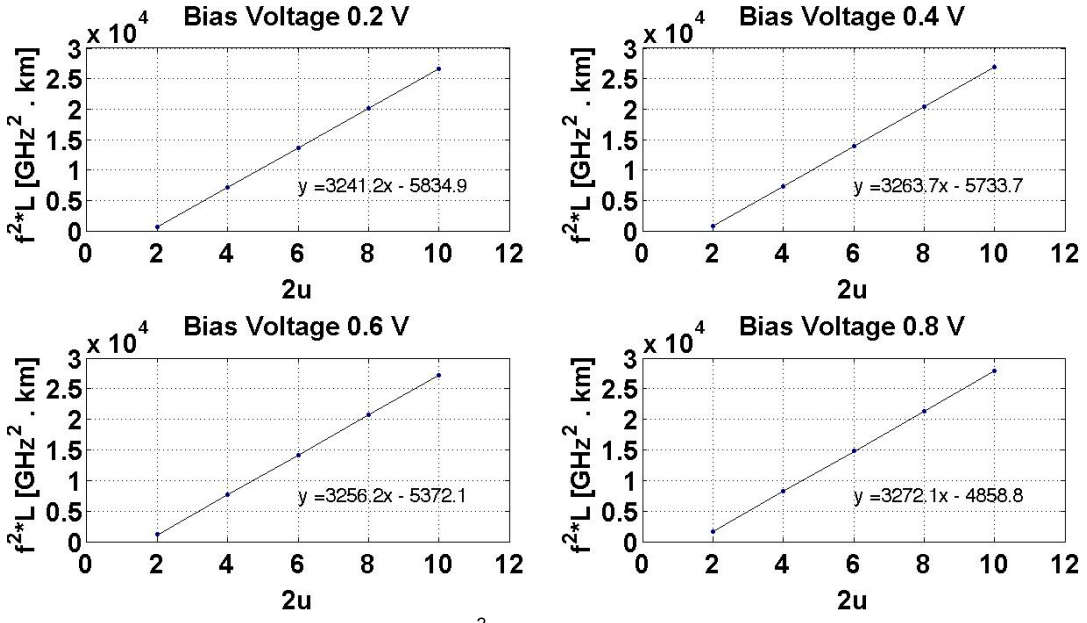

Figure A.30 – Linear regression realized over the f_u^2L parameter versus two times the order of the resonance for a wavelength of 1579 nm, a laser output power level of 3 dBm and the reverse bias voltage of 0.2 to 0.8 V

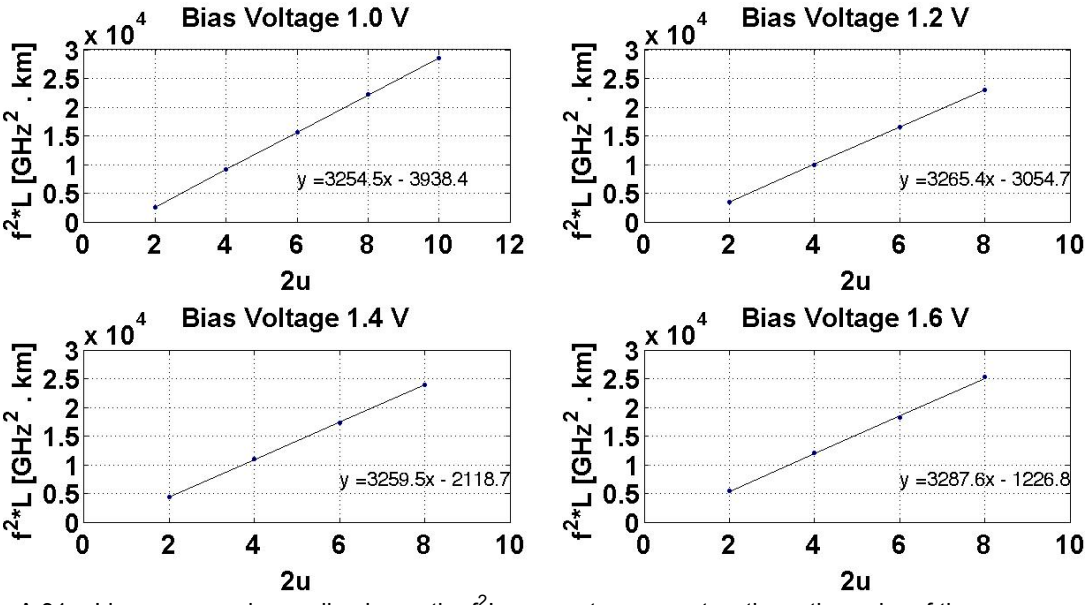

Figure A.31 – Linear regression realized over the f_u^2L parameter versus two times the order of the resonance for a wavelength of 1579 nm, a laser output power level of 3 dBm and the reverse bias voltage of 1.0 to 1.6 V

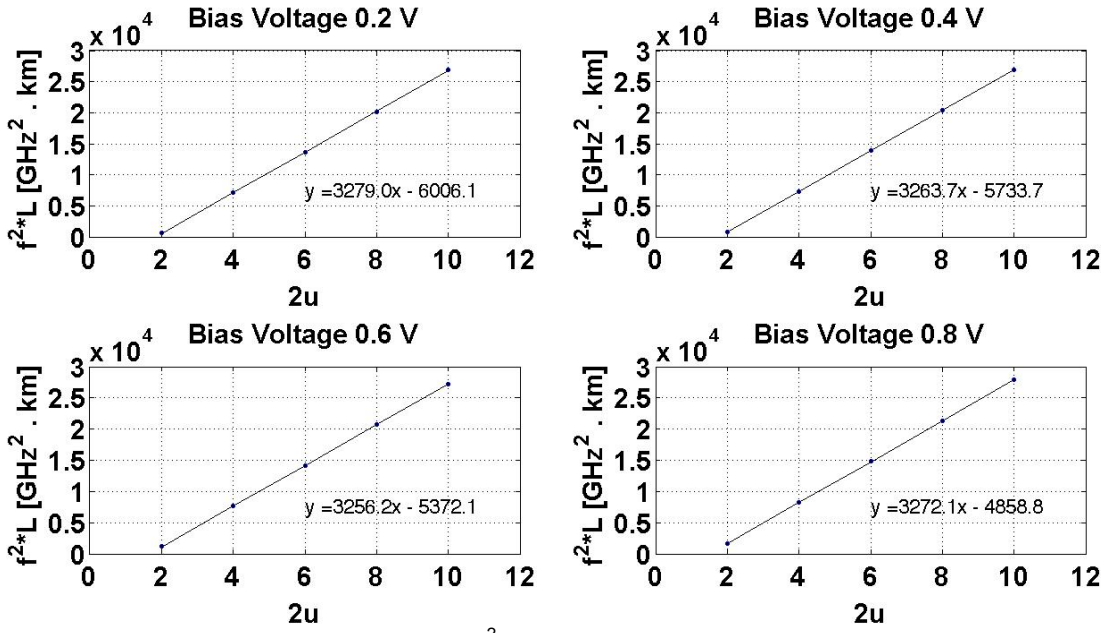

Figure A.32 – Linear regression realized over the f_u^2L parameter versus two times the order of the resonance for a wavelength of 1579 nm, a laser output power level of 6.5 dBm and the reverse bias voltage of 0.2 to 0.8 V

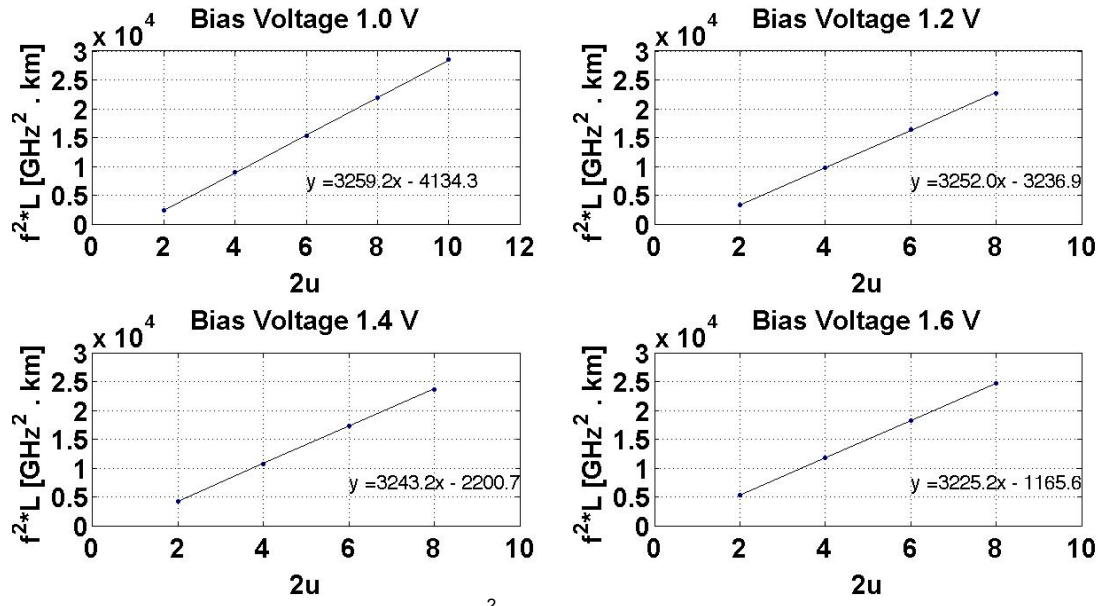

Figure A.33 – Linear regression realized over the f_u^2L parameter versus two times the order of the resonance for a wavelength of 1579 nm, a laser output power level of 6.5 dBm and the reverse bias voltage of 1.0 to 1.6 V

Inspection of figures A.26 to A.33 shows that the relation between the sharp dips and the points of the linear regression is still verified.

A.4 Comparison between experimental results and theoretical model approach to the amplitude response

In order to confirm the estimation through the theoretical process, two assessments were made. Figure A.34 shows the estimation for an operative wavelength of 1575 nm, a laser output power level of 3 dBm and a reverse bias voltage of 0.6 V (positive chirp value). This estimation was performed

with the Excel tool. In figure A.34 the value of dispersion factor used was 18.241 ps/(nm.km) and the value of the chirp parameter was 1.3103.

In figure A.35, it can be seen that the estimation for an operative wavelength of 1579 nm, a laser output power level of 6.5 dBm and a reverse bias voltage of 1.2 V (negative chirp value). In figure A.35, the value of dispersion factor used was 18.641 ps/(nm.km) and the value of the chirp parameter was -1.5682.

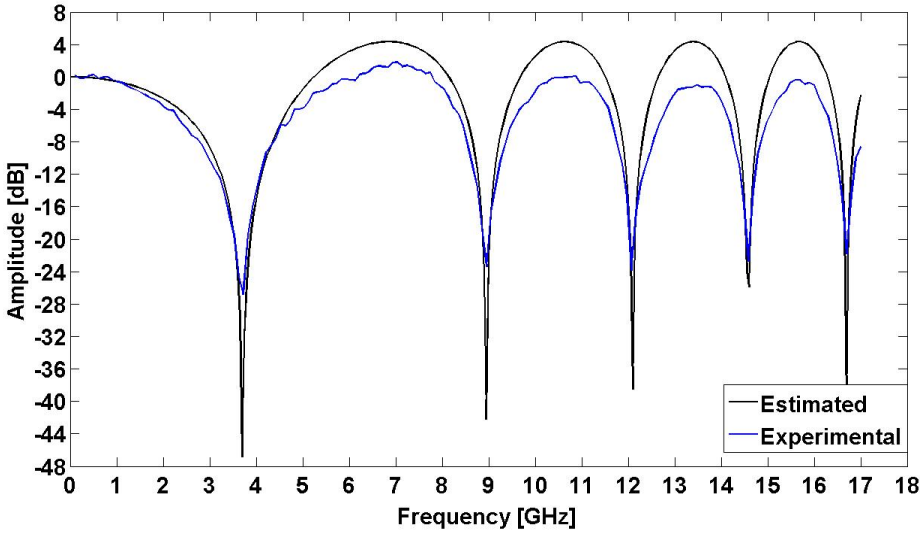

Figure A.34 – Comparison of the estimated amplitude response and the experimental amplitude response with a wavelength of 1575 nm, a laser output power level of 3 dBm and reverse bias voltage of 0.6 V

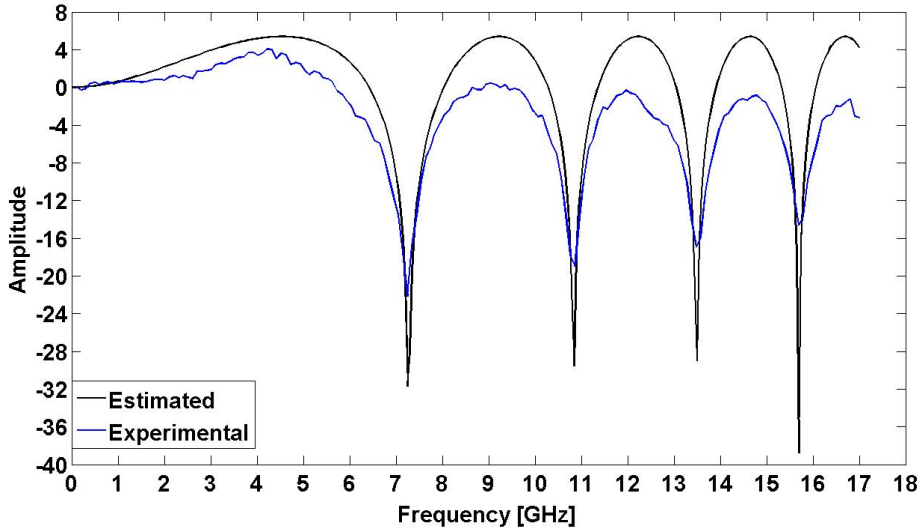

Figure A.35 – Comparison of the estimated amplitude response and the experimental amplitude response with a wavelength of 1579 nm, a laser output power level of 6.5 dBm and a reverse bias voltage of 1.2

Either figure A.34 and A.35 shows that, these two made estimations represent a very good approximation of the experimental measure. As it can be seen by figures A.34 and A.35, the position of the frequency dips of the estimation and the experimental measure are very similar. The behavior of the estimation amplitude response is also very similar to the experimental response, although some device limitations are presented. The experimental measure doesn't reach, for the frequency dips, the same amplitude response value of the estimation measure, because the sampling rate of the vector signal generator is smaller. The estimation was performed with 341 samples and the experimental

measurement was realized with 170 samples. This last validation finishes the dispersion and the chirp parameter for the EAM device.

Appendix B

Additional information for the experimental demonstration of a 10 Gbit/s signal in a downstream transmission employing an EAM

In this appendix, additional information of the experimental demonstration of a downstream transmission in a 10 Gbit/s system employing an EAM.

is presented. In section B.1, a calculation of the extinction ratio is presented. This section describes and identifies two extinction ratio scenarios from the optical power values found in the static characteristic measured in section 3.1 of chapter 3.

Section B.2 presents additional information of the experimental setup used for the evaluation of the performance of a 10 Gbit/s signal in a optic link, which emulates the downstream direction of a XG-PON1 architecture. In this section, some photographs of the setup deployed in the laboratory are presented.

In section B.3, additional information of waveforms of the 10 Gbit/s signal measured at the PIN output is presented. In this section, the waveforms of the 10 Gbit/s signal measured by the DSA are presented and analyzed. The waveforms presented in this section are measured considering the two extinction ratio scenarios defined in this work.

In section B.4, the waveforms of the 10 Gbit/s signal obtained by the BER measurement without optical fiber, are presented and analyzed. These waveforms are obtained considering the minimum extinction ratio scenario.

In section B.5, the waveforms of the 10 Gbit/s signal obtained by the BER measurement without optical fiber, are presented and analyzed. These waveforms are obtained considering the maximum extinction ratio scenario.

B.1 Calculation of the extinction ratio

It is important that the experimental demonstration shown is this work follows the standard given by XG-PON1. The standard indicates that the minimum value of the extinction ratio is 8.2 dB. In order to estimate the extinction ratio in this work some calculations had to made from the table A.1 presented in section A.1 of Appendix A. The reverse bias voltage of 0 V will be considered the reference voltage. The extinction ratio is calculated by subtracting all the optical powers of all the reverse bias voltage by the reference value, for each wavelength. Table B.1 presents the results of the calculation performed when making the reference value of 0 V.

	Operating Wavelength [nm] / Optical Power at the output of the laser source [dBm]											
Reverse bias [V]	1575				1577				1579			
	1	3	5	7	1	3	5	7	1	3	5	6.5
0.0	0	0	0	0	0	0	0	0	0	0	0	0
0.2	0.2	0.2	0.2	0.2	0.2	0.1	0.1	0.1	0.2	0.2	0.2	0.2
0.4	0.4	0.4	0.4	0.5	0.4	0.3	0.3	0.3	0.4	0.4	0.4	0.4
0.6	0.9	0.9	0.9	0.9	0.8	0.7	0.7	0.7	0.7	0.7	0.7	0.7
0.8	1.9	1.8	1.8	1.7	1.7	1.6	1.5	1.4	1.5	1.4	1.4	1.4
1.0	3.5	3.4	3.3	3.1	3.1	3	2.9	2.7	2.8	2.7	2.6	2.6
1.2	5.5	5.4	5.2	5	5.1	4.9	4.8	4.5	4.6	4.5	4.4	4.3
1.4	7.3	7.3	7.2	7	6.9	6.8	6.7	6.5	6.5	6.4	6.3	6.2
1.6	8.4	8.4	8.4	8.4	8.1	8	8	7.9	7.7	7.7	7.7	7.7
1.8	8.8	8.9	8.9	9	8.6	8.5	8.6	8.6	8.3	8.3	8.4	8.5
2.0	8.8	8.8	8.9	9.1	8.6	8.6	8.6	8.8	8.4	8.4	8.5	8.6

Table B.1 – Extinction ratio for all the operating wavelengths and optical input power values

The inspection of table B.1 reveals the maximum value of extinction ratio that this work permits. The reverse bias voltage of 2 V, with a wavelength of 1575 and an optical input power of 7 dB can achieve a maximum value of extinction ratio of 9.1 dB. From table B.1 it is also possible to identify the minimum value of 8.2 dB for extinction rate. This value is obtained between the reverse bias voltage of 0.6 and 2 V. This interval is defined close to the reverse bias voltage of 2 V because, when remembering the linear region identified in the static characterization of the EAM device performed in section 3.1 of chapter 3, the reverse bias voltage of 2 V is inside this linear region. This interval also results in negative values of the chirp parameter. These chirp parameter values are helpful, because they induced a negative dispersion, which will mitigate to the dispersion coming from the optical fiber. Therefore the reverse bias voltages between 0 and 0.5 V are not considered.

B.2 Photos of the devices, equipment and experimental setup

In this section, some photographs of the experimental setup implemented in the laboratory are presented.

The laser source used in this experimental demonstration is presented in figure B.1.

Figure B.1 – Laser source used in the experimental setup

In figure B.1 it is possible to see the laser source used. In this device it is possible to control the operating wavelength and the optical power level. This optical source is a tunable laser source.

The EAM device used in the experimental demonstration is presented in figure B.2

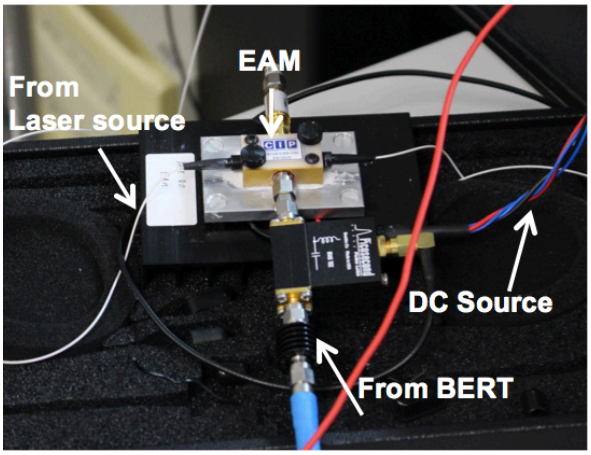

Figure B.2 – EAM device used in the experimental demonstration

From figure B.2 it is possible to see all the connections of the EAM device. From figure B.2 it is possible the fiber cable coming from the laser source which carriers the optical power. Applied to the EAM device is a module that is connected to the DC source and to the BERT device. Also it is possible to see from figure B.2 that applied to the electric module is another DC source, which controls the EAM temperature.

Some of the DC sources used in this experimental demonstration are presented in figure B.3

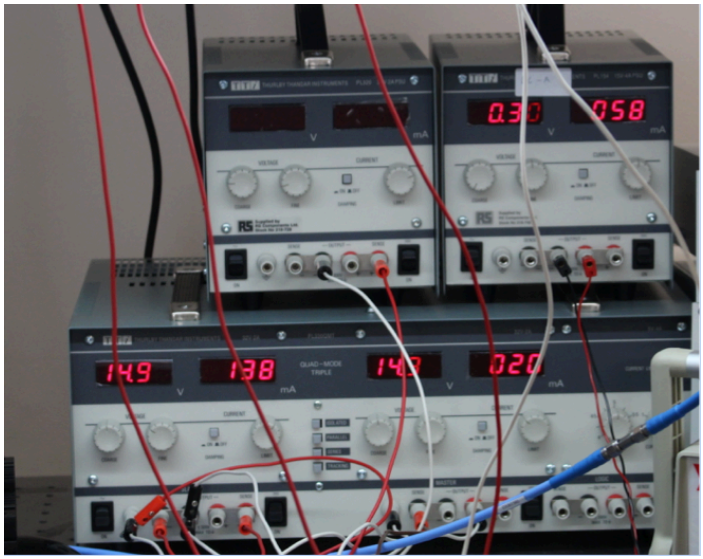

Figure B.3 –DC sources used in the experimental demonstration

From figure B.3, it is possible to see some of the DC sources and their current and amplitude values. For example, the DC source on the bottom is the one that is connected to the EAM device, which controls the temperature of the optical modulator.

The optical amplifier used in the experimental demonstration is presented in figure B.4.

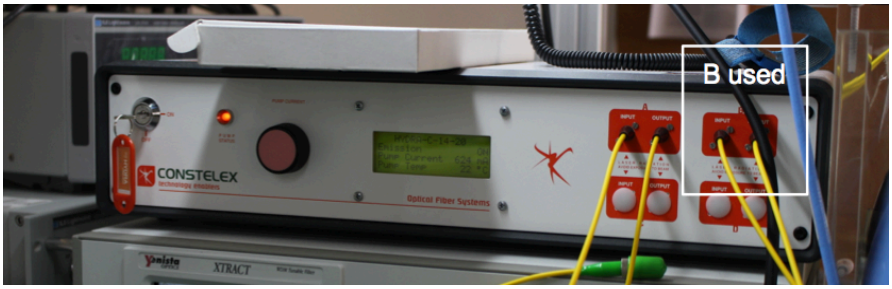

Figure B.4 – Optical amplifier used in the experimental demonstration

From figure B.4, it is possible to see the optical fiber cables coming from the EAM device and optical cables leaving the optical amplifier and going to the optical filter. As it was stated in section 3.3 of chapter 3, this optical amplifier amplifies the optical power level at the device's input into the optical level value of around 14 dBm.

The optical filter used in the experimental demonstration is presented in figure B.5.

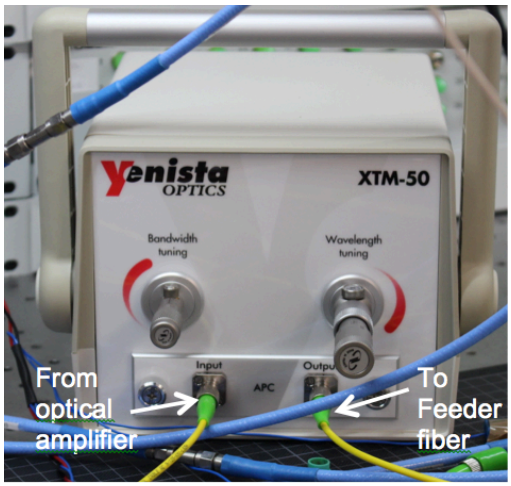

Figure B.5 – Optical filter used in the experimental demonstration

Figure B.5 shows the optical filter used to filter the optical power level at a chosen operating wavelength. In figure B.5 it is possible to see the tunable buttons used to search through the wavelength domain.

In figure B.6, it can be seen the optical fiber cables used in the experimental demonstration to implement a feeder fiber length of 20 km after the optical filter.

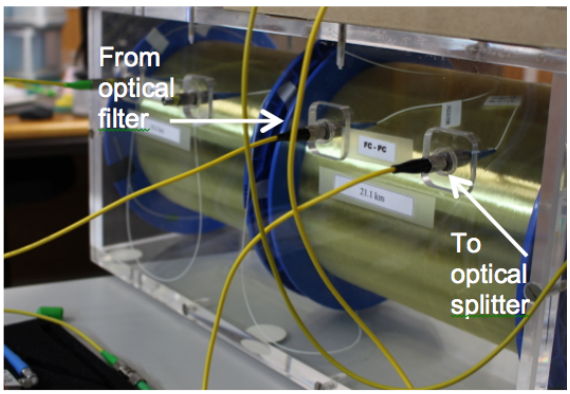

Figure B.6 – Optical fiber cable to used to implement a fiber length of 20 km

Figures B.7 and B.8 shows the optical splitters used in this experimental demonstration.

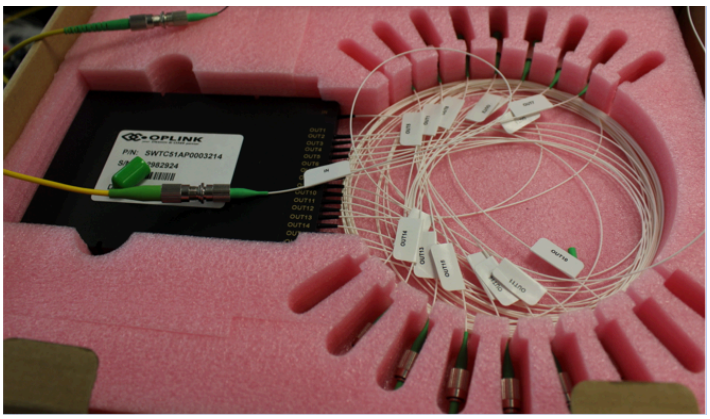

Figure B.7 – Optical splitter with splitting factor of 1/16

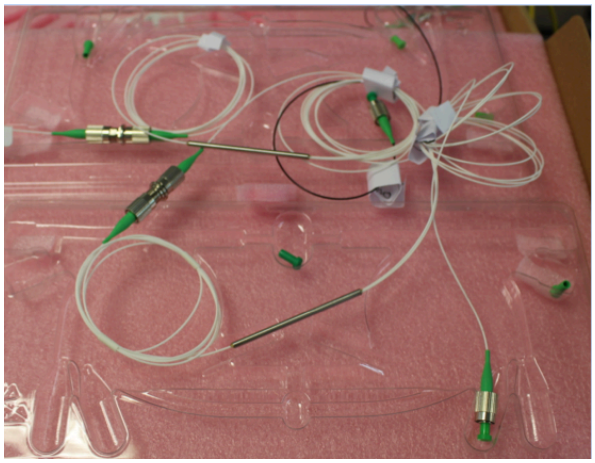

Figure B.8 – Optical splitters with splitting factor of 1/2

Figure B.9 shows the PIN photodetector used in this experimental demonstration.

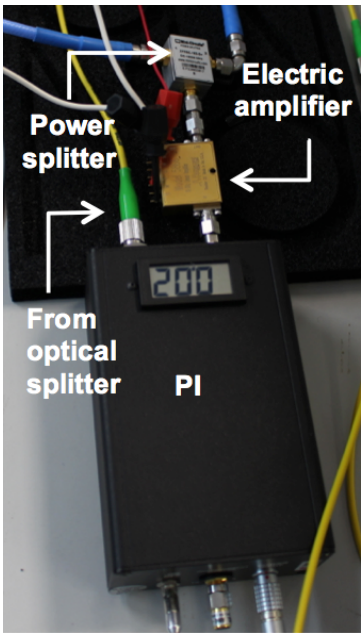

Figure B.9 – PIN device used in the experimental demonstration

From figure B.9, it is possible to see the electric amplifier and the electric splitter already described in section 4.1 of chapter 4.

The BERT and the DSA are presented in figure B.10

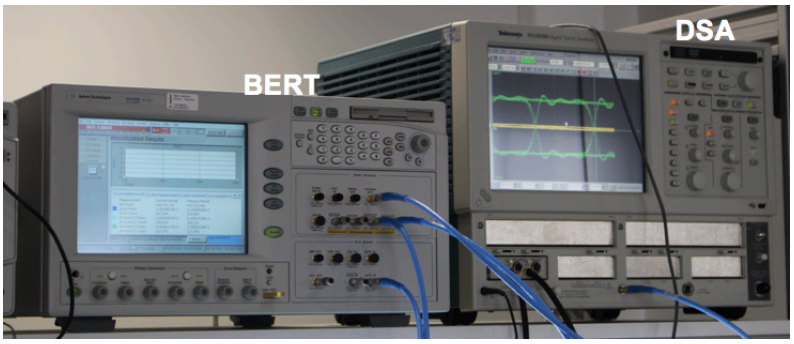

Figure B.10 – BERT and DSA devices used in the experimental demonstration

Figures B.11 and B.12 shows an overall layout of the setup implemented in the laboratory.

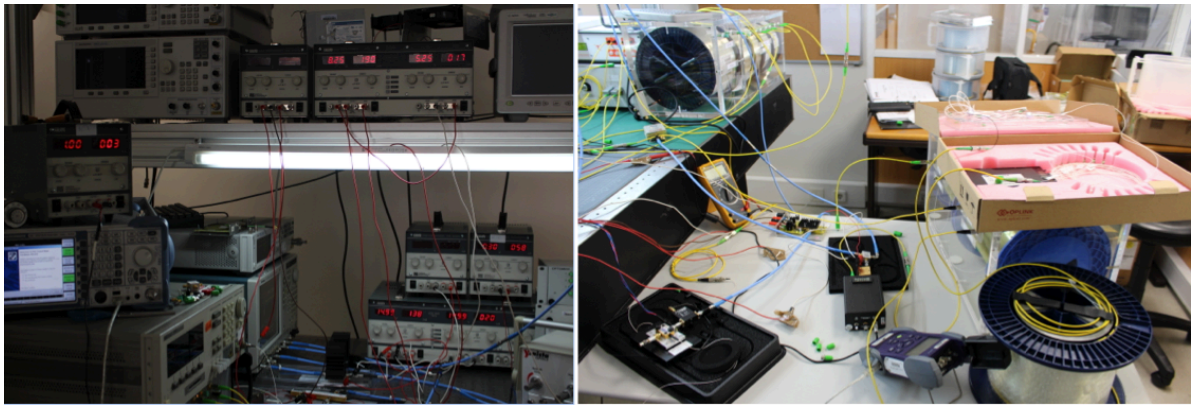

Figure B.11 and B.12 – Overall setup implemented in the laboratory

B.3 Waveforms of the 10 Gbit/s signal measured at the PIN output

In this section, the additional waveforms of the 10 Gbit/s signal measured at the PIN output are presented. The waveform measured at the Pin device output, considering the minimum extinction ratio scenario, distribution fiber of 0 km and an optical splitter of 1/16 is presented in figure 4.4, located in section 4.2 of chapter 4. After this measurement, optical fiber sections of 5 km were added to the distribution fiber. The result of all the waveforms of the 10 Gbit/s signal at the PIN output considering a minimum extinction ratio scenario, a splitting factor of 1/16, an operating wavelength of 1575 nm, and all fiber sections used are presented in figure B.13.

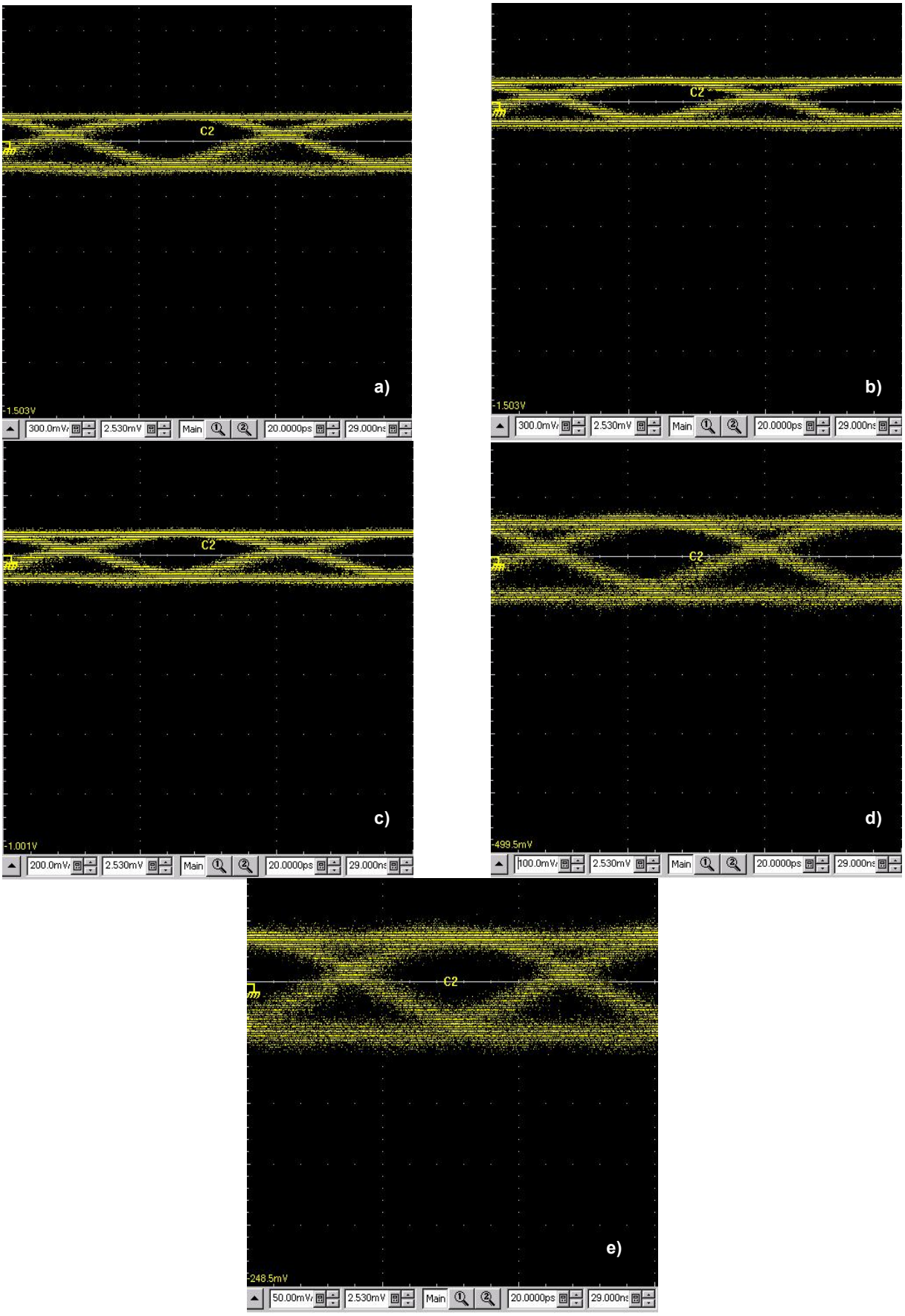

Figure B.13 - Waveforms of the 10 Gbit/s signal at the PIN output with a splitting factor of 1/16, considering the minimum extinction ratio scenario and fiber sections of a) 5 km, b) 10 km, c) 15 km, d) 25 km and e) 30 km

From figure B.13 it is possible to see that, the amplitude of the waveform at the PIN's input is decreasing with each fiber section added. The definition of the eye in the eye diagram is also declining with each fiber section. In figure B.13 e) it is possible to see the dispersion present in a fiber section of 30 km. With this fiber section, the vertical scale was changed to 50 mV in order to see that, the eye for this waveform is almost closed.

The result of all the waveforms of the 10 Gbit/s signal at the PIN output considering a minimum extinction ratio scenario, a splitting factor of 1/32, an operating wavelength of 1575 nm, and all fiber sections used are presented in figure B.14.

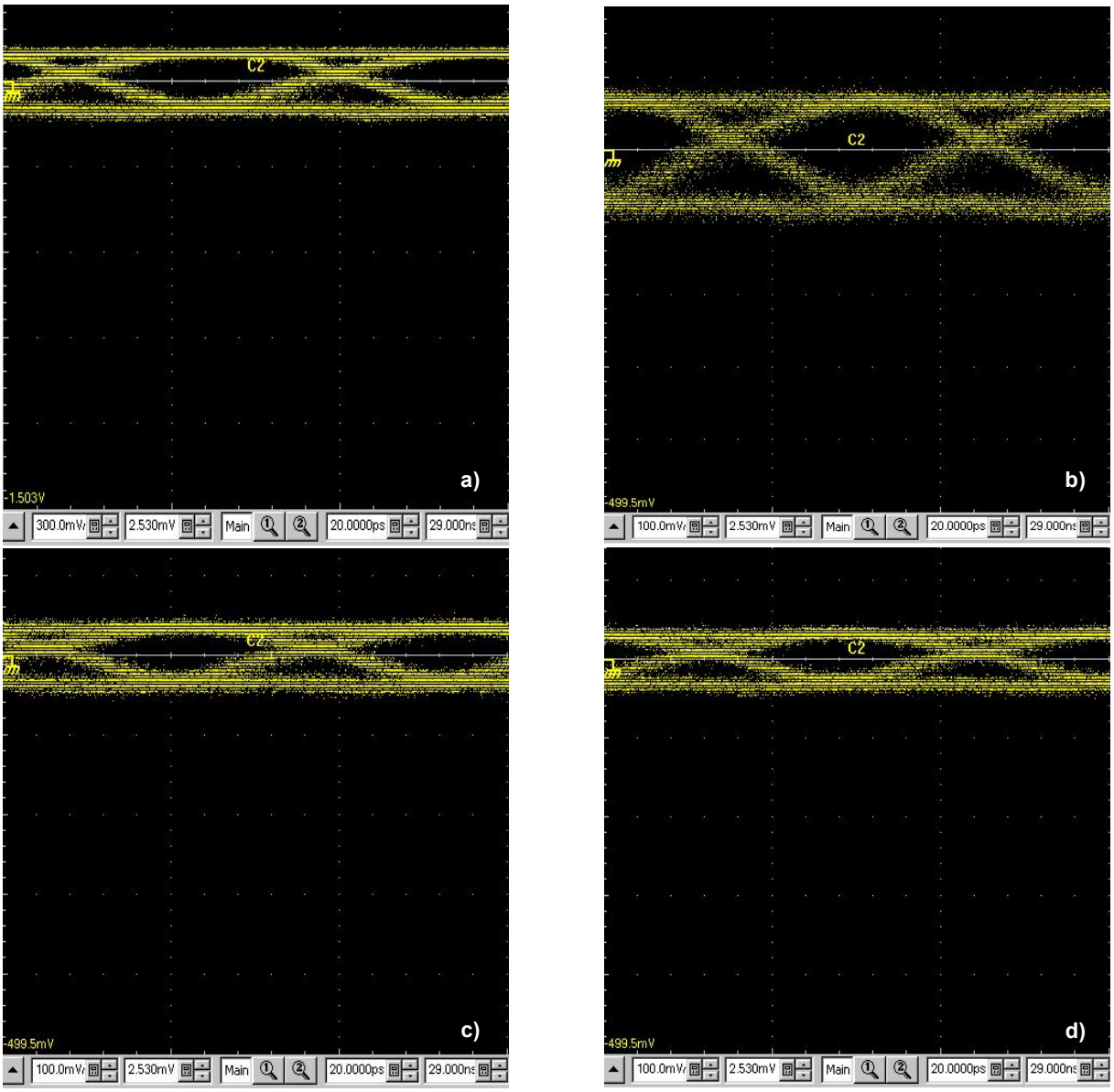

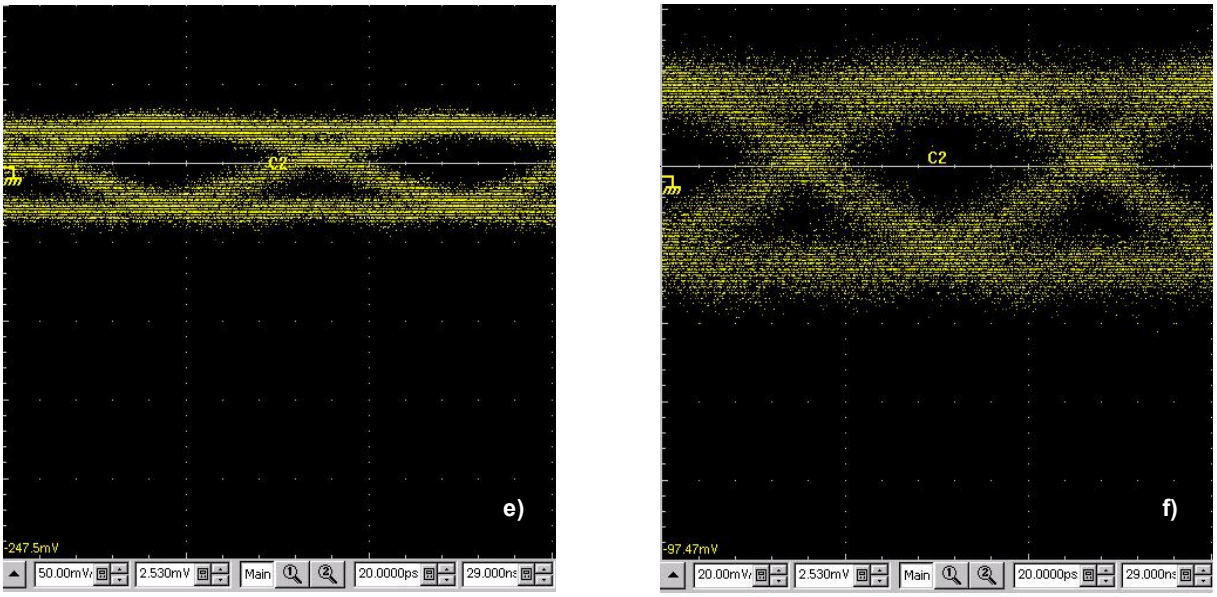

Figure B.14 - Waveforms at the PIN output with a splitting factor of 1/32, considering the minimum extinction ratio scenario and fiber sections of a) 0 km, b) 5 km, c) 10 km, d) 15 km, e) 25 km and f) 30 km

From figure B.14 it is possible to see that, the amplitude of the waveform at the PIN's input is decreasing with each fiber section added. The definition of the eye in the eye diagram is also declining with each fiber section. In figure B.14 e) it is possible to see the dispersion and noise present in a fiber section of 30 km. With this fiber section, the vertical scale was changed to 20 mV in order to see that, the eye for this waveform is almost closed and the dispersion is considerably visible and present.

The result of all the waveforms at the PIN output considering a minimum extinction ratio scenario, a splitting factor of 1/64, an operating wavelength of 1575 nm, and all fiber sections used are presented in figure B.15.

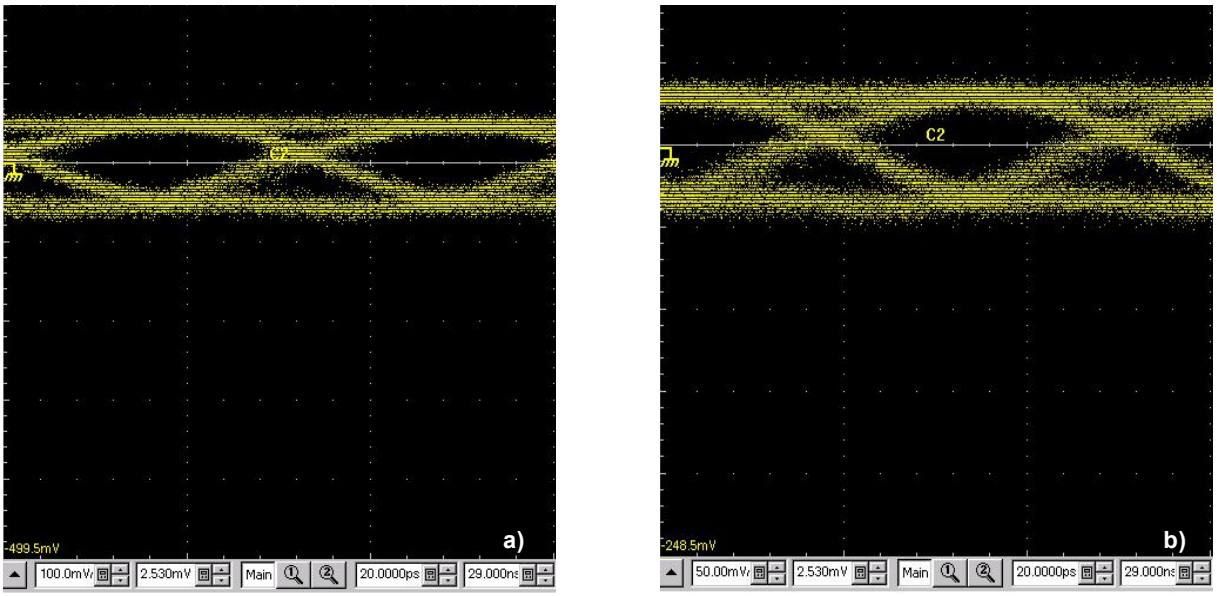

Figure B.15 - Waveforms of the 10 Gbit/s signal at the PIN output with a splitting factor of 1/64, considering the minimum extinction ratio scenario and fiber sections of a) 0 km and b) 5 km

Figure B.15 b) presents the waveform with the most losses because it using a splitting factor of 1/64 and a optical fiber section of 5 km. The waveform from figure B.15 a) presents a well defined eye however, the vertical scale had to be change to 100 mV in order to see it because it is slightly closed.

B. ADDITIONAL INFORMATION FOR THE EXPERIMENTAL DEMONSTRATION OF A 10 GBIT/S SIGNAL IN A DOWNSTREAM TRANSMISSION EMPLOYING AN EAM

With the fiber section of 5 km, the vertical scale was changed to 50 mV in order to see that, the eye for this waveform is almost closed and the dispersion is considerably visible and present.

The result of all the waveforms of the 10 Gbit/s signal at the PIN output considering a minimum extinction ratio scenario, a splitting factor of 1/16, an operating wavelength of 1579 nm, and all fiber sections used are presented in figure B.16.

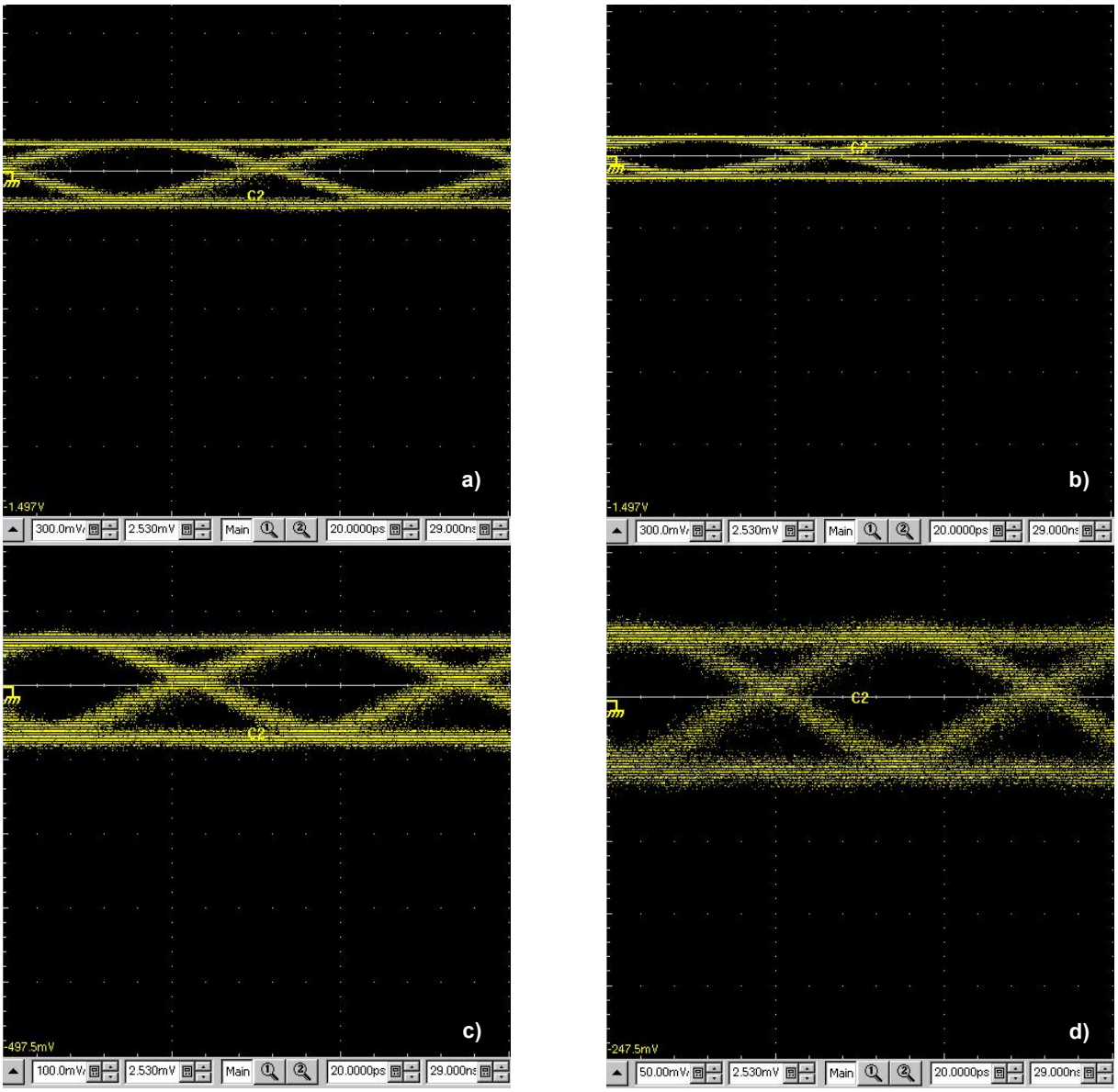

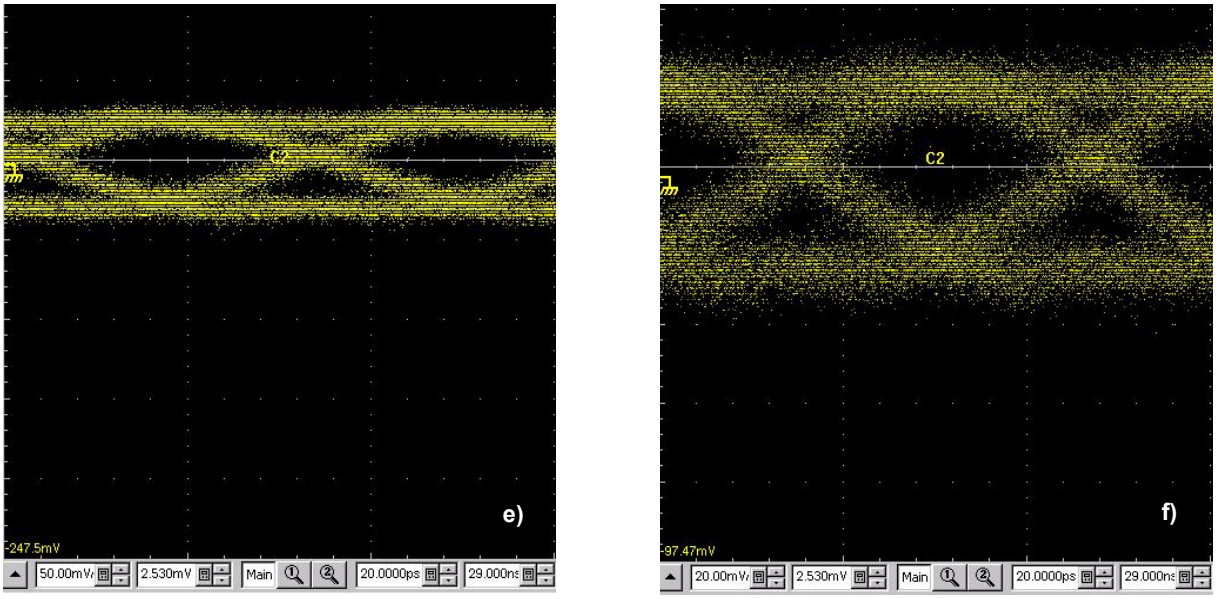

Figure B.16 - Waveforms at the PIN output with a splitting factor of 1/16, considering the minimum extinction ratio scenario and fiber sections of a) 0 km, b) 5 km, c) 10 km, d) 15 km, e) 25 km and f) 30 km

From figure B.16 it is possible to see that, the amplitude of the waveform at the PIN's input is decreasing with each fiber section added. The definition of the eye in the eye diagram is also declining with each fiber section. In figure B.16 e) it is possible to see that the dispersion and noise are considerably visible and present in the fiber section of 30 km. With this fiber section, the vertical scale was changed to 20 mV in order to see that, the eye for this waveform is almost closed.

The result of all the waveforms at the PIN output considering a minimum extinction ratio scenario, a splitting factor of 1/32, an operating wavelength of 1579 nm, and all fiber sections used are presented in figure B.17.

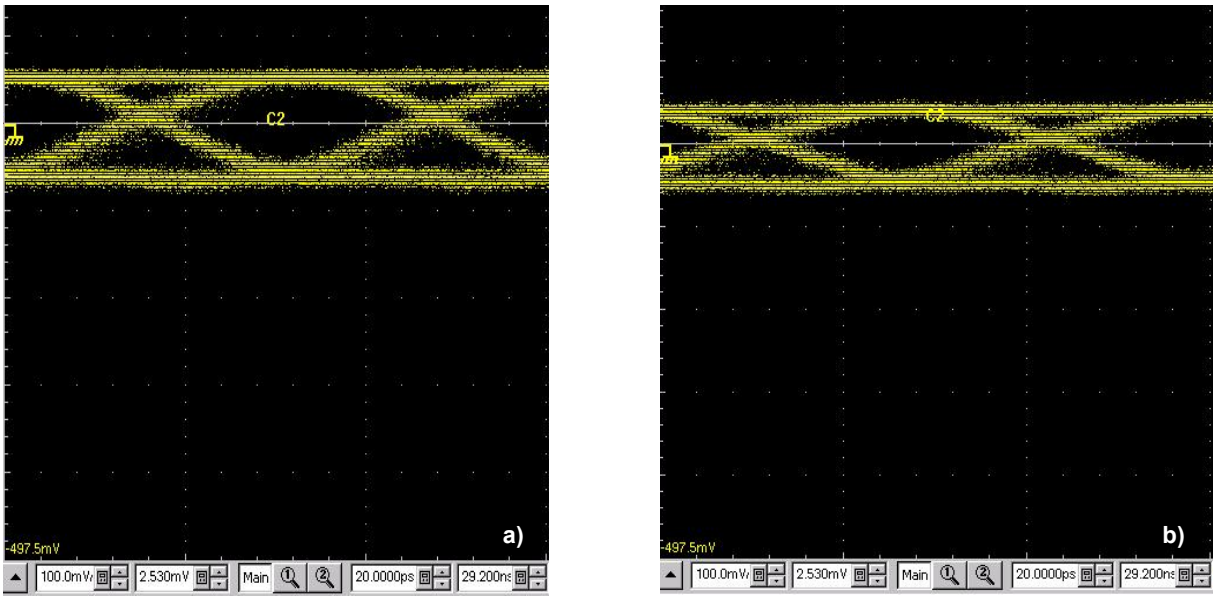

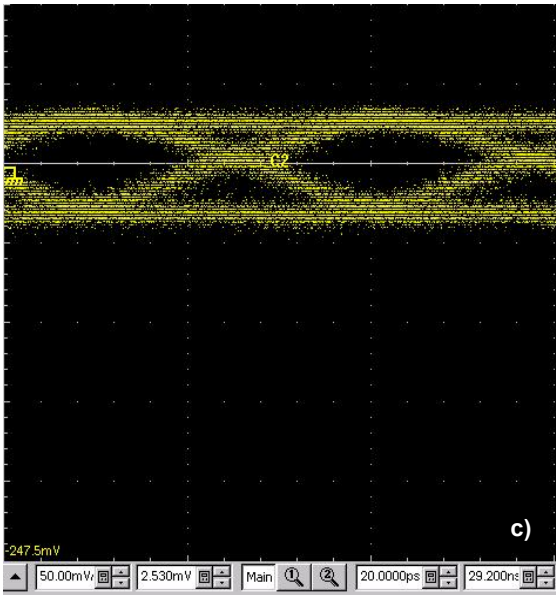

Figure B.17 - Waveforms at the PIN output with a splitting factor of 1/32, considering the minimum extinction ratio scenario and fiber sections of a) 0 km, b) 5 km and c) 10 km

From figure B.17 it is possible to see that, the amplitude of the waveform at the PIN's input is decreasing with each fiber section added. The definition of the eye in the eye diagram is also declining with each fiber section. In figure B.17 c) it is possible to see that the dispersion and noise are considerably visible and present in the fiber section of 10 km. With this fiber section, the vertical scale was changed to 50 mV in order to see that, the eye for this waveform is almost closed.

The result of all the waveforms of the 10 Gbit/s signal at the PIN output considering a minimum extinction ratio scenario, a splitting factor of 1/64, an operating wavelength of 1579 nm, and all fiber sections used are presented in figure B.18.

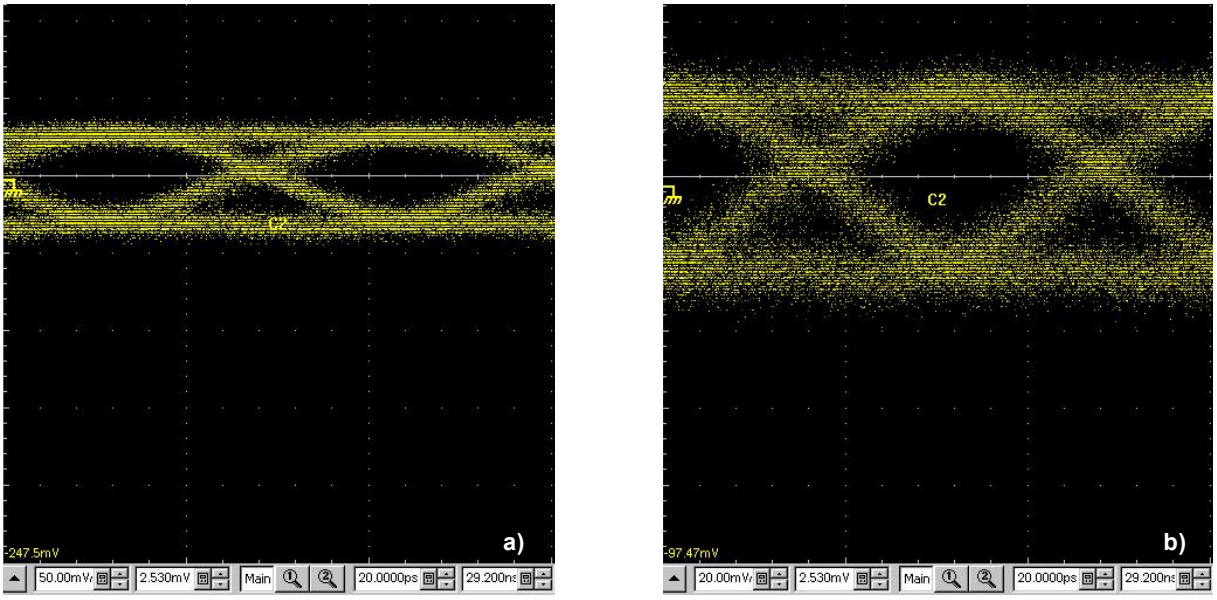

Figure B.18 - Waveforms at the PIN output with a splitting factor of 1/64, considering the minimum extinction ratio scenario and fiber sections of a) 0 km and b) 5 km

From figure B.18 it is possible to see that, the amplitude of the waveform at the PIN's input is decreasing with each fiber section added. The definition of the eye in the eye diagram is also declining

with each fiber section. Figure B.18 b) presents the waveform with the most losses because it using a splitting factor of 1/64 and a optical fiber section of 5 km. The waveform from figure B.18 a) presents a well defined eye however, the vertical scale had to be change to 50 mV in order to see it because it is slightly closed. With the fiber section of 5 km, the vertical scale was changed to 20 mV in order to see that, the eye for this waveform is almost closed and the dispersion is considerably visible and present.

The result of all the waveforms of the 10 Gbit/s signal at the PIN output considering a maximum extinction ratio scenario, a splitting factor of 1/16, an operating wavelength of 1575 nm, and all fiber sections used are presented in figure B.19.

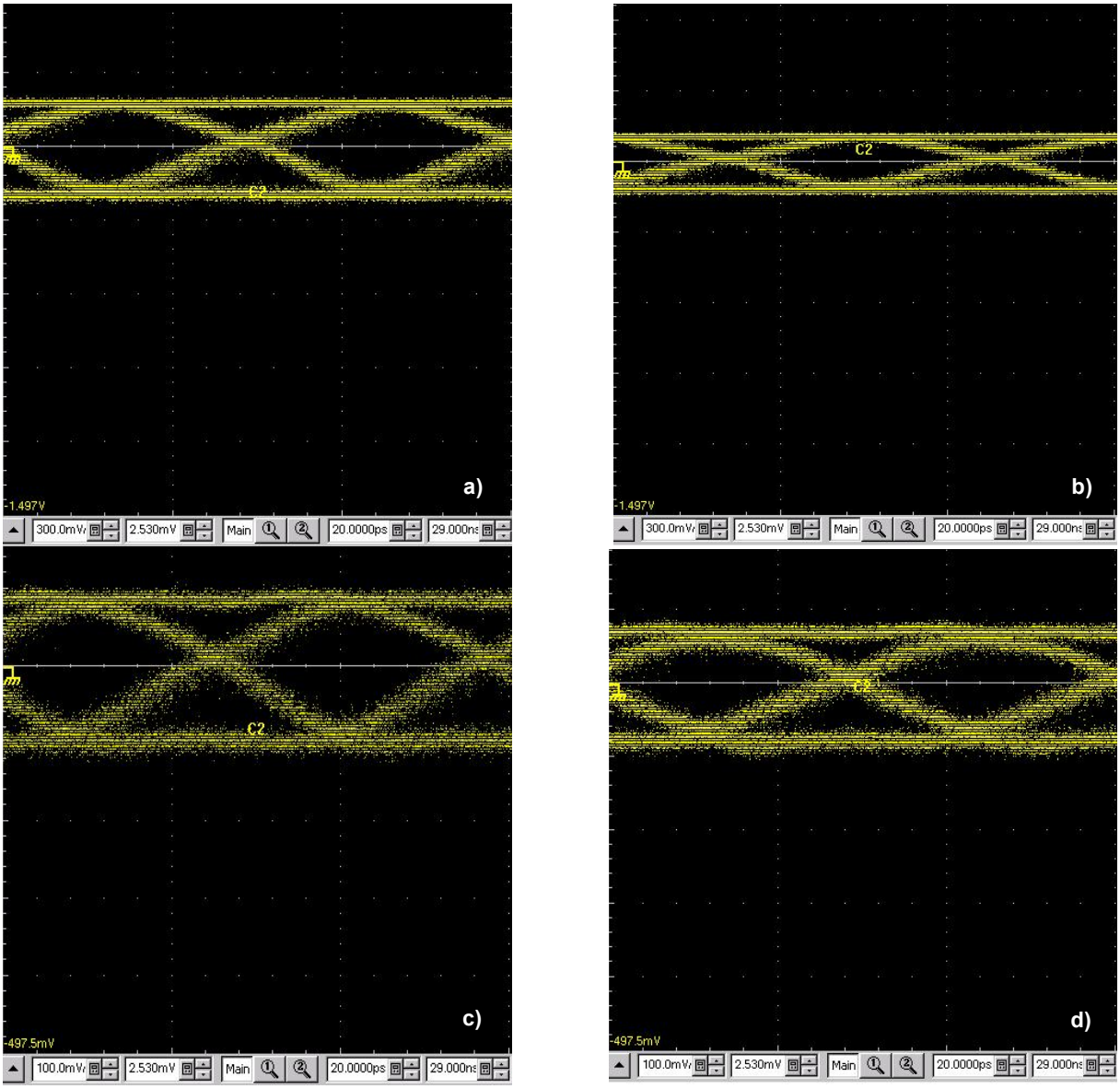

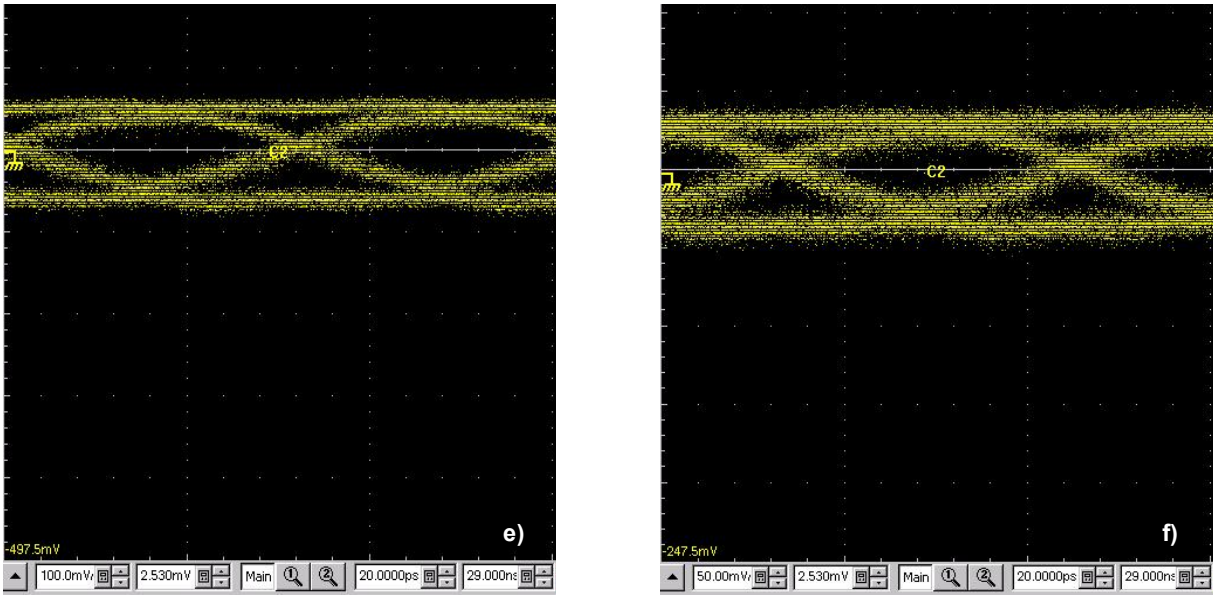

Figure B.19 - Waveforms at the PIN output with a splitting factor of 1/16, considering the maximum extinction ratio scenario and fiber sections of a) 5 km, b) 10 km, c) 15 km, d) 25 km, e) 30 km and f) 35 km

From figure B.19 it is possible to see that, the amplitude of the waveform at the PIN's input is decreasing with each fiber section added. The definition of the eye in the eye diagram is also declining with each fiber section. From figure B.19 e) and f), it is possible to see that the dispersion and noise are considerably visible and present in the fiber section of 30 and 35 km. With these fiber sections, the vertical scale was changed to 100 and 50 mV in order to see that, the eye for this waveform is almost closed.

The result of all the waveforms of the 10 Gbit/s signal at the PIN output considering a maximum extinction ratio scenario, a splitting factor of 1/32, an operating wavelength of 1575 nm, and all fiber sections used are presented in figure B.20.

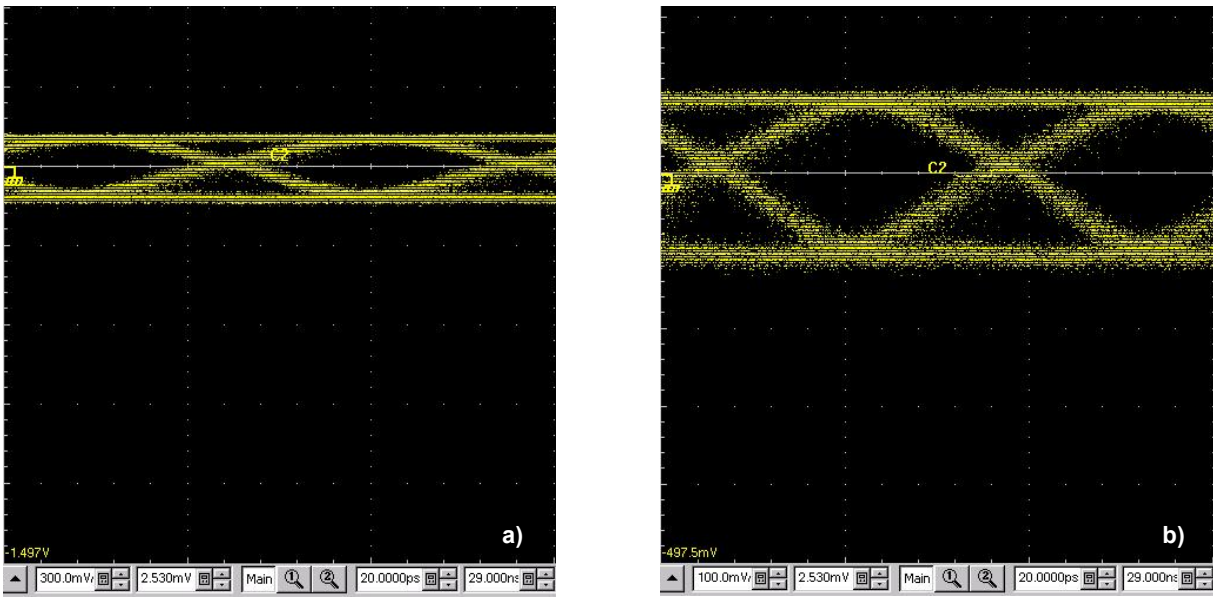

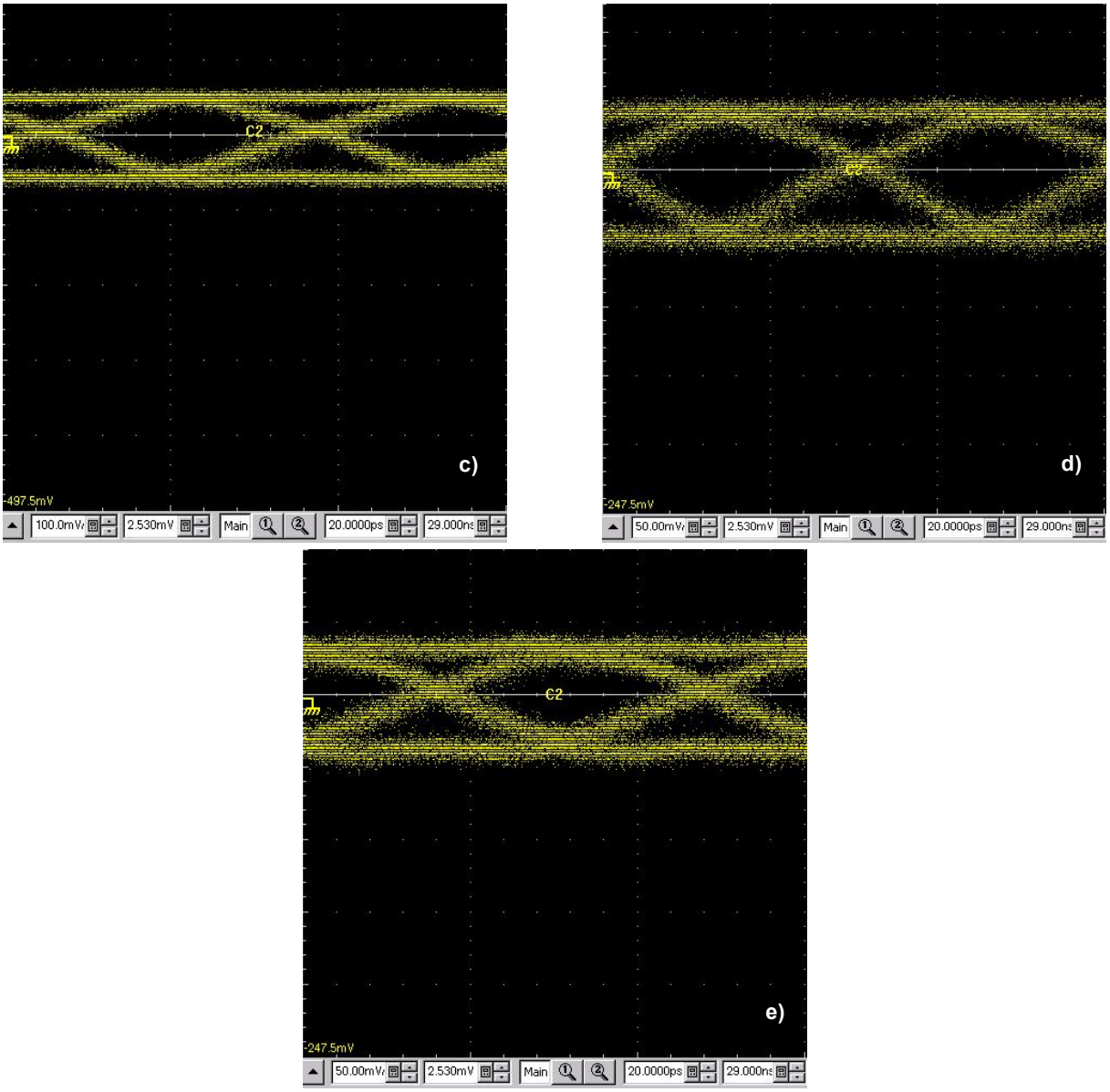

Figure B.20 - Waveforms at the PIN output with a splitting factor of 1/32, considering the maximum extinction ratio scenario and fiber sections of a) 0 km, b) 5 km, c) 10 km, d) 15 km and e) 25 km

From figure B.20 it is possible to see that, the amplitude of the waveform at the PIN's input is decreasing with each fiber section added. The definition of the eye in the eye diagram is also declining with each fiber section. From figure B.20 d) and e), it is possible to see that the dispersion and noise are considerably visible and present in the fiber section of 15 and 25 km. With these fiber sections, the vertical scale was changed to 50 mV in order to see that, the eye for this waveform is almost closed.

The result of all the waveforms of the 10 Gbit/s signal at the PIN output considering a maximum extinction ratio scenario, a splitting factor of 1/64, an operating wavelength of 1575 nm, and all fiber sections used are presented in figure B.21.

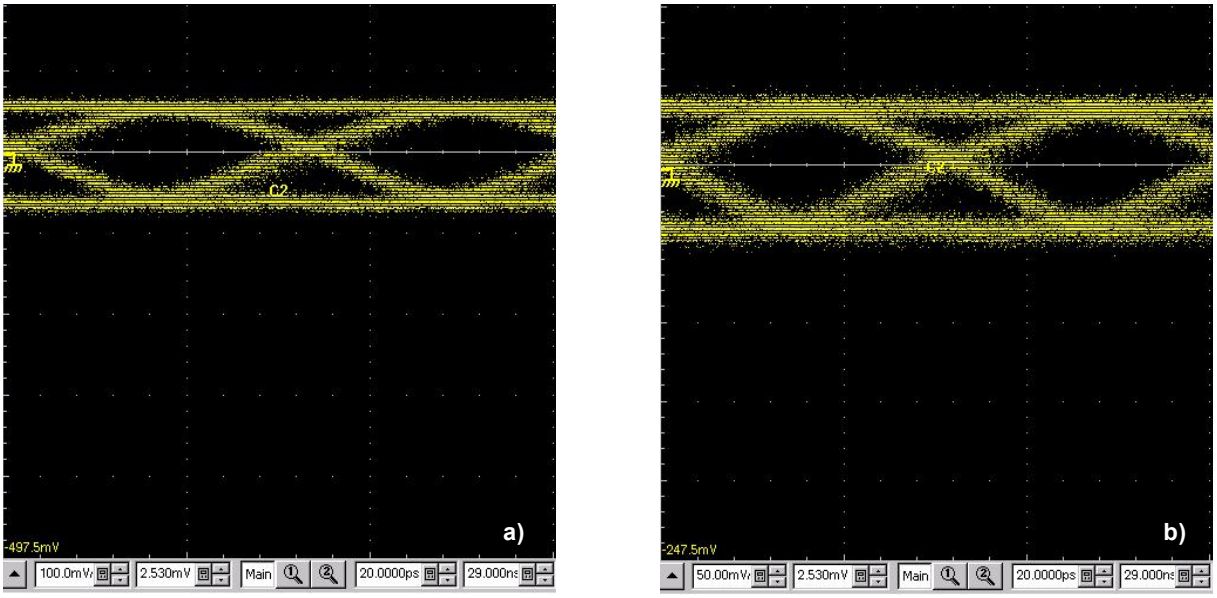

Figure B.21 - Waveforms at the PIN output with a splitting factor of 1/64, considering the maximum extinction ratio scenario and fiber sections of a) 0 km and b) 5 km

From figure B.21 it is possible to see that, the amplitude of the waveform at the PIN's input is decreasing with each fiber section added. The definition of the eye in the eye diagram is also declining with each fiber section. Figure B.21 b) presents the waveform with the most losses because it using a splitting factor of 1/64 and a optical fiber section of 5 km. The waveform from figure B.21 a) presents a well defined eye however, the vertical scale had to be change to 100 mV in order to see it because it is slightly closed. With the fiber section of 5 km, the vertical scale was changed to 50 mV in order to see that, the eye for this waveform is almost closed and the dispersion and noise are considerably visible and present.

B.4 Waveforms of the 10 Gbit/s signal obtained by the BER measurement without optical fiber, considering the minimum extinction ratio scenario

The result of all the waveforms of the 10 Gbit/s signal at the PIN output considering a minimum extinction ratio scenario, a splitting factor of 1/16, an operating wavelength of 1575 nm, and all attenuation values used to simulate the optical fiber path loss are presented in figure B.22

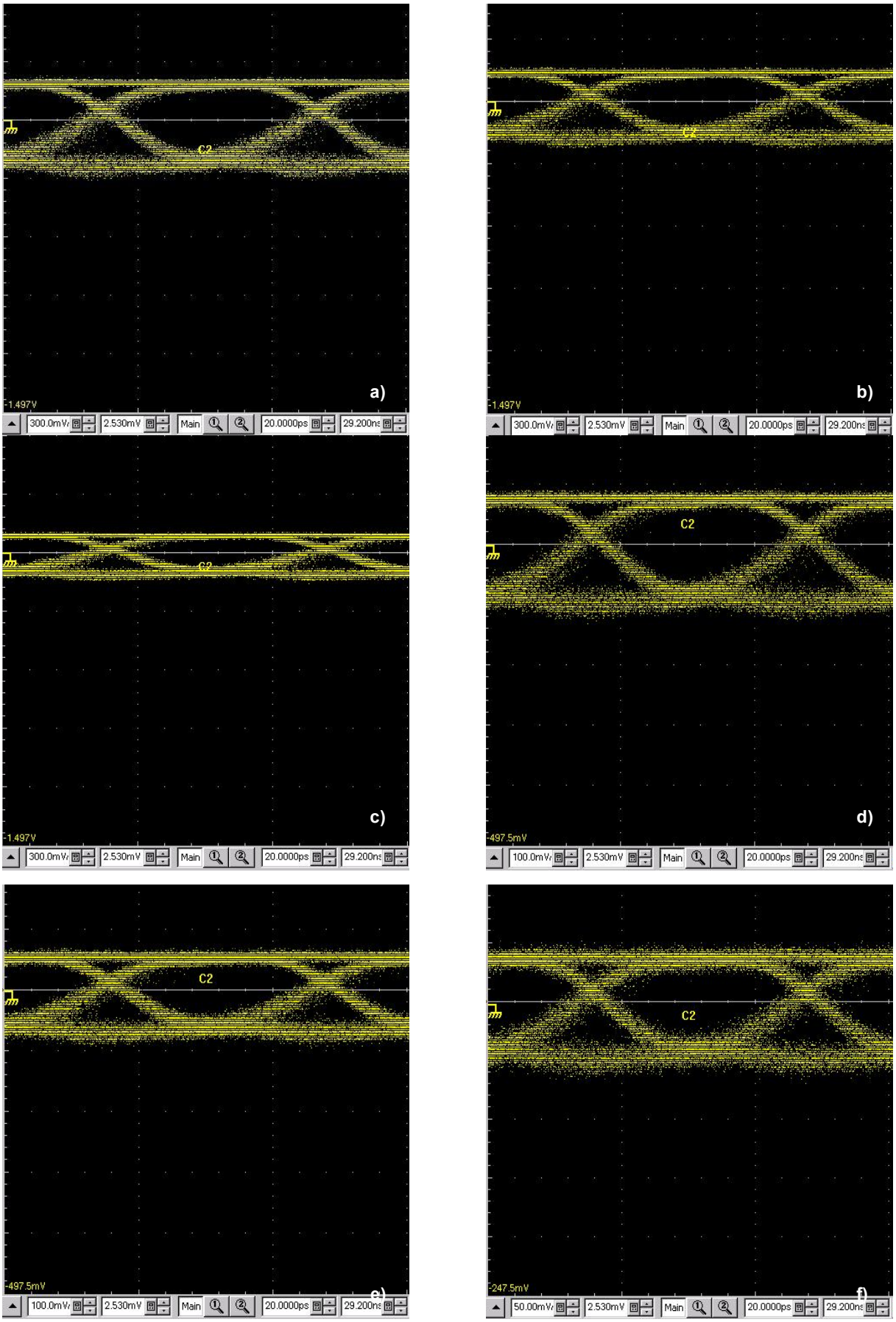
C2
-1.497V
300.0mV
2.530mV
Main
20.0000ps
29.200ns
a)
b)
c)
-497.5mV
100.0mV
d)
-247.5mV
50.00mV
e)
f)

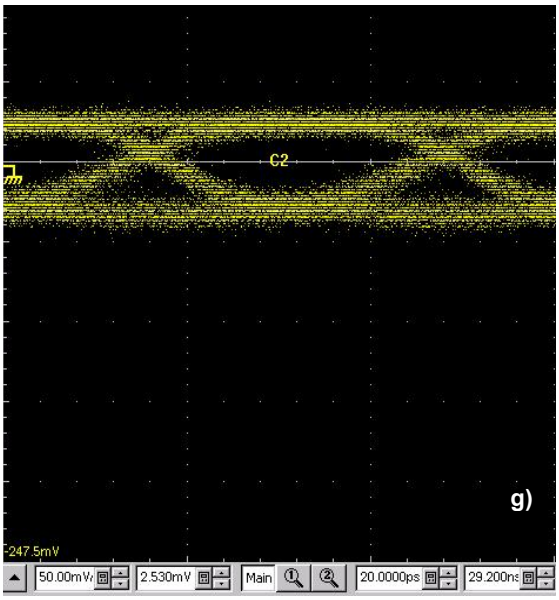

Figure B.22 - Waveforms at the PIN output with a splitting factor of 1/16, considering the minimum extinction ratio scenario and simulated fiber sections of a) 0 km, b) 5 km, c) 10 km, d) 15 km, e) 25 km f) 30 km and g) 35 km

From figure B.22 it is possible to see that, the amplitude of the waveform at the PIN's input is decreasing with each fiber section added. The definition of the eye in the eye diagram is also declining with each fiber section. From figure B.22 e), f) and g), it is possible to see that the dispersion and noise are considerably visible and present in the attenuation value that simulates the fiber sections of 25, 30 and 35 km. With these attenuation values, the vertical scale was changed to 100 and 50 mV in order to see that, the eye for this waveform is almost closed.

The result of all the waveforms of the 10 Gbit/s signal at the PIN output considering a minimum extinction ratio scenario, a splitting factor of 1/32, an operating wavelength of 1575 nm, and all attenuation values used to simulate the optical fiber path loss are presented in figure B.23.

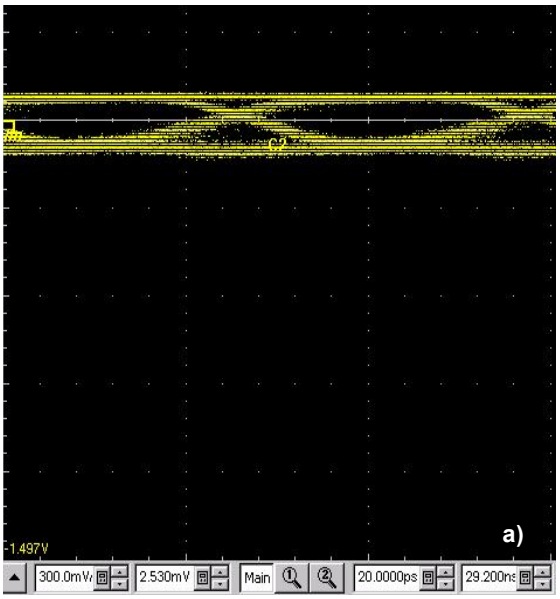

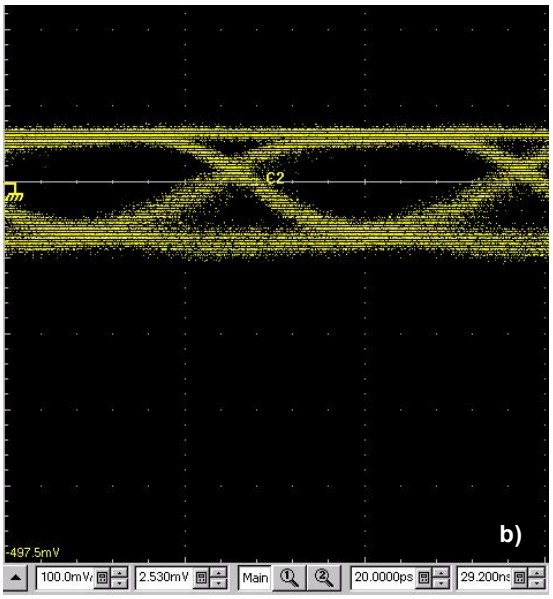

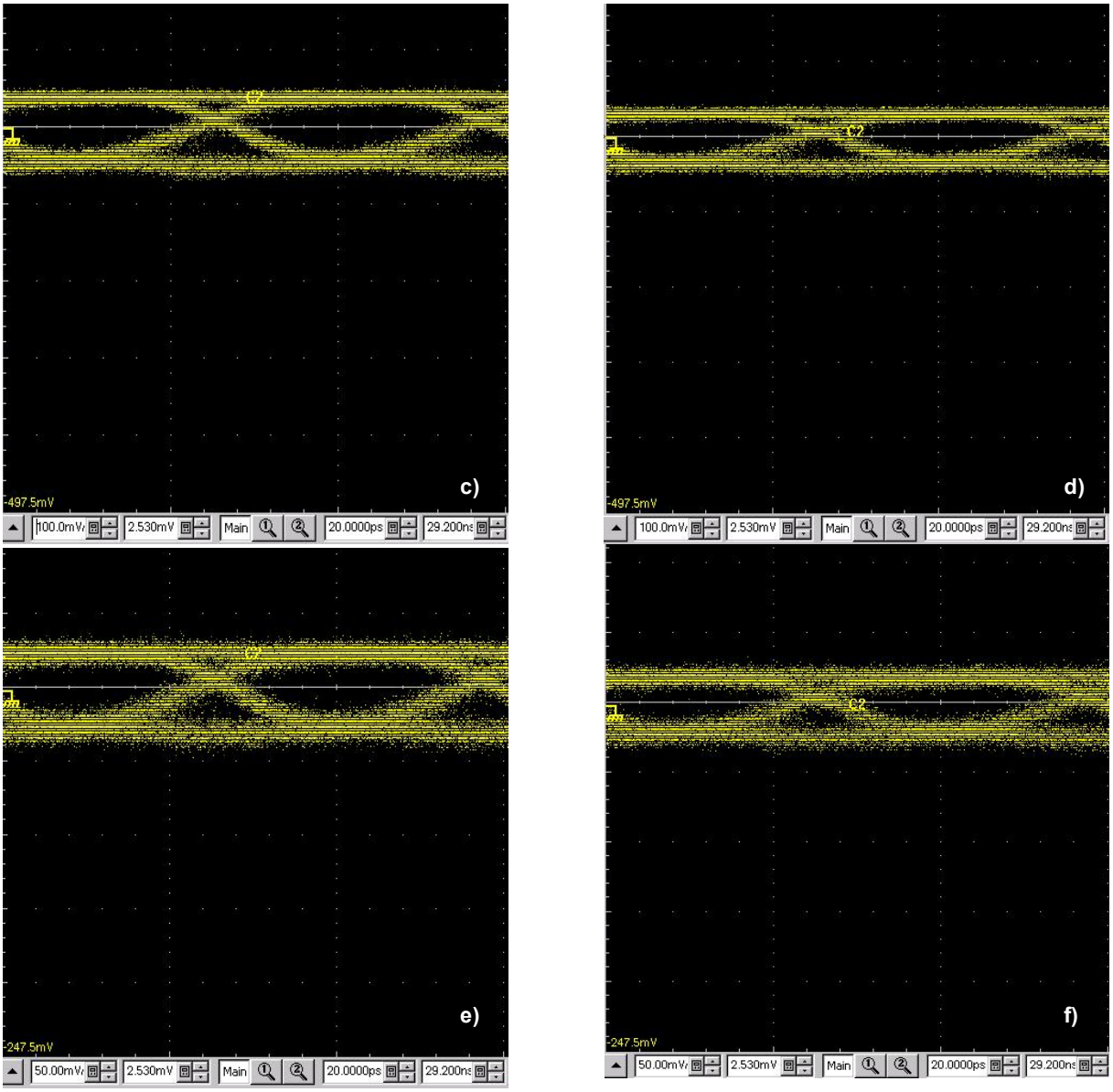

Figure B.23 - Waveforms at the PIN output with a splitting factor of 1/32, considering the minimum extinction ratio scenario and simulated fiber sections of a) 0 km, b) 5 km, c) 10 km, d) 15 km, e) 25 km and f) 30 km

From figure B.23 it is possible to see that, the amplitude of the waveform at the PIN's input is decreasing with each fiber section added. The definition of the eye in the eye diagram is also declining with each fiber section. From figure B.23 e) and f) it is possible to see that the dispersion and noise are considerably visible and present in the attenuation value that simulates the fiber sections of 25 and 30 km. With these attenuation values, the vertical scale was changed to 50 mV in order to see that, the eye for this waveform is almost closed.

The result of all the waveforms of the 10 Gbit/s signal at the PIN output considering a minimum extinction ratio scenario, a splitting factor of 1/64, an operating wavelength of 1575 nm, and all attenuation values used to simulate the optical fiber path loss are presented in figure B.24.

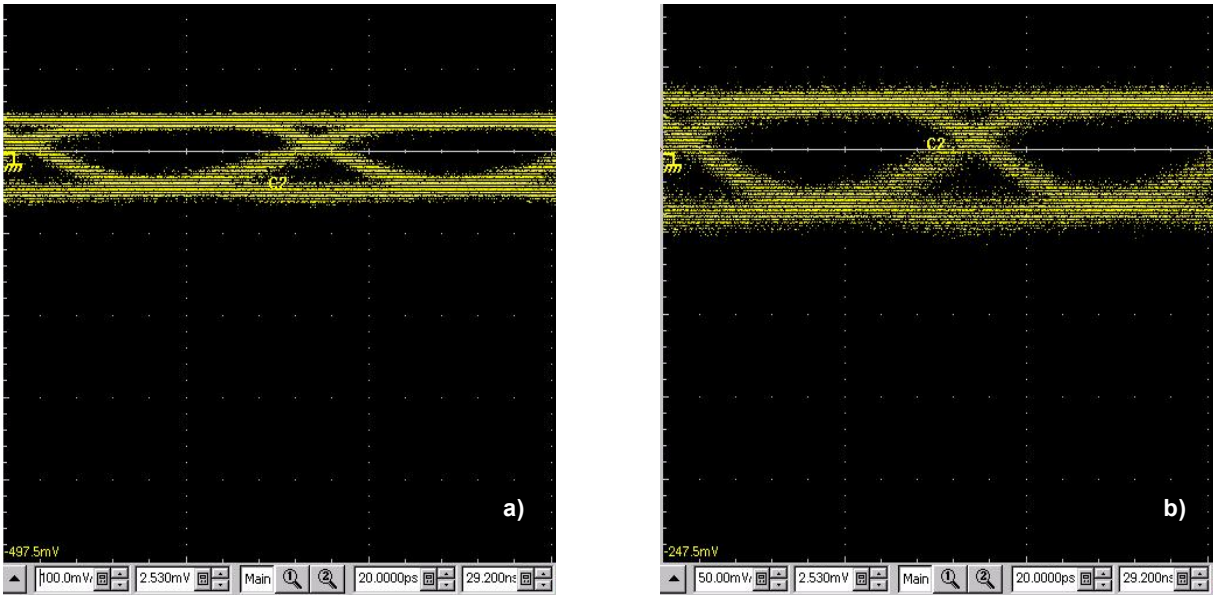

B.24 - Waveforms at the PIN output with a splitting factor of 1/64, considering the minimum extinction ratio scenario and simulated fiber sections of a) 0 km and b) 5 km

From figure B.24 it is possible to see that, the amplitude of the waveform at the PIN's input is decreasing with each fiber section added. The definition of the eye in the eye diagram is also declining with each fiber section. Figure B.24 b) presents the waveform with the most losses because it using a splitting factor of 1/64 and a attenuation value that simulates the fiber section of 5 km. The waveform from figure B.24 a) presents a well defined eye however, the vertical scale had to be change to 100 mV in order to see it because it is slightly closed. With the fiber section of 5 km, the vertical scale was changed to 50 mV in order to see that, the eye for this waveform is almost closed and the dispersion and noise is considerably visible and present.

B.5 Waveforms of the 10 Gbit/s signal obtained by the BER measurement without optical fiber, considering the maximum extinction ratio scenario

In addition to the BER measurement performed in section 4.4 of chapter 4, for the minimum extinction ratio scenario without optical fiber cables, the maximum extinction ratio scenario was also addressed. The setup was correctly assembled and the attenuation values applied to the VOA, in order to simulate the path loss of the optical fiber cable, are presented in table B.2.

	Fiber Length [km]						
Splitter	**0**	**5**	**10**	**15**	**25**	**30**	**35**
1/16	4.8	6.1	8.2	9.0	10.1	11.6	13.7
1/32	4.7	5.9	8.5	9.3	10.2	11.3	-
1/64	4.8	6.3	8.6	-	-	-	-

Table B.2 – Attenuation values, in dB, applied to the VOA for the maximum extinction ratio scenario

The result of all the waveforms of the 10 Gbit/s signal at the PIN output considering a maximum extinction ratio scenario, a splitting factor of 1/16, an operating wavelength of 1575 nm, and all attenuation values used to simulate the optical fiber path loss are presented in figure B.25.

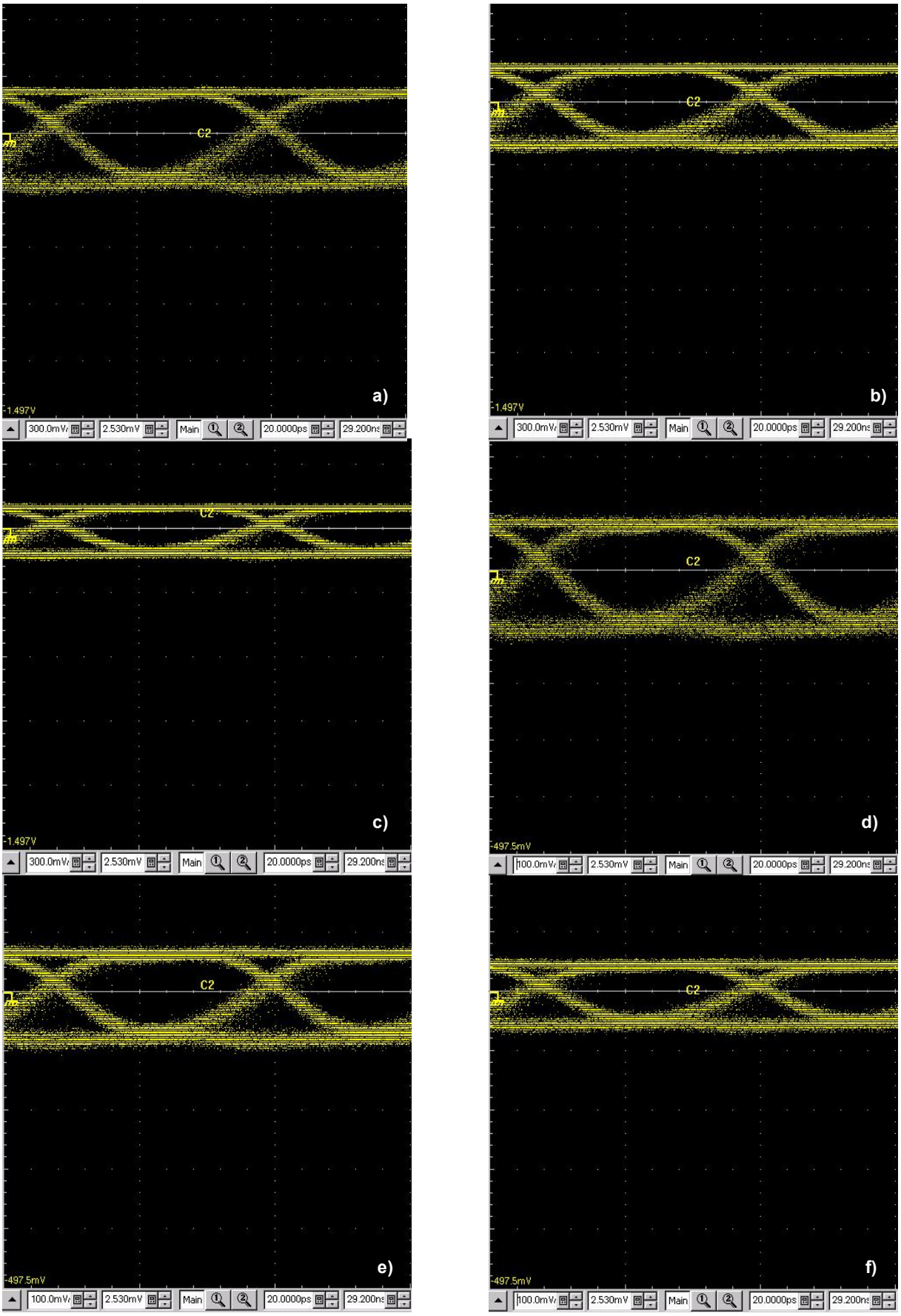

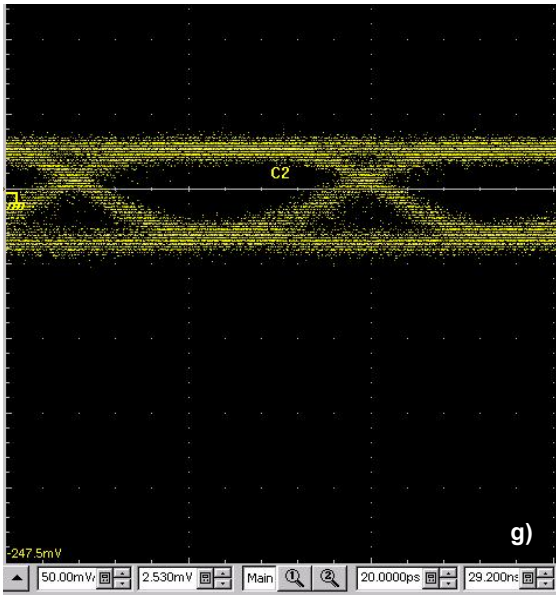

Figure B.25 - Waveforms at the PIN output with a splitting factor of 1/16, considering the maximum extinction ratio scenario and simulated fiber sections of a) 0 km, b) 5 km, c) 10 km, d) 15 km, e) 25 km f) 30 km and g) 35 km

From figure B.25 it is possible to see that, the amplitude of the waveform at the PIN's input is decreasing with each fiber section added. The definition of the eye in the eye diagram is also declining with each fiber section. From figure B.25 e), f) and g), it is possible to see that the dispersion and noise are considerably visible and present in the attenuation value that simulates fiber sections of 25, 30 and 35 km. With these attenuation values, the vertical scale was changed to 100 and 50 mV in order to see that, the eye for this waveform is almost closed.

The result of all the waveforms of the 10 Gbit/s signal at the PIN output considering a maximum extinction ratio scenario, a splitting factor of 1/32, an operating wavelength of 1575 nm, and all attenuation values used to simulate the optical fiber path loss are presented in figure B.26.

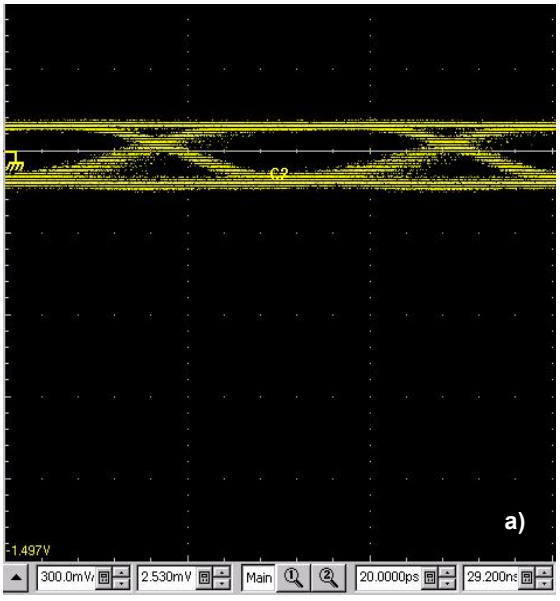

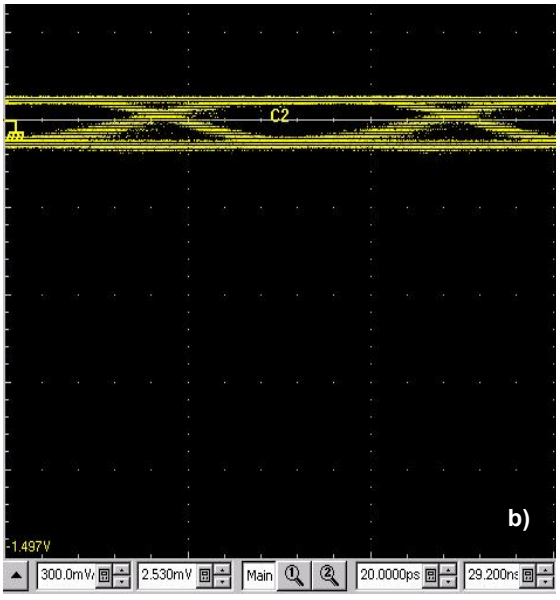

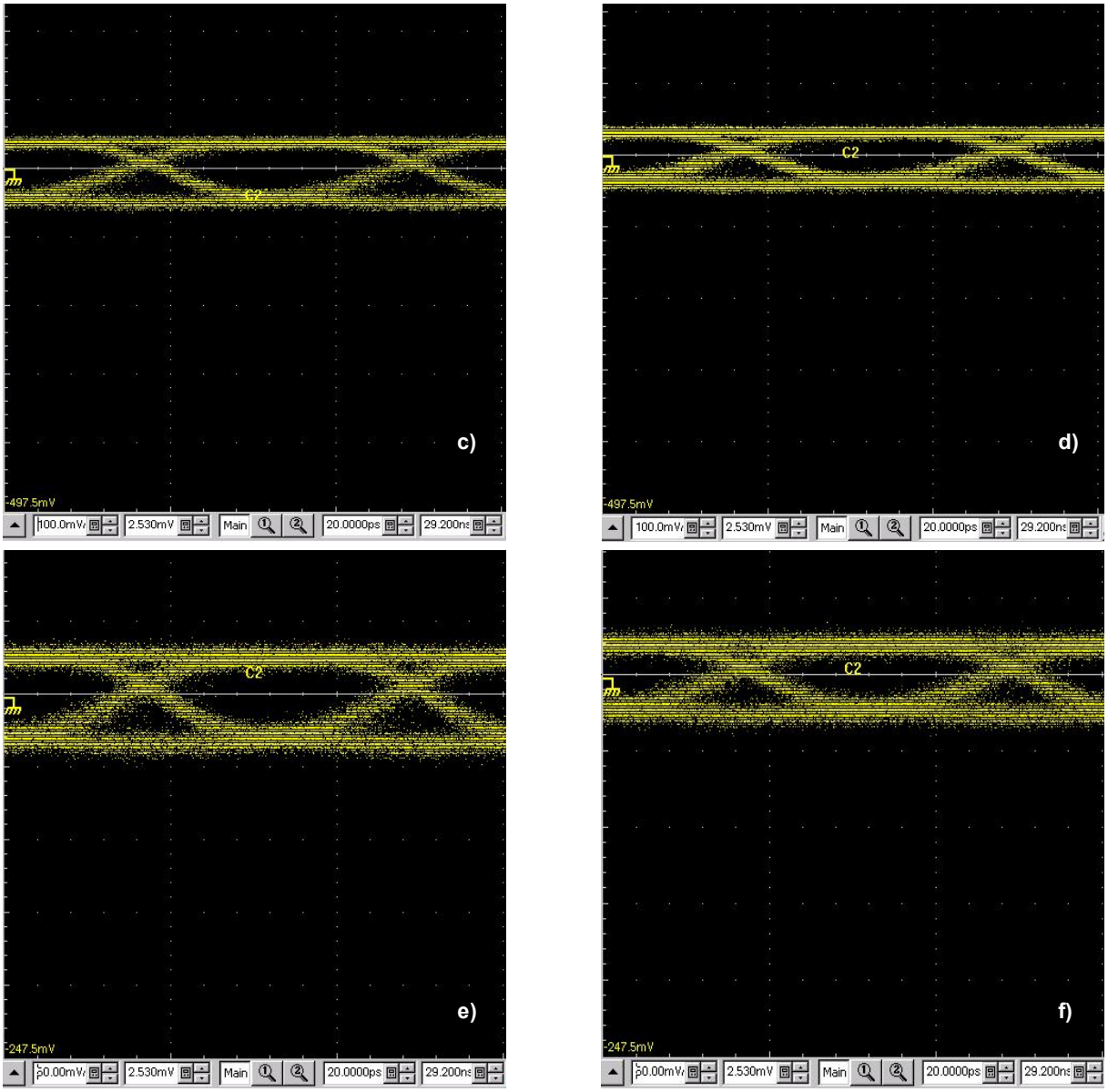

Figure B.26 - Waveforms at the PIN output with a splitting factor of 1/32, considering the maximum extinction ratio scenario and simulated fiber sections of a) 0 km, b) 5 km, c) 10 km, d) 15 km, e) 25 km and f) 30 km

From figure B.26 it is possible to see that, the amplitude of the waveform at the PIN's input is decreasing with each fiber section added. The definition of the eye in the eye diagram is also declining with each fiber section. From figure B.26 e) and f), it is possible to see that the dispersion and noise are considerably visible and present in the attenuation value that simulates fiber sections of 25, 30 and 35 km. With these attenuation values, the vertical scale was changed to 50 mV in order to see that, the eye for this waveform is almost closed.

The result of all the waveforms of the 10 Gbit/s signal at the PIN output considering a maximum extinction ratio scenario, a splitting factor of 1/64, an operating wavelength of 1575 nm, and all attenuation values used to simulate the optical fiber path loss are presented in figure B.27.

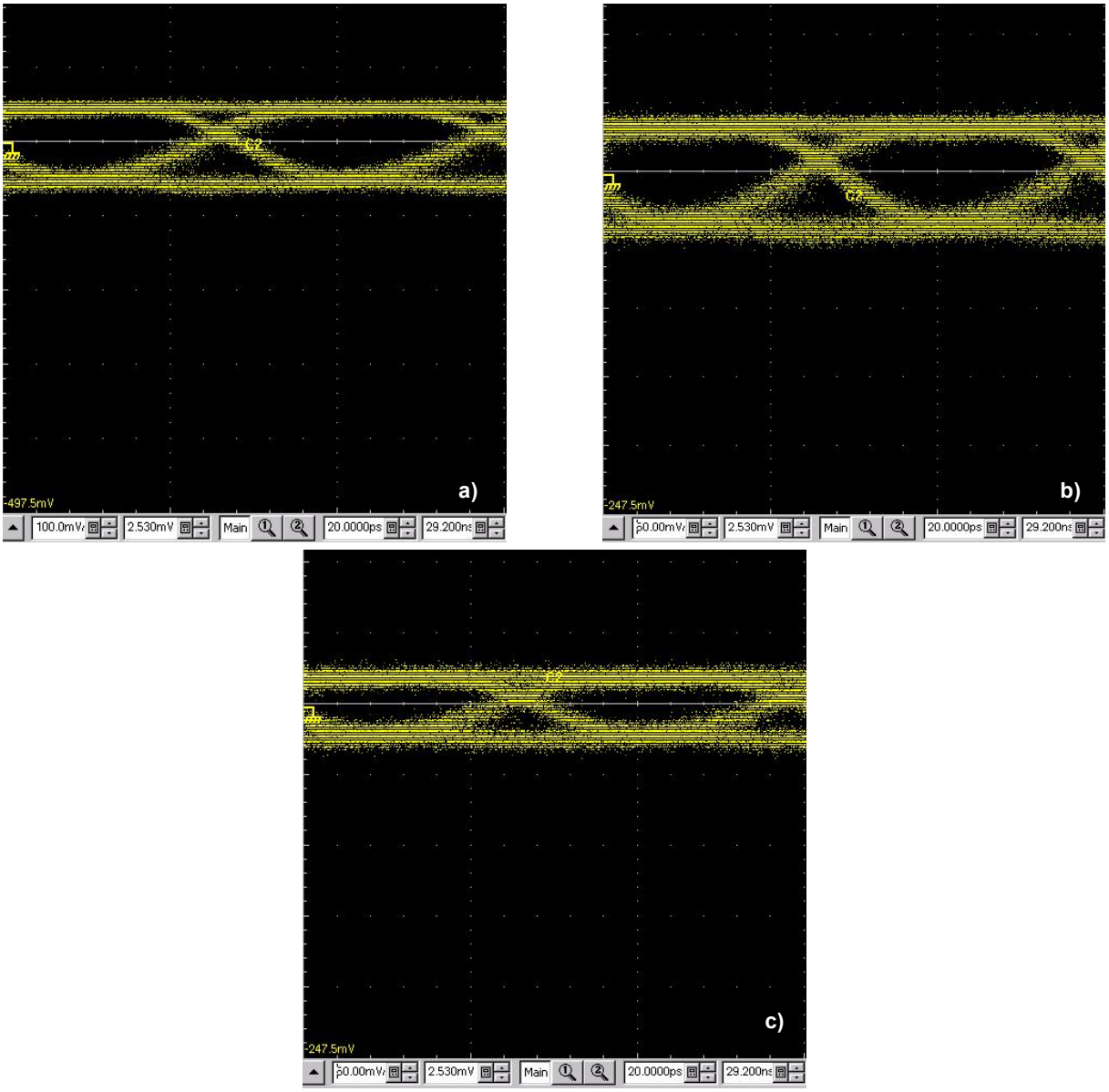

Figure B.27 - Waveforms at the PIN output with a splitting factor of 1/64, considering the maximum extinction ratio scenario and simulated fiber sections of a) 0 km, b) 5 km and c) 10 km

From figure B.27 it is possible to see that, the amplitude of the waveform at the PIN's input is decreasing with each fiber section added. The definition of the eye in the eye diagram is also declining with each fiber section. Figure B.27 b) and c) presents the waveform with the most losses because it using a splitting factor of 1/64 and a attenuation value that simulates fiber sections of 5 and 10 km. The waveform from figure B.27 a) presents a well defined eye however, the vertical scale had to be change to 100 mV in order to see it because it is slightly closed. With the fiber section of 5 and 10 km, the vertical scale was changed to 50 mV in order to see that, the eye for this waveform is almost closed and the dispersion is considerably visible and present.

With the values obtained from table B.2 applied to the VOA, the BER parameter was measured. The measurements results are presented in table B.3.

	Fiber Length [km]						
Splitter	**0**	**5**	**10**	**15**	**25**	**30**	**35**
1/16	<-12.0	<-12.0	<-12.0	<-12.0	<-12.0	-11.4	-7.0
1/32	<-12.0	<-12.0	-10.0	-7.9	-6.8	-4.1	X
1/64	-12.4	-8.5	-4.0	X	X	X	X

Table B.3 – Log_{10}BER measured using the VOA device and considering the maximum extinction ratio scenario

By watching the information presented in table B.3 it is possible to do a comparison with the results obtained for the minimum extinction ratio scenario in section 4.4 of chapter 4. It is possible to conclude that for both scenarios the BER has similar results. However, with the maximum extinction ratio scenario, the BERT device was able to measure better values for the BER, which indicates a better performance.